

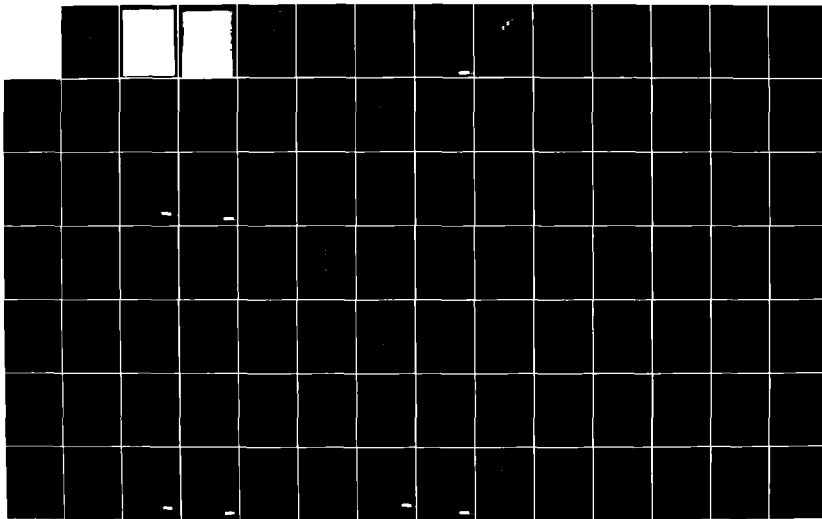
AD-A435 156

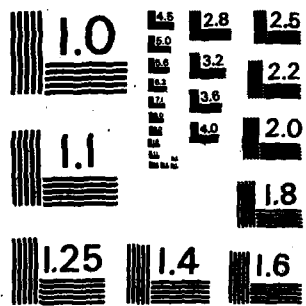
SIMPLE POLARIMETRIC SIMULATION FOR SMALL COMPUTERS(U)
ARMY MISSILE COMMAND REDSTONE ARSENAL AL ADVANCED
SENSORS DIRECTORATE J S COLE DEC 82 DRSMI-RE-83-B-TR
SBI-AD F950 462 F/G 17/9

1/2

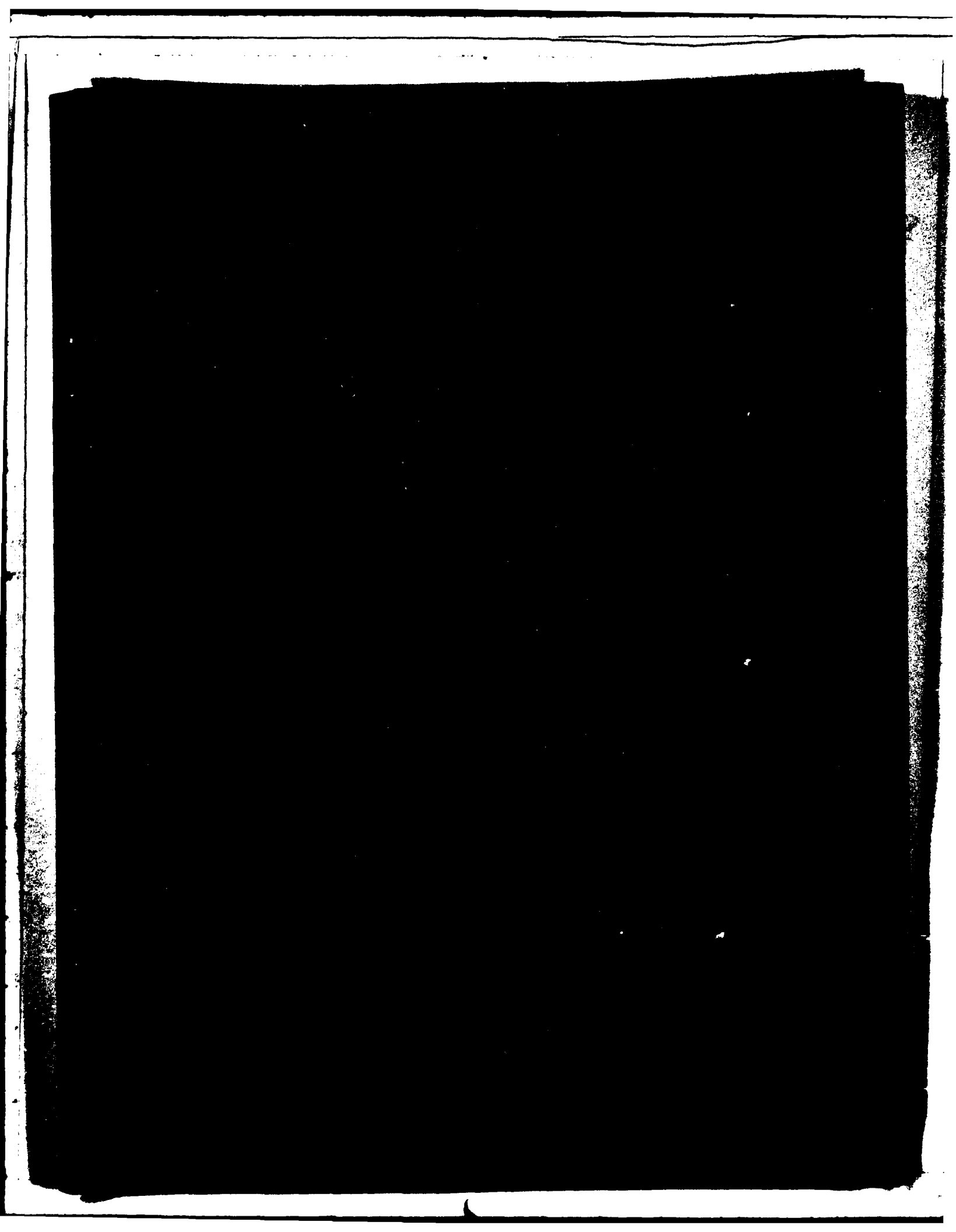
UNCLASSIFIED

NL





MICROCOPY RESOLUTION TEST CHART
NATIONAL BUREAU OF STANDARDS-1963-A





UNCLASSIFIED

SECURITY CLASSIFICATION OF THIS PAGE (When Data Entered)

REPORT DOCUMENTATION PAGE		READ INSTRUCTIONS BEFORE COMPLETING FORM
1. REPORT NUMBER TR-RE-83-8	2. GOVT ACCESSION NO. AD-A135 156	3. RECIPIENT'S CATALOG NUMBER
4. TITLE (and Subtitle) SIMPLE POLARIMETRIC SIMULATION FOR SMALL COMPUTERS		5. TYPE OF REPORT & PERIOD COVERED Technical Report
		6. PERFORMING ORG. REPORT NUMBER
7. AUTHOR(s) John S. Cole		8. CONTRACT OR GRANT NUMBER(s)
9. PERFORMING ORGANIZATION NAME AND ADDRESS Commander, US Army Missile Command ATTN: DRSMI-RE Redstone Arsenal, AL 35812		10. PROGRAM ELEMENT, PROJECT, TASK AREA & WORK UNIT NUMBERS
11. CONTROLLING OFFICE NAME AND ADDRESS Commander, US Army Missile Command ATTN: DRSMI-RPT Redstone Arsenal, AL 35812		12. REPORT DATE December 1982
		13. NUMBER OF PAGES
14. MONITORING AGENCY NAME & ADDRESS (if different from Controlling Office)		15. SECURITY CLASS. (of this report) UNCLASSIFIED
		15a. DECLASSIFICATION/DOWNGRADING SCHEDULE
16. DISTRIBUTION STATEMENT (of this Report) Approved for public release; distribution unlimited.		
17. DISTRIBUTION STATEMENT (of the abstract entered in Block 20, if different from Report)		
18. SUPPLEMENTARY NOTES		
19. KEY WORDS (Continue on reverse side if necessary and identify by block number) Polarization Scattering Matrix Radar FFT		
20. ABSTRACT (Continue on reverse side if necessary and identify by block number) A simple method of simulating polarization dependent radar is presented. The polarization scattering matrix is derived. Transform techniques for radar processing is presented.		

Acknowledgements

The author wishes to express his appreciation to the following persons for their guidance and counsel:

Lloyd W. Root, Jr.

Robert F. Russell

Fred W. Sedenquist

DeWayne C. Garner

Accession For	
NTIS GRA&I	<input checked="" type="checkbox"/>
DTIC TAB	<input type="checkbox"/>
Unannounced	<input type="checkbox"/>
Justification	
By _____	
Distribution/	
Availability Codes	
Dist	Avail and/or Special
A/1	



CONTENTS

	<u>Page No.</u>
I. INTRODUCTION.....	3
II. CONCEPT OF POLARIZED ELECTROMAGNETIC WAVES.....	3
III. THE POLARIZATION SCATTERING MATRIX.....	4
IV. SCATTERING MATRICES FOR SIMPLY SHAPED OBJECTS.....	10
V. REPRESENTATION OF COMPLEX TARGETS USING THE POLARIZATION SCATTERING MATRIX.....	17
VI. ANTENNA CROSS COUPLING AND ITS EFFECT ON THE RECEIVED WAVE.....	19
VII. FREQUENCY AGILITY AND THE PHASE DELAY FUNCTION.....	22
VIII. CONCLUSIONS.....	24
Appendix A - Simulation and Data.....	27
Appendix B - Linear to Circular Transformation.....	85
Appendix C - Poincaré Sphere.....	91

I. INTRODUCTION

Much research has been done in recent years with the objective of understanding, quantifying, and exploiting the polarization properties of radar targets. The purpose of this report is to further this effort by describing a simple algorithm for polarimetric modeling of targets and clutter. The hypothesis which is the basis for the algorithm is that targets and clutter can be modeled as a collection of odd and even bounce scattering centers. Odd bounce scatterers are modeled as trihedrals and even bounce scatterers are modeled as dihedrals. Depolarization effects are simulated by canted dihedrals. The monostatic only case is addressed and no attempt has been made to account for aspect angle or motion dependent phenomena such as glint, scintillation, fading, or doppler shift. Polarization scattering matrices will be used to describe the transformation between incident and reflected waves. The report concludes with a brief description of some simple polarimetric signal processing techniques.

II. CONCEPT OF POLARIZED ELECTROMAGNETIC WAVES

If by convention we neglect the magnetic field vector, an electromagnetic wave can be expressed as the sum of a horizontal and a vertical component as follows:

$$\vec{E} = A_h \cos(\omega t) \hat{h} + A_v \cos(\omega t + \beta) \hat{v} \quad (1)$$

where

\vec{E} = Electric field vector

A_h = Magnitude of horizontal component

A_v = Magnitude of vertical component

\hat{h} = Unit vector in the horizontal direction

\hat{v} = Unit vector in the vertical direction

β = Phase angle between the horizontal and vertical components

As the wave propagates through space, the tip of the electric field vector describes a locus that is elliptical in shape. By varying the magnitude of the horizontal and vertical components and the phase angle between them, any ellipticity desired can be generated. Some special cases of elliptical polarization are presented in Figure 2. The locus diagrams in Figure 2 should be viewed as the trace the tip of the electric field vector makes as the wave is propagated through a stationary planar surface (in this case the page) aligned normal to the direction of propagation. As illustrated in Figure 2, left-hand circular appears to rotate clockwise and right-hand circular counter clockwise. This conforms to the familiar right-hand rule and to the IEEE standard¹ definition of circular polarization and is the convention that will be used throughout this report. Figure 3 is a block diagram of a generic polarimetric radar. The antenna is capable of transmitting and receiving any combination of horizontal, vertical, or circular polarization of either right or left-hand sense. Polarization agility is necessary to generate the elements

- \hat{h} = Unit vector in the horizontal direction
- \hat{v} = Unit vector in the vertical direction
- β = Phase angle between the horizontal and vertical components

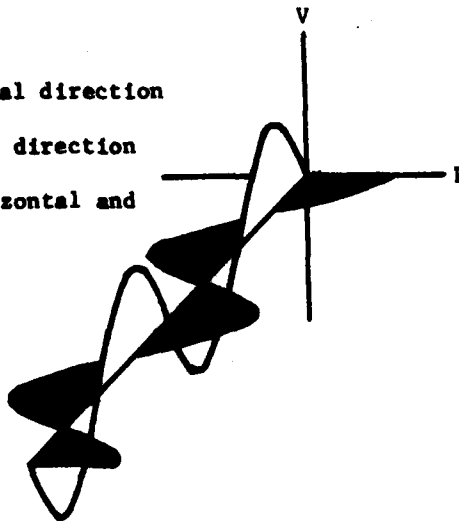


Figure 1. Horizontal and vertical component of elliptically polarized electromagnetic wave.

in the polarization scattering matrix. Complete characterization of a radar target (or clutter cell) is possible given the information contained in the polarization scattering matrix.

Any polarization desired can be generated from two orthogonal polarizations. Linear polarization can be produced by combining RHC and LHC; right and left circular can be produced by combining horizontal and vertical.

III. THE POLARIZATION SCATTERING MATRIX

Sinclair² introduced the concept that a radar target in the far field has a polarization response which can be described by a 2 x 2 matrix known as the polarization scattering matrix [S]. [S] completely characterizes the scattering properties of a target such that:

$$[\vec{E}^S] = [S] [\vec{E}^T] \frac{1}{\sqrt{4\pi R^2}} \quad (2)$$

where

\vec{E}^S = scattered electric field vector (at the target)

\vec{E}^T = transmitted electric field vector

$\frac{1}{\sqrt{4\pi R^2}}$ = amplitude scaling factor. R is range to target

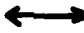





Ah	Av	β	Locus of E	Type of Polarization
E	0	Undefined		Horizontal
0	E	Undefined		Vertical
$\frac{E}{\sqrt{2}}$	$\frac{E}{\sqrt{2}}$	-90°		Right hand circular
$\frac{E}{\sqrt{2}}$	$\frac{E}{\sqrt{2}}$	$+90^\circ$		Left hand circular
$\frac{E}{\sqrt{2}}$	$\frac{E}{\sqrt{2}}$	-180°		Slant right 45°
$\frac{E}{\sqrt{2}}$	$\frac{E}{\sqrt{2}}$	$+180^\circ$		Slant left 45°

Figure 2. Special cases of elliptical polarization. Direction of propagation is out of the page.

The scattering matrix [S] relates the incident electric field to the scattered electric field. The matrix formulation of the target scattering function is justified if the following assumptions are made.

- a. The medium of propagation is homogeneous.
- b. The relationship between the incident and scattered field is linear.

The elements of [S] are complex vector quantities. In order to define individual elements of [S], a polarization basis must be chosen. A polarization basis is a set of orthonormal vectors that span the complex vector space S of which [S] is a subset. If we define S as the set of all 2 x 2 matrices describing the target scattering properties as a function of cross polarized and co-polarized response, then it is easy to see that the choice of polarization bases are infinite, due to the infinite choice of transmitted waveforms. The polarization bases that will be considered herein are the linear (horizontal and vertical) and circular (right and left hand). Choosing a linear

polarization basis, and restricting the transmitted wave to horizontal only yields the following matrix representation of \vec{E}^T :

$$\vec{E}_H^T = \begin{bmatrix} A_H \cos(\omega t + \phi_H) \\ 0 \end{bmatrix} \begin{bmatrix} \hat{h} \\ \hat{v} \end{bmatrix}^T$$

where

A_H = magnitude of horizontal component

ϕ_H = phase angle of horizontal component

\hat{h}, \hat{v} = unit vectors in h and v direction

Similarly for vertical only:

$$\vec{E}_V^T = \begin{bmatrix} 0 \\ A_V \cos(\omega t + \phi_V) \end{bmatrix} \begin{bmatrix} \hat{h} \\ \hat{v} \end{bmatrix}^T$$

where

A_V = magnitude of vertical component

ϕ_V = phase angle of vertical component

Combining the two matrices yields the general case

$$\vec{E}^T = \begin{bmatrix} A_H \cos(\omega t) \\ A_V \cos(\omega t + \beta) \end{bmatrix} \begin{bmatrix} \hat{h} \\ \hat{v} \end{bmatrix}^T$$

$\beta = \phi_V - \phi_H$ if we choose the time reference such that E_V^T is maximum at t equal zero.

If the time dependence of \vec{E}^T is suppressed, the matrix notation becomes

$$\vec{[E^T]} = \begin{bmatrix} E_H^T \\ E_V^T \end{bmatrix} \begin{bmatrix} \hat{h} \\ \hat{v} \end{bmatrix}^T$$

where E_H^T and E_V^T are complex phasors of the form $A_H e^{j\theta_H}$ and $A_V e^{j\theta_V}$.

Decomposing $(\vec{E^S})$ in a similar manner yields:

$$\vec{[E^S]} = \begin{bmatrix} E_H^S \\ E_V^S \end{bmatrix} \begin{bmatrix} \hat{h} \\ \hat{v} \end{bmatrix}^T$$

For brevity, the unit vector matrix will be dropped allowing Equation (2) to be rewritten as:

$$\begin{bmatrix} \vec{E_H^S} \\ \vec{E_V^S} \end{bmatrix} = \begin{bmatrix} S_{11} & S_{12} \\ S_{21} & S_{22} \end{bmatrix} \begin{bmatrix} \vec{E_H^T} \\ \vec{E_V^T} \end{bmatrix}^T \frac{1}{\sqrt{4\pi R^2}} \quad (3)$$

From Equation (3) it can be seen that the scattered wave horizontal component is related to the incident wave in the following manner:

$$\vec{E_H^S} = S_{11} \vec{E_H^T} + S_{12} \vec{E_V^T} .$$

The vertical component of the scattered wave is represented by:

$$\vec{E_V^S} = S_{21} \vec{E_H^T} + S_{22} \vec{E_V^T} .$$

S_{11} and S_{22} are referred to as the co-polarized terms of the scattering matrix, while S_{12} and S_{21} are the cross polarized terms. For a linear polarization basis, S_{11} is that quantity that defines the targets horizontal response to a horizontally polarized transmitted wave. S_{22} defines the targets vertical response to a vertically polarized transmitted wave. S_{12} and S_{21} are terms that quantify the targets depolarization response. For clarity, the subscript numbers will be replaced by the corresponding polarization designating letter with the first letter indicating the scattered polarization and the

second the incident polarization. For a linear polarization basis, [S] will have the form:

$$[S] = \begin{bmatrix} S_{HH} & S_{HV} \\ S_{VH} & S_{VV} \end{bmatrix}$$

For a circular polarization basis [S] would have the form:

$$[S] = \begin{bmatrix} S_{RR} & S_{RL} \\ S_{LR} & S_{LL} \end{bmatrix}$$

Where R is right-hand circular polarization,

and L is left-hand circular polarization.

Equation (3) for a circular polarization basis is:

$$\begin{bmatrix} \vec{E}_R^S \\ \vec{E}_L^S \end{bmatrix} = \begin{bmatrix} S_{RR} & S_{RL} \\ S_{LR} & S_{LL} \end{bmatrix} \begin{bmatrix} \vec{E}_R^T \\ \vec{E}_L^T \end{bmatrix} \frac{1}{\sqrt{4\pi R^2}}$$

Mentzer³ et al. have shown that the scattering matrix is a function of radar cross section and has the form

$$[S] = \begin{bmatrix} \sqrt{\sigma_{HH}} e^{j\phi_{HH}} & \sqrt{\sigma_{HV}} e^{j\phi_{HV}} \\ \sqrt{\sigma_{VH}} e^{j\phi_{VH}} & \sqrt{\sigma_{VV}} e^{j\phi_{VV}} \end{bmatrix}$$

σ_{HH} = RCS for horizontal transmit, horizontal receive

σ_{HV} = RCS for vertical transmit, horizontal receive

σ_{VH} = RCS for horizontal transmit, vertical receive

σ_{VV} = RCS for vertical transmit, vertical receive

ϕ_{HH} = Absolute phase for horizontal transmit, horizontal receive

ϕ_{HV} = Absolute phase for vertical transmit, horizontal receive

ϕ_{VH} = Absolute phase for horizontal transmit, vertical receive

ϕ_{VV} = Absolute phase for vertical transmit, vertical receive

For a circular polarization basis, [S] will have the form:

$$[S] = \begin{bmatrix} \sqrt{\sigma_{RR}} e^{j\phi_{RR}} & \sqrt{\sigma_{RL}} e^{j\phi_{RL}} \\ \sqrt{\sigma_{LR}} e^{j\phi_{LR}} & \sqrt{\sigma_{LL}} e^{j\phi_{LL}} \end{bmatrix}$$

σ_{RR} = RCS for RHC transmit, RHC receive

σ_{RL} = RCS for LHC transmit, RHC receive

σ_{LR} = RCS for RHC transmit, LHC receive

σ_{LL} = RCS for LHC transmit, LHC receive

ϕ_{RR} = Absolute phase for RHC transmit, RHC receive

ϕ_{RL} = Absolute phase for LHC transmit, RHC receive

ϕ_{LR} = Absolute phase for RHC transmit, LHC receive

ϕ_{LL} = Absolute phase for LHC transmit, LHC receive

As defined above, [S] is the absolute phase scattering matrix. Definition of each element in the absolute phase scattering matrix requires the measurement radar to be coherent. If a coherent system is not available, then the phase measurements may be made relative to one of the elements. The resulting scattering matrix is called the relative phase scattering matrix. For a linear polarization basis with horizontal transmit, vertical receive as the phase reference, [S] will have the form:

$$[S] = \begin{bmatrix} \sqrt{\sigma_{HH}} e^{j(\phi_{HH} - \phi_{HV})} & \sqrt{\sigma_{HV}} \\ \sqrt{\sigma_{VH}} e^{j(\phi_{VH} - \phi_{HV})} & \sqrt{\sigma_{VV}} e^{j(\phi_{VV} - \phi_{HV})} \end{bmatrix}$$

For a monostatic radar the theorem of reciprocity⁴ holds such that:

$$\sigma_{HV} = \sigma_{VH}$$

$$\phi_{HV} = \phi_{VH}$$

Rewriting [S] yields:

$$[S] = \begin{bmatrix} \sqrt{\sigma_{HH}} e^{j(\phi_{HH} - \phi_{HV})} \sqrt{\sigma_{HV}} & \\ \sqrt{\sigma_{HV}} & \sqrt{\sigma_{VV}} e^{j(\phi_{VV} - \phi_{HV})} \end{bmatrix}$$

This is the relative phase scattering matrix. It should be noted that scattering matrices can be transformed from one polarization basis to another through use of congruent transformation matrices. Derivation of a transformation matrix to transform between linear and circular polarization bases is included as Appendix B. Only five measurements are needed to completely define the relative phase scattering matrix.

IV. SCATTERING MATRICES FOR SIMPLY SHAPED OBJECTS

A. Flat Plate

For a linear polarization basis and a perfectly conducting flat plate oriented normal to the direction of propagation of the incident wave, the scattered wave must have an amplitude equal to the incident wave and a phase shift of 180° in order for the zero tangential field boundary condition to hold. Simply put, this means that if we transmit vertical we will receive vertical and if we transmit horizontal, we will receive horizontal. The scattering matrix for the flat plate will have zeros for the cross polarized terms and unity for the co-polarized terms. The 180° phase shift is handled by setting ϕ_{HH} and ϕ_{VV} equal to π . [S] will have the form:

$$[S] = \begin{bmatrix} \sqrt{\sigma_{HH}} e^{j\pi} & 0 \\ 0 & \sqrt{\sigma_{VV}} e^{j\pi} \end{bmatrix} = \begin{bmatrix} -1 & 0 \\ 0 & -1 \end{bmatrix} \sqrt{\sigma}$$

by symmetry $\sqrt{\sigma_{HH}} = \sqrt{\sigma_{VV}} = \sqrt{\sigma}$

also

$$e^{j\pi} = -1$$

Equation (3) for a flat plate would have the form:

$$\begin{bmatrix} \vec{E}_H^S \\ \vec{E}_H^S \\ \vec{E}_V^S \\ \vec{E}_V^S \end{bmatrix} = \begin{bmatrix} -1 & 0 \\ 0 & -1 \end{bmatrix} \begin{bmatrix} \vec{E}_H^T \\ \vec{E}_H^T \\ \vec{E}_V^T \\ \vec{E}_V^T \end{bmatrix}^T \sqrt{\frac{\sigma}{4\pi R^2}}$$

Normalizing yields:

$$\begin{bmatrix} \vec{E}_H^S \\ \vec{E}_H^S \\ \vec{E}_V^S \\ \vec{E}_V^S \end{bmatrix} = \begin{bmatrix} -1 & 0 \\ 0 & -1 \end{bmatrix} \begin{bmatrix} \vec{E}_H^T \\ \vec{E}_H^T \\ \vec{E}_V^T \\ \vec{E}_V^T \end{bmatrix}^T$$

Solving for \vec{E}_H^S and \vec{E}_V^S :

$$\vec{E}_H^S = -\vec{E}_H^T$$

$$\vec{E}_V^S = -\vec{E}_V^T$$

which is the expected result.

B. Trihedral Corner Reflector

If the three sided corner reflector is modeled as a series of three reflections from flat plates, it is easy to see that [s] will be the same as for the flat plate

Reflection	\vec{E}_H^T	\vec{E}_H^S	\vec{E}_V^T	\vec{E}_V^S
1	1	-1	1	-1
2	-1	1	-1	1
3	1	-1	1	-1

For odd bounce reflectors oriented normal to the direction of propagation, [S] will have the form:

$$[S] = \begin{bmatrix} e^{jn\pi} & 0 \\ 0 & e^{jn\pi} \end{bmatrix}$$

where $n = 1, 3, 5, \dots$.

It should be noted that the odd bounce reflector is rotation angle independent.

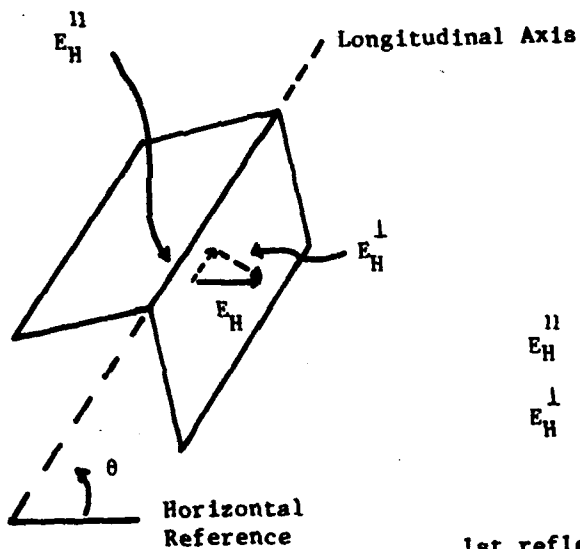
C. Dihedral Corner Reflector

Due to the asymmetrical nature of the dihedral reflector, cross polarized terms will appear in its scattering matrix for any rotation angle other than zero. Figure 4.a. shows a dihedral reflector at an arbitrary angle θ . For a horizontally polarized incident wave, the reflected wave can be derived by breaking the incident wave into two components. The first component is parallel and the second perpendicular to the longitudinal axis of the reflector. The parallel component undergoes a 180° phase shift at the first reflection and 180° phase shift at the second reflection. The net phase shift is 0° . To determine the phase shift of the perpendicular component, it is necessary to decompose it into components parallel and perpendicular to the first plate. At the first reflection, the parallel component will undergo a 180° phase shift and the perpendicular component (which is now parallel to the second plate) will undergo a 180° phase shift and the parallel component (which is now perpendicular to the second plate) will undergo a 0° phase shift (Figure 4.b.). The net result is E_H^\perp has a final phase shift of 180° . Combining the reflections of E_H^\perp and $E_H^{||}$ yields a scattered wave which is rotated an angle of 2θ relative to the horizontal.

The horizontal cross and co-polarized terms of the scattering matrix become $\sin 2\theta$ and $\cos 2\theta$, respectively. A similar analysis for a vertically polarized incident wave will yield cross and co-polarized terms of $\sin 2\theta$ and $-\cos 2\theta$. The scattering matrix for a dihedral reflector is:

$$[S] = \begin{bmatrix} \cos 2\theta & \sin 2\theta \\ \sin 2\theta & -\cos 2\theta \end{bmatrix} .$$

$E_H^{||}$ is reflected from surface (1) and (2). Total phase shift is 0° . A top view of the reflector is shown below. E_H^\perp is broken into two components as shown:



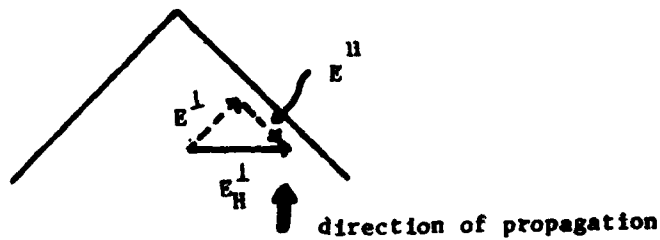
$$E_H^{\parallel} = E_H \cos \theta$$

$$E_H^{\perp} = E_H \sin \theta$$

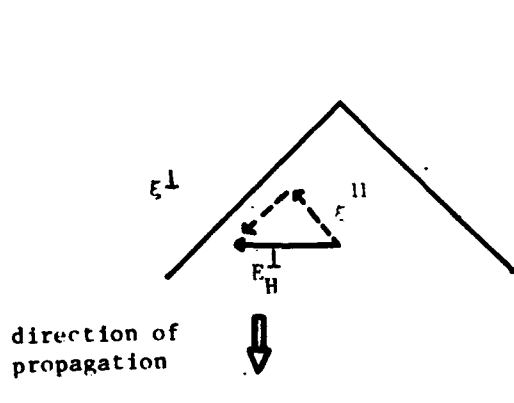
1st reflection - E^{\parallel} undergoes
 180° phase shift. E^{\perp} undergoes
 0° phase shift

Figure 4. Reflection of horizontal wave from a dihedral corner reflector.

TOP VIEW

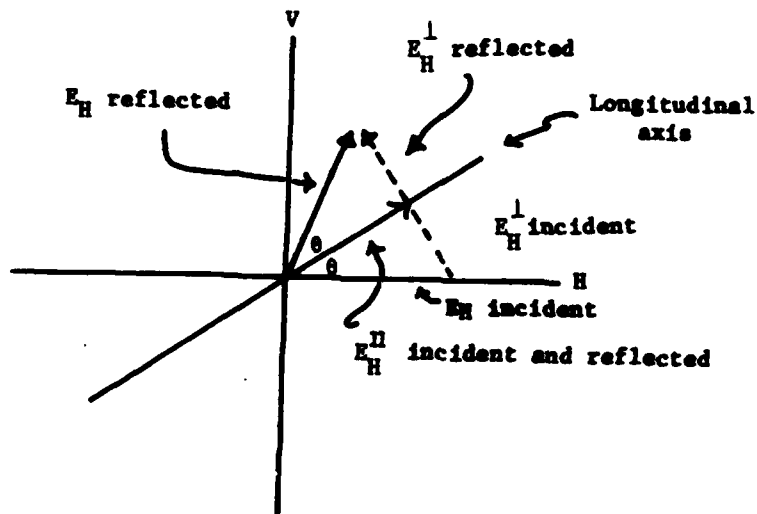


b. direction of propagation



Net result: E_H has a 180° phase shift.

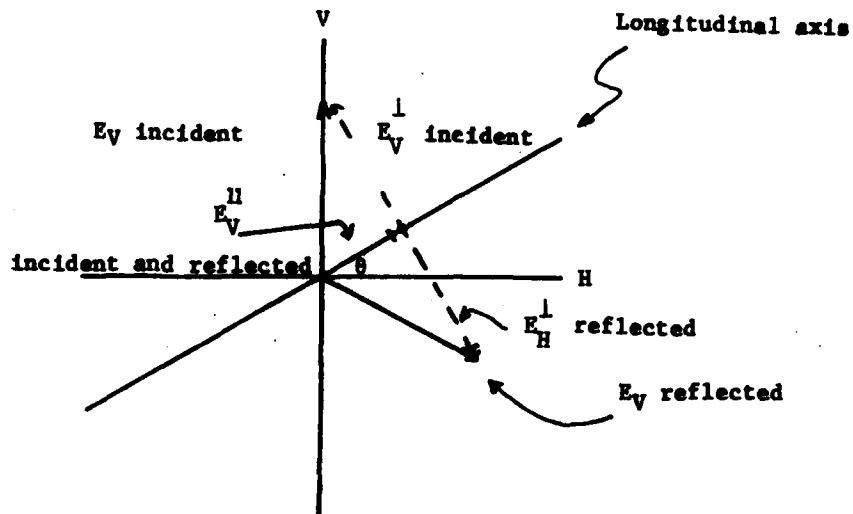
2nd reflection - E_1 undergoes a 180° phase shift. E_2 undergoes a 0° phase shift.



$$\vec{E}_H^{\perp} \text{ cross polarized} = E_H \sin 20^\circ$$

$$\vec{E}_H^{\parallel} \text{ co-polarized} = E_H \cos 20^\circ$$

Figure 5. Reflected wave for a horizontally polarized incident wave.



$$\begin{aligned} \phi &= 180^\circ - (90^\circ + \theta) - \theta \\ &= 90^\circ - 2\theta \end{aligned}$$

$$\begin{aligned} \vec{E}_V \text{ cross polarized} &= E \sin \phi \\ &= E \sin (90^\circ - 2\theta) \\ &= E \sin 2\theta \end{aligned}$$

$$\begin{aligned} \vec{E}_V \text{ co-polarized} &= E_V (-\cos \phi) \\ &= E_V (-\cos (90^\circ - 2\theta)) \\ &= E_V (-\cos 2\theta) \end{aligned}$$

Figure 6. Reflected wave for a vertically polarized incident wave.

V. REPRESENTATION OF COMPLEX TARGETS USING THE POLARIZATION SCATTERING MATRIX

The hypothesis that targets and clutter can be modeled as a collection of odd and even bounce reflectors is the basis for the simulation. The matrix equation for an ensemble of odd and even bounce reflectors will have the form:

$$\begin{bmatrix} \vec{E}_H^R \\ \vec{E}_V^R \end{bmatrix} = \left(\underbrace{\sum_{i=1}^{N_1} \begin{bmatrix} -1 & 0 \\ 0 & -1 \end{bmatrix} \sqrt{\sigma_i} e^{-jKd_i}}_{\text{odd}} + \sum_{j=1}^{N_2} \begin{bmatrix} \cos 2\theta_j & \sin 2\theta_j \\ \sin 2\theta_j & -\cos 2\theta_j \end{bmatrix} \sqrt{\sigma_j} e^{-jKd_j}}_{\text{even}} \right) \begin{bmatrix} \vec{E}_H^T \\ \vec{E}_V^T \end{bmatrix}^T$$

N_1 = number of odd reflectors

N_2 = number of even reflectors

σ_i = RCS of the i th odd reflector

σ_j = RCS of the j th even reflector

d_i = distance to the i th odd reflector

d_j = distance to the j th even reflector

\vec{E}_H^R = Horizontal received electromagnetic wave

\vec{E}_V^R = Vertical received electromagnetic wave

\vec{E}_H^T = Horizontal transmitted electromagnetic wave

\vec{E}_V^T = Vertical transmitted electromagnetic wave

θ_j = Rotation angle of j th even reflector

$K = \frac{4\pi f}{c}$ = two way intrinsic phase constant

solving for \vec{E}_H^R and \vec{E}_V^R yields:

$$\vec{E}_H^R = \sum_{i=1}^{N1} -\sqrt{\sigma_i} e^{-jKdi} \vec{E}_H^T + \sum_{j=1}^{N2} \sqrt{\sigma_j} (\cos 2\theta_j \vec{E}_H^T + \sin 2\theta_j \vec{E}_V^T) e^{-jKdj}$$

$$\vec{E}_V^R = \sum_{i=1}^{N1} -\sigma_i e^{-jKdi} \vec{E}_V^T + \sum_{j=1}^{N2} \sigma_j (\sin 2\theta_j \vec{E}_H^T - \cos 2\theta_j \vec{E}_V^T) e^{-jKdj}$$

Utilizing Eulers Identity and decomposing the result into real and imaginary parts produces the following relationships:

$$\begin{aligned} \text{Re}\{\vec{E}_H^R\} &= \vec{E}_H^T \sum_{i=1}^{N1} -\sqrt{\sigma_i} \cos Kdi + \sum_{j=1}^{N2} \sqrt{\sigma_j} (\cos 2\theta_j \cos Kdj \vec{E}_H^T + \\ &\quad \sin 2\theta_j \cos Kdj \vec{E}_V^T) \end{aligned}$$

$$\begin{aligned} \text{Im}\{\vec{E}_H^R\} &= \vec{E}_H^T \sum_{i=1}^{N1} \sqrt{\sigma_i} \sin Kdi - \sum_{j=1}^{N2} \sqrt{\sigma_j} (\cos 2\theta_j \sin Kdj \vec{E}_H^T + \\ &\quad \sin 2\theta_j \sin Kdj \vec{E}_V^T) \end{aligned}$$

$$\begin{aligned} \text{Re}\{\vec{E}_V^R\} &= \vec{E}_V^T \sum_{i=1}^{N1} -\sqrt{\sigma_i} \cos Kdi + \sum_{j=1}^{N2} \sqrt{\sigma_j} (\sin 2\theta_j \cos Kdj \vec{E}_H^T - \\ &\quad \cos 2\theta_j \cos Kdj \vec{E}_V^T) \end{aligned}$$

$$\begin{aligned} \text{Im}\{\vec{E}_V^R\} &= \vec{E}_V^T \sum_{i=1}^{N1} \sqrt{\sigma_i} \sin Kdi - \sum_{j=1}^{N2} \sqrt{\sigma_j} (\sin 2\theta_j \sin Kdj \vec{E}_H^T - \\ &\quad \cos 2\theta_j \sin Kdj \vec{E}_V^T) \end{aligned}$$

These are the general equations that define the horizontal and vertical (in-phase and quadrature) components of the received electromagnetic wave. \vec{E}_H^T and \vec{E}_V^T are vectors and therefore have an amplitude and phase associated with them. One major objective of the simulation is to model the effects of a less than perfect radar antenna. Figure 7 is a graphical representation of a non-ideal antenna. The amplitude and phase coupling between the horizontal and vertical channels of the antenna is derived in Section VI and the specific equations as used in the simulation are developed.

VI. ANTENNA CROSS COUPLING AND ITS EFFECT ON THE TRANSMITTED WAVE

Figure 7 is a model of a non-ideal antenna with cross coupling between the horizontal and vertical channels. The cross coupling ratio ρ (RHO) is defined in terms of voltage. Equal power is assumed for the horizontal and vertical channel.

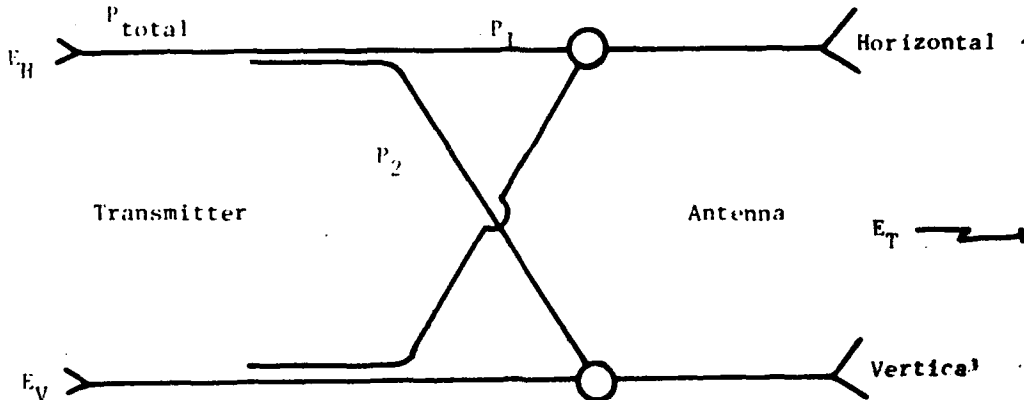


Figure 7. Non-ideal antenna model.

$$\vec{E}^T = E_H \hat{h} + E_V \hat{v} \text{ for no cross coupling}$$

$$\vec{E}^T = \text{transmitted wave}$$

For lossless coupling (no I^2R losses) and considering the horizontal channel of Figure 7;

$$P_{total} = P_1 + P_2 \quad \text{where } P = \text{power}$$

$$\text{db of coupling} = 10 \left(\frac{P_2}{P_t} \right)$$

then

$$P_2 = 10^{\frac{-\text{db}}{10}} P_{total}$$

$$P_1 = (1 - 10^{\frac{-\text{db}}{10}}) P_{total}$$

in terms of voltage (Z normalized);

$$E_2 = \sqrt{10 \frac{-db}{10}}$$

$$E_1 = \sqrt{1 - 10 \frac{-db}{10}}$$

\vec{E}_H^T will have the form:

$$\vec{E}_H^T = A \vec{E}_H + B \vec{E}_V \text{ where } A = \sqrt{1 - 10 \frac{-db}{10}}$$

$$\text{and } B = \sqrt{10 \frac{-db}{10}}$$

let $\rho = 10 \frac{-db}{10}$

then

$$A = \sqrt{1 - \rho}$$

$$B = \sqrt{\rho}$$

\vec{E}_V^T will have the form:

$$\vec{E}_V^T = B \vec{E}_H + A \vec{E}_V$$

For simplicity in the simulation, the transmitted signal is restricted to horizontal, vertical, RHC, or LHC only. For RHC transmit, \vec{E}_H^T and \vec{E}_V^T are equal to:

$$\vec{E}_H^T = A \vec{E}_H + j B \vec{E}_V$$

$$\vec{E}_V^T = B \vec{E}_H + j A \vec{E}_V$$

For LHC transmit \vec{E}_H^T and \vec{E}_V^T are:

$$\vec{E}_H^T = A \vec{E}_H - j B \vec{E}_V$$

$$\vec{E}_V^T = \vec{B}\hat{E}_H - jA\hat{E}_V$$

A dummy variable n is introduced to provide circular polarization agility.

\vec{E}_H^T and \vec{E}_V^T are defined as:

$$\vec{E}_H^T = A\hat{H} + njB\hat{V}$$

$$\vec{E}_V^T = B\hat{H} + njA\hat{V}$$

H = horizontal magnitude

V = vertical magnitude

Replacing \vec{E}_H^T and \vec{E}_V^T in the general equations with the expressions developed above and separating the real and imaginary parts yields:

$$\text{RE} \left\{ \vec{E}_H^T \right\}^* = \sum_{i=1}^{N1} -\sqrt{\sigma_i} (AH \cos Kdi - nBV \sin Kdi) + \sum_{j=1}^{N2} \sqrt{\sigma_j} (AH \cos 2\theta_j \cos Kdj + nBV \sin 2\theta_j \sin Kdj + BH \sin 2\theta_j \cos Kdj + nAV \sin 2\theta_j \sin Kdj)$$

$$\text{Im} \left\{ \vec{E}_H^T \right\}^* = \sum_{i=1}^{N1} \sqrt{\sigma_i} (AH \sin Kdi - nBV \cos Kdi) + \sum_{j=1}^{N2} \sqrt{\sigma_j} (nBV \sin 2\theta_j \cos Kdj - AH \cos 2\theta_j \sin Kdj + nAV \sin 2\theta_j \cos Kdj - BH \sin 2\theta_j \sin Kdj)$$

* Indicates received field at antenna

$$\text{RE} \left\{ \vec{E}_V^T \right\}^* = \sum_{i=1}^{N1} -\sigma_i (BH \cos Kdi + nAV \sin Kdi) + \sum_{j=1}^{N2} \sigma_j (AH \sin 2\theta_j \cos Kdj + nBV \sin 2\theta_j \sin Kdj - BH \cos 2\theta_j \cos Kdj - nAV \cos 2\theta_j \sin Kdj)$$

$$\text{Im} \left\{ \vec{E}_V^T \right\}^* = \sum_{i=1}^{N1} \sqrt{\sigma_i} (BH \sin Kdi - nAV \cos Kdi) + \sum_{j=1}^{N2} \sqrt{\sigma_j} (nBV \sin 2\theta_j \cos Kdj - AH \sin 2\theta_j \sin Kdj - nAV \cos 2\theta_j \cos Kdj + BH \cos 2\theta_j \sin Kdj)$$

n = ±1 RHC or LHC transmitted

V = 0 Horizontal transmitted

H = 0 Vertical transmitted

These equations define the received electromagnetic wave seen by the antenna. Determination of the signal at the antenna terminals is accomplished through multiplication of these equations by the cross coupling coefficients. The resulting equations are:

$$\operatorname{Re} \left\{ \vec{E}_H^R \right\} = A \cdot \operatorname{Re} \left\{ \vec{E}_H^R \right\}^* + B \cdot \operatorname{Re} \left\{ \vec{E}_V^R \right\}^*$$

$$\operatorname{Im} \left\{ \vec{E}_H^R \right\} = A \cdot \operatorname{Im} \left\{ \vec{E}_H^R \right\}^* + B \cdot \operatorname{Im} \left\{ \vec{E}_V^R \right\}^*$$

$$\operatorname{Re} \left\{ \vec{E}_V^R \right\} = A \cdot \operatorname{Re} \left\{ \vec{E}_V^R \right\}^* + B \cdot \operatorname{Re} \left\{ \vec{E}_H^R \right\}^*$$

$$\operatorname{Im} \left\{ \vec{E}_V^R \right\} = A \cdot \operatorname{Im} \left\{ \vec{E}_V^R \right\}^* + B \cdot \operatorname{Im} \left\{ \vec{E}_H^R \right\}^*$$

These are the equations used in the simulation. The real equations define the in-phase components, while the imaginary equations define the quadrature components of the vertical and horizontal received signals.

VII. FREQUENCY AGILITY AND THE PHASE DELAY FUNCTION

Determination of the phase delay function [5] is the objective of any polarimetric radar. The phase delay function defines the location, type, and size (RCS) of the predominant scatterers that comprise a target. For a stationary ergodic process, which is a function of a random variable (frequency in this case), the output of the process can be determined in a number of ways. Sampling of a long time duration output record with a constantly changing input is identical to instantaneous, time coincident sampling of a large number of output records generated by different inputs. Simply put, in order to generate a sample set for signal processing, two options are available:

1. Simultaneously transmit a large number of different frequency signals (i.e., an impulse) and record a large number of discrete bandpass samples of the echo.

2. Sequentially change frequency and sequentially record the echo. (This is the method used in this simulation and in most radars.)

The final result will be the same. The range resolution of a pulsed radar is defined as:

$$\Delta R = \frac{cT}{2}$$

where

$$C = 2.997 \times 10^8 \text{ m/sec}$$

τ = Pulsewidth in sec.

For a frequency agile, coherent radar with matched receiver, the range resolution is:

$$\Delta R = \frac{C}{2B}$$

where B = frequency agile bandwidth.

The amplitude of the scattered field as a function of frequency is the Fourier transform of the phase delay function⁵. Through use of the complex inverse Fourier Transform, the phase delay function can be found. The complex inverse Fourier Transform for circularly polarized signals will yield the following information:

1. Scatterer position relative to a zero reference (i.e., the leading edge of a range gate)
2. Scatterer Radar Cross Section
3. Scatterer type (odd or even bounce)

The real inverse Fourier Transform for linear polarized signals provides inter-scatterer spacing. The FFT (Fast Fourier Transform) algorithm is used in the simulation to generate all data records. To minimize processing time, 64 point FFT's are used exclusively. Higher order FFT's (128, 256, etc) have an advantage of integration gain which will improve the signal-to-noise ratio of the output. Noise is not modeled in this simulation so no real advantage is gained by use of higher order FFT's. Distance can be related to frequency on the FFT plot in the following manner:

$$f = kd$$

where

f = FFT line frequency

d = relative distance

$$k = \frac{2B}{c\Delta T}$$

where

$$C = 2.997 \times 10^8 \text{ m/sec}$$

B = frequency agile bandwidth

ΔT = sweep time (time to step through the agile bandwidth)

for a stepped system ΔT will have the form

$$\Delta T = (N-1) t$$

where

N = number of different frequencies

$$t = \frac{1}{\text{PRF}} \text{ (pulse repetition frequency)}$$

Solving for d :

$$d = \frac{C (N-1) f}{2B (\text{PRF})}$$

f = FFT line frequency

$$f = \frac{n f_s}{N}$$

where

f_s = sampling frequency

n = line number

N = number of points in FFT

f_s = PRF for a sample per pulse.

$$d = \frac{C (N-1) n}{2NB}$$

The amplitude of complex and real FFT lines are directly proportional to the RCS of the scatterer (or pairs of scatterers in the real case) that generated the line. Scatterer types can be determined by transmitting RHC, receiving RHC and LHC, and running complex FFT's on the result. The odd bounce scatterers will appear in the left hand FFT. The even bounce scatterers will appear in the right hand FFT. Reciprocity holds such that transmitting LHC will yield opposite results.

VIII. CONCLUSION

The algorithm described in this report provides a simple, cost effective method for polarimetric simulation that should appeal to resource limited organizations. This algorithm is intended only as a first order of model of a polarimetric radar. The radar range equation, noise simulation, doppler shift, rain, EMI, multipath, and hardware induced measurement errors are a few of the many parameters that should be incorporated into any radar model. The new generation of small computers should make it possible to add these important variables to the simulation without an intolerable increase in processing time. The HP9830 used for this simulation is not the optimum choice of computers. A machine with complex arithmetic could significantly decrease the processing time and is recommended.

The data presented clearly illustrates the potential for polarimetric radar. Definition of a feature space for target recognition might start with a ratio of odd-to-even bounce scattering centers. The distribution of scatterers, relative amplitude of returns, and phase information could all be exploited for target recognition. Ongoing work in the R.F. Guidance Technology branch includes:

1. Clutter modelling
2. Target modeling
3. Polarimetric measurements of targets and clutter

A more powerful FORTRAN simulation that includes most of the parameters enumerated above has been developed by this office. For further information contact F. W. Sedenguist, Autovon 746-7198.

APPENDIX A

PRECEDING PAGE

SIMULATION

Figure 8 is a flowchart of the simulation. Transmitted signals are assumed to have unity amplitude. The simulation was coded in BASIC and implemented on an HP9830 desk top calculator. The output matrix, K, contains all data generated by the algorithm. K is a 64 by 14 matrix. Plots of RHC, LHC, Horizontal, and Vertical were generated on standard plot routines (not shown).

DATA PRESENTATION

Two Reflectors

Figures 9 and 10 are complex FFT plots for a 100m^2 trihedral located at 2.950m and a 100m^2 dihedral located at 5.900m. The start frequency is 34.75 GHz with a 500 MHz bandwidth. The distances were carefully chosen to eliminate FFT sidelobes ($d = .2950\lambda$ for a 500 MHz bandwidth). The transmitted waveform was RHC. The trihedral alone is seen in the complex LHC plot, and the dihedral alone in the complex RHC plot. The antenna coupling factor was 100 dB (equivalent to a near perfect antenna) for all plots in this section. The dihedral was rotated 45° . The D.C. component is not included on any plots. All plots are normalized to the highest A.C. component.

Figures 11 and 12 are complex FFT's of the linear signals (H and V) both reflectors show up in these plots.

Figures 13 and 14 are real linear FFT's. The inter-reflector spacing is found on these plots (along with the image always present in Real FFT's). A brief summary of FFT information content is presented below:

FFT TYPE

1. Complex Circular - Scatter size, location, and type.
2. Complex Linear - Scatter size and location.
3. Real Linear - Inter-scatterer spacing for all reflectors.
Number of combinations are:

$$\sum_{i=1}^{N_T} (N_T - i)$$

where N_T = total number of reflectors.

4. Real circular - Spacing for pairs of like reflectors. The number of combinations are:

$$\sum_{i=1}^{N_L} (N_L - i)$$

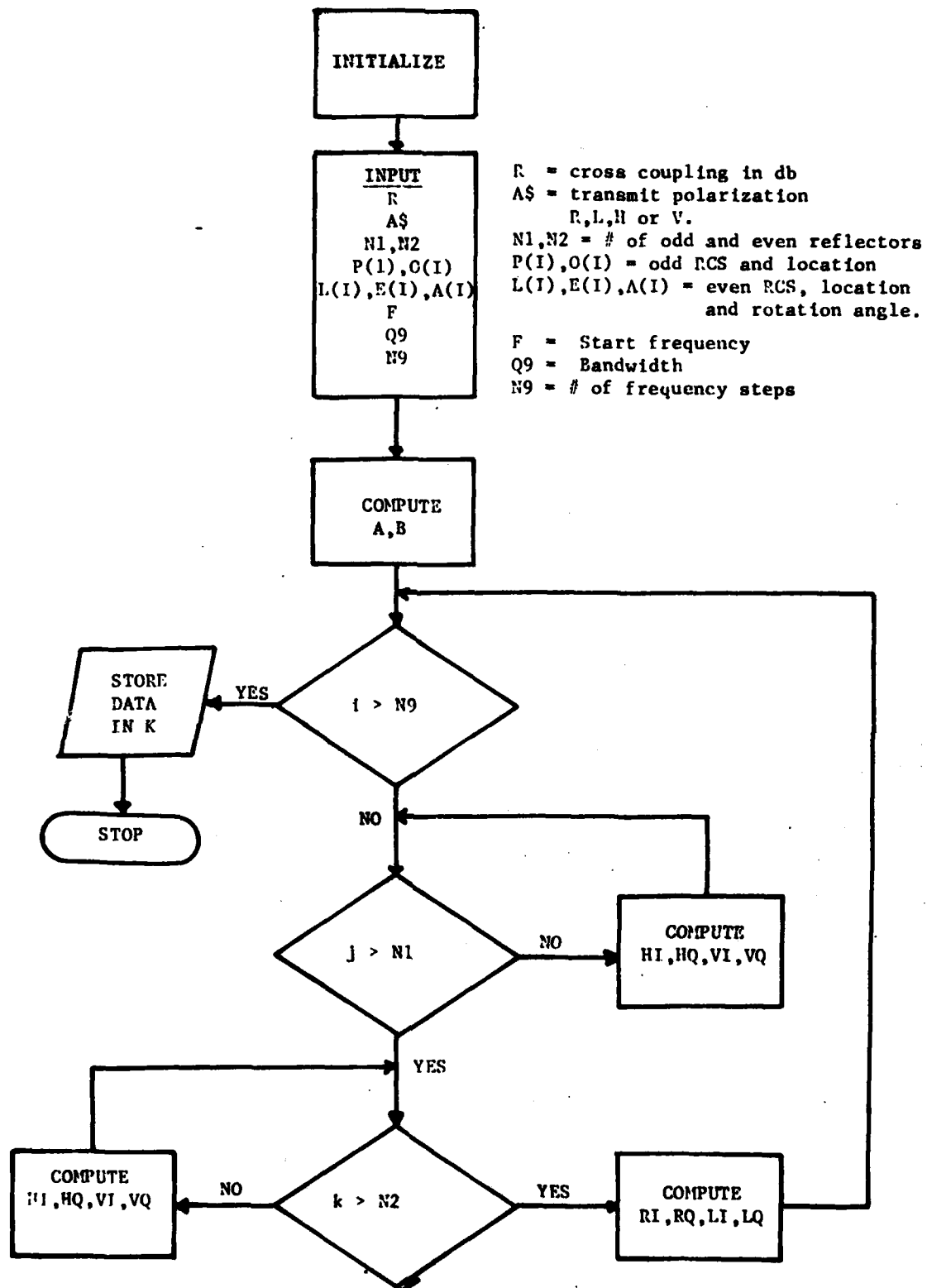


Figure 8. Simulation flowchart.

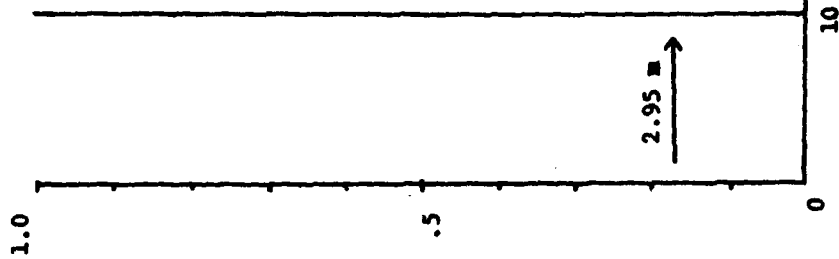


Figure 9. Complex LHC FFT for 100 m^2 trihedral at 2.95 m and 100 m^2 dihedral at 5.90 m. EHC transmit, 500 MHz bandwidth antenna cross coupling 100 db.

64

A
M
P
L
I
T
U
D
E

(Normalized)

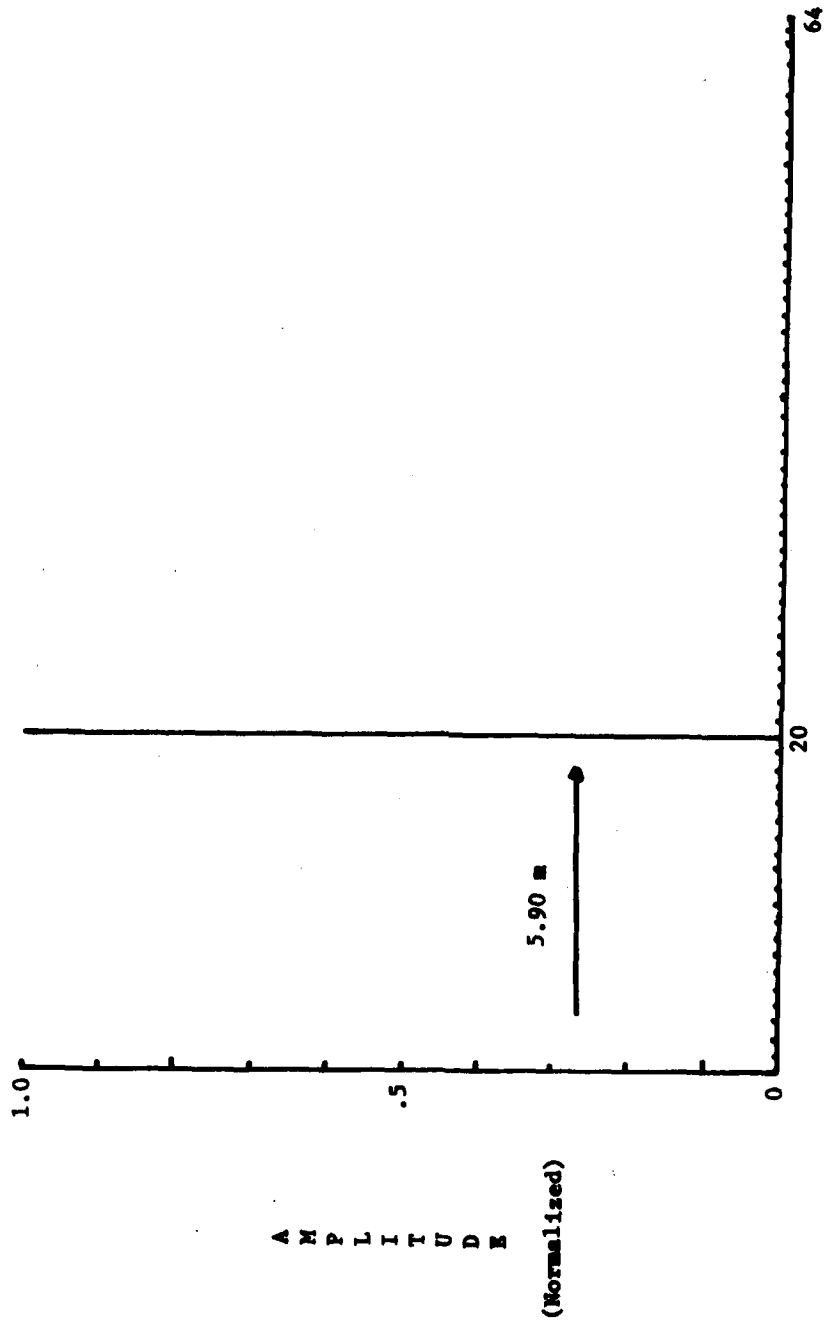
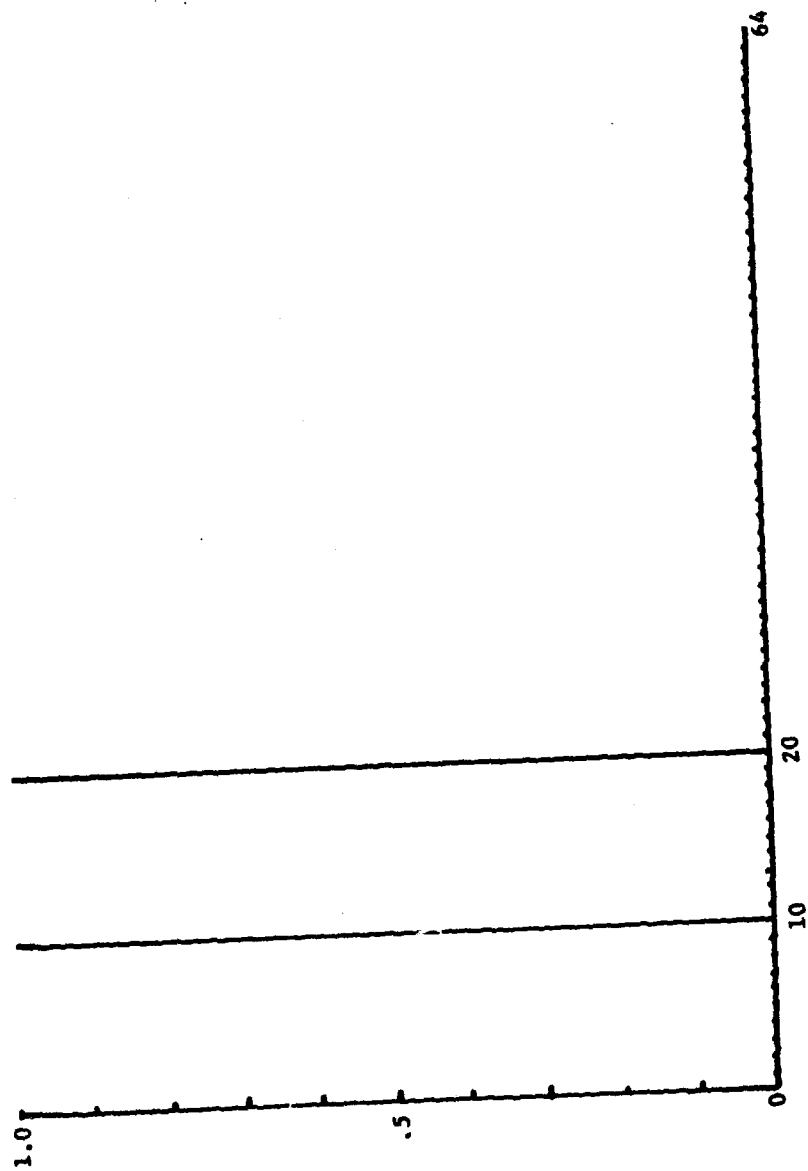


Figure 10. Complex RHC FFT for 100m^2 trihedral at 2.95m and 100m^2 dihedral at 5.90m. RHC transmit, 500 MHz bandwidth antenna cross coupling 100 db.



AMPLITUDE
(Normalized)

Figure 11. Complex horizontal FFT for 100m² trihedral and 100m² dihedral at 2.95m and 5.90m.

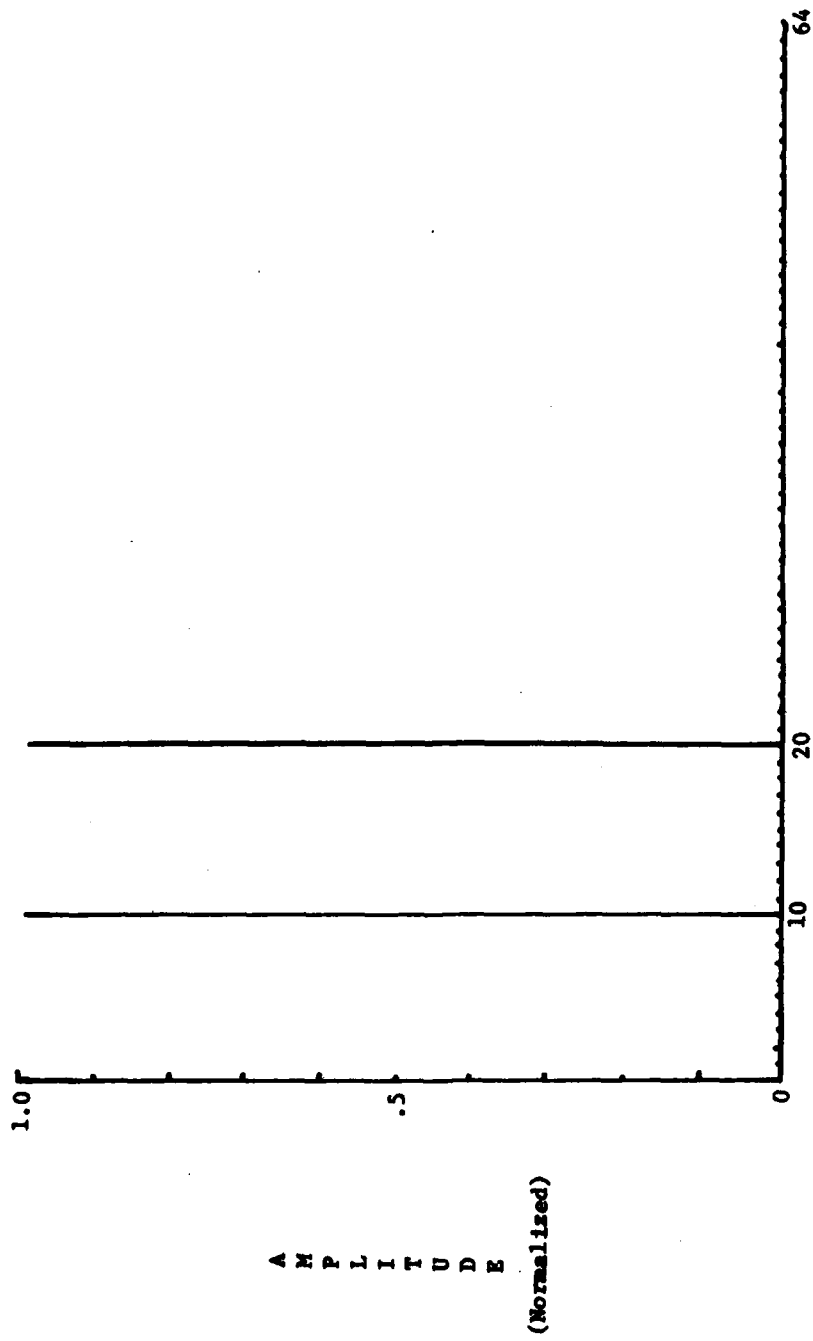


Figure 12. Complex vertical FFT for 100m^2 trihedral and 100m^2 dihedral at 2.95m and 5.90m.

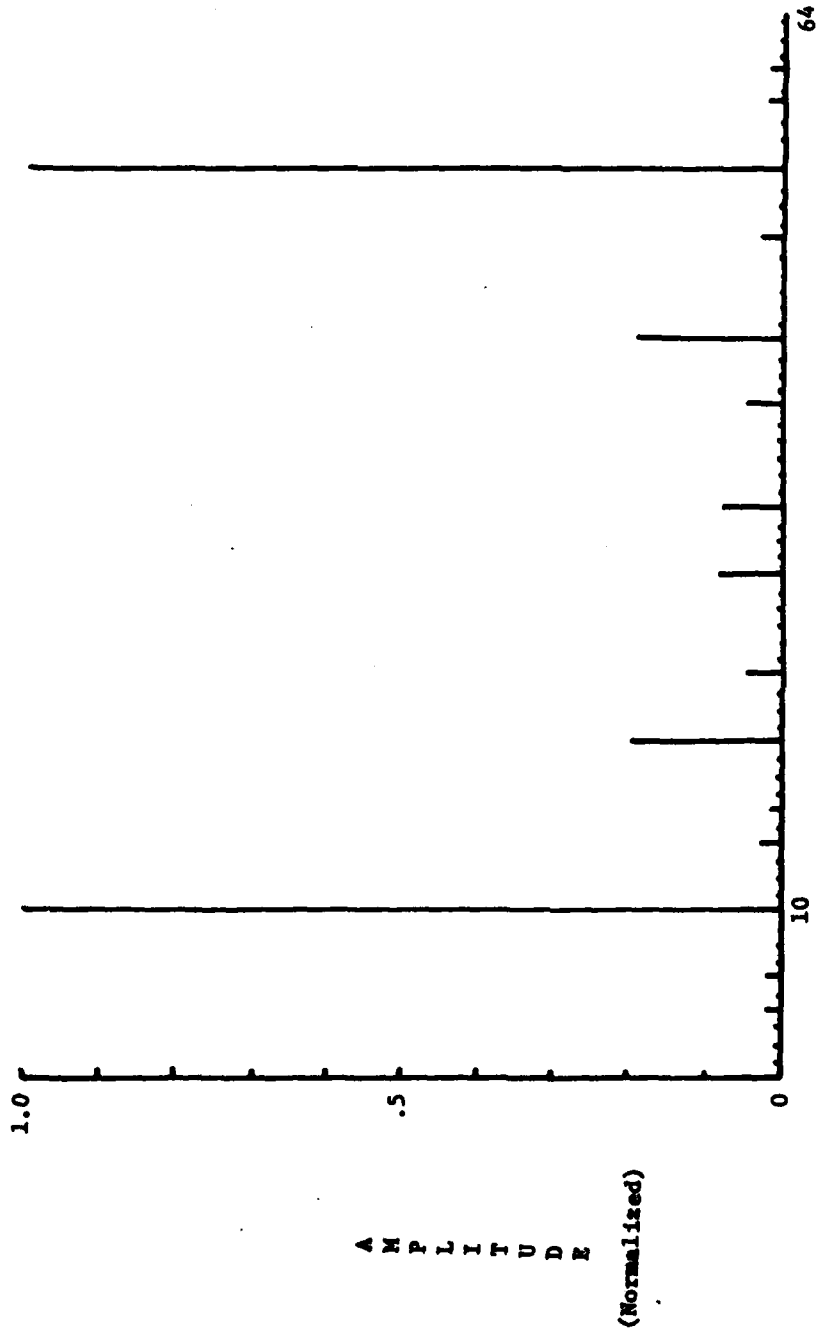
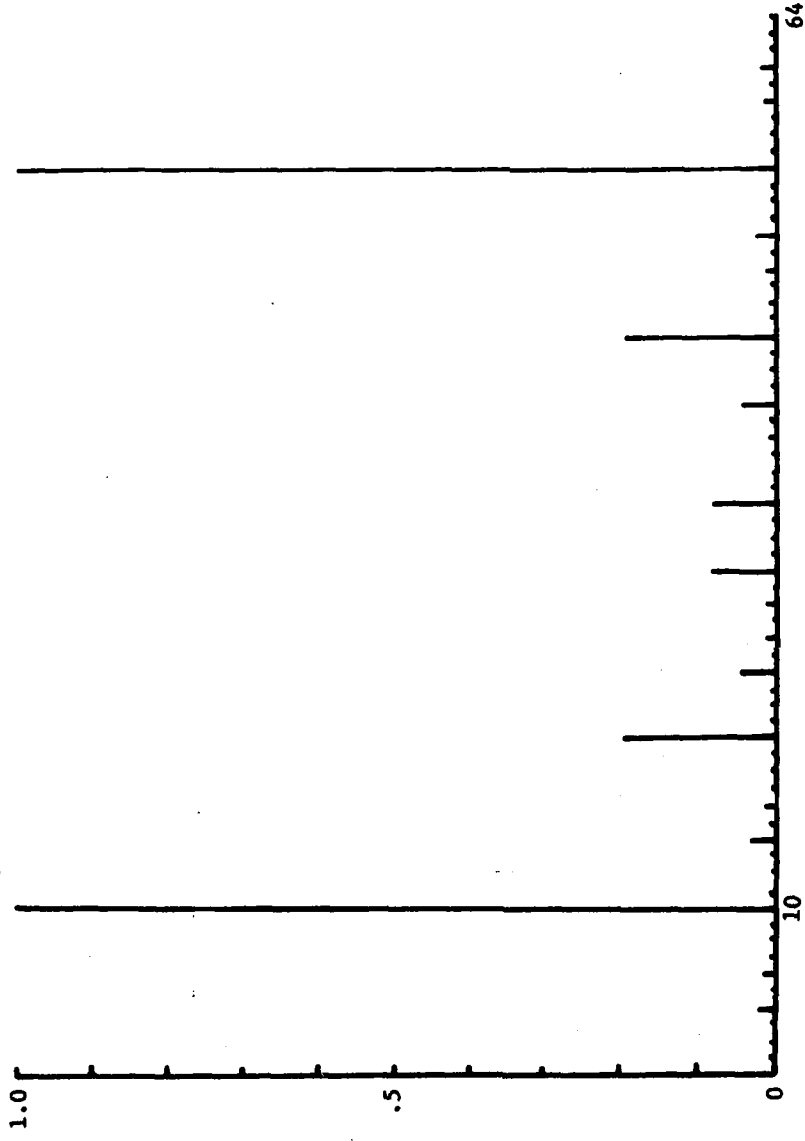


Figure 13. Real FFT of horizontal return for 100m² trihedral at 2.95m and 100m² dihedral at 5.9m.

$$H = \sqrt{HI^2 + HQ^2}$$



A M P L I T U D E

(Normalized)

Figure 14. Real FFT of vertical return for 100m² trihedral at 2.95m and 100m² dihedral at 5.90m.

$$V = \sqrt{VI^2 + VQ^2}$$

where N_L = number of like reflectors.

Figures 15 through 20 are the same 100m^2 reflectors displaced so the response is between filter bins on the FFT. The sidelobe structure is now very evident. Figure 21 is a complex horizontal FFT where the dihedral RCS has been reduced to 50m^2 . The remaining plots are described by their respective captions. In sections to follow only FFT plots will be presented.

Four Reflectors

Figures 31 through 38 are for the 4 reflector array illustrated in Figure 30. All reflectors are 100m^2 . The frequency was stepped from 34.75 GHz to 35.25 GHz in 64 steps. RHC was transmitted. Antenna cross coupling was 100 dB.

Four Reflectors With Variable Antenna Cross Coupling

Figures 39 through 54 are complex FFT plots for the same 4 reflector array seen in the previous data section. Antenna cross coupling is varied from 50 to 3 dB.

As the cross coupling coefficient decreases, the odd bounce reflectors begin to appear in the even bounce FFT and the even bounce reflectors in the odd bounce FFT. The relative amplitude of the lines on the linear FFT plots fluctuates as a function of cross coupling. The need for a good antenna is evident from these plots.

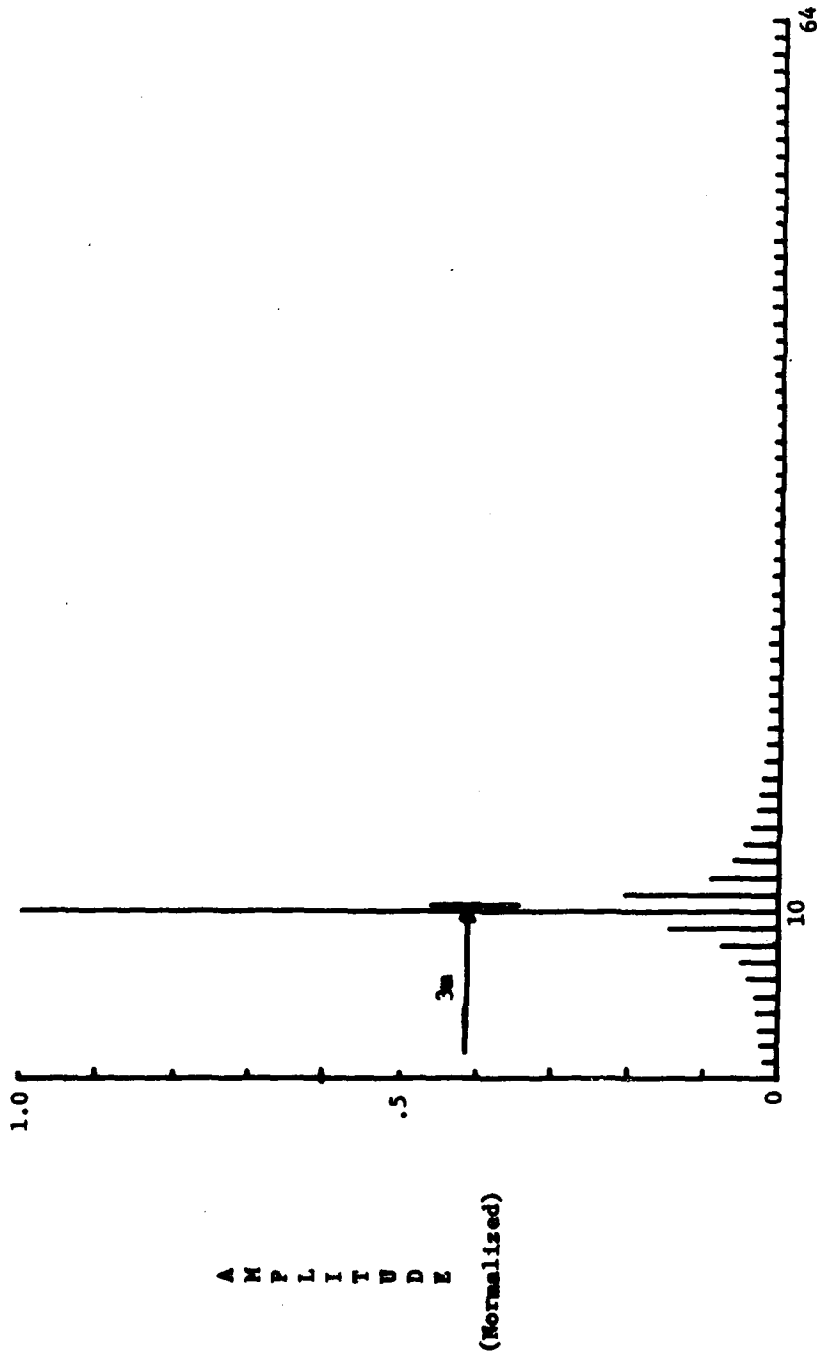


Figure 15. Complex LHC FFT for 100m^2 trihedral at 3m and 100m^2 dihedral at 6m.

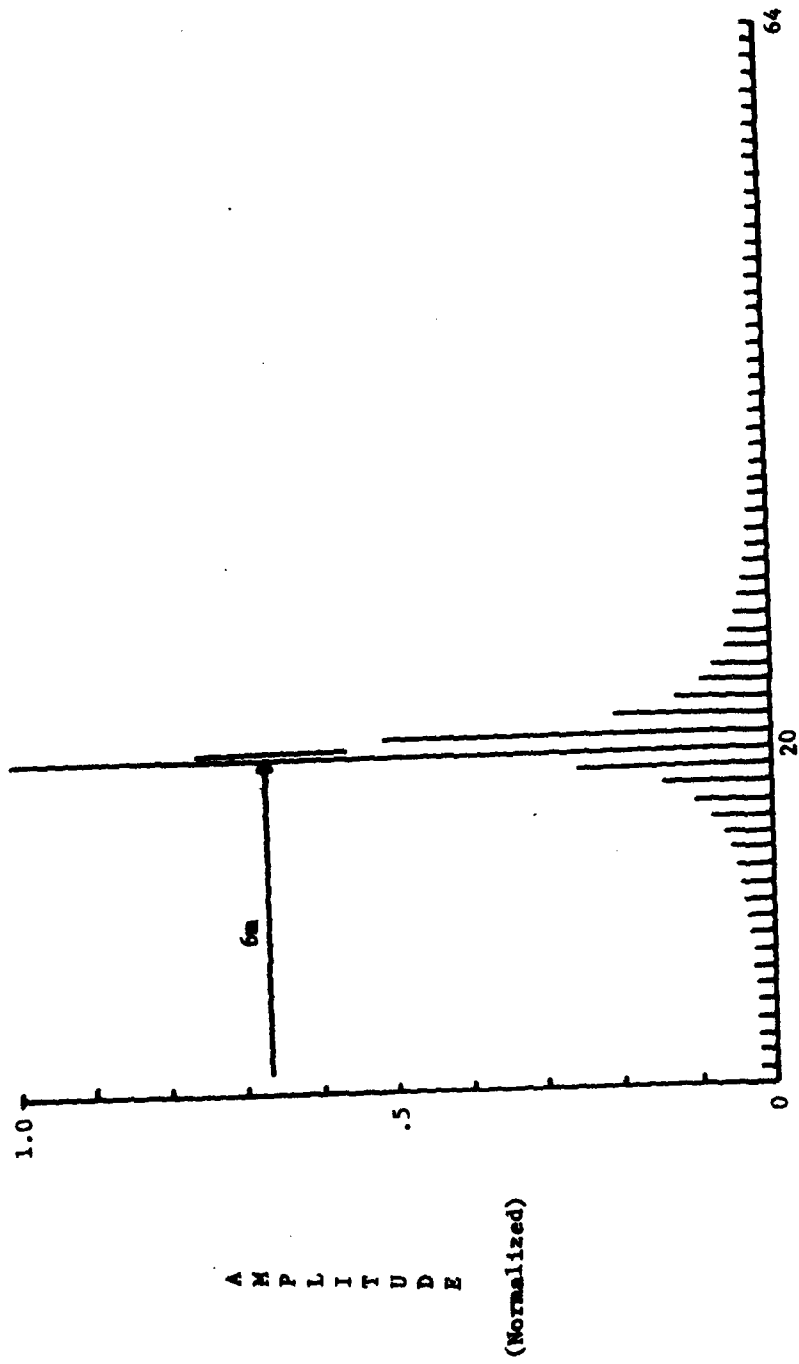


Figure 16. Complex RHC PFI for 100m² trihedral at 3m and 100m² at 6m.

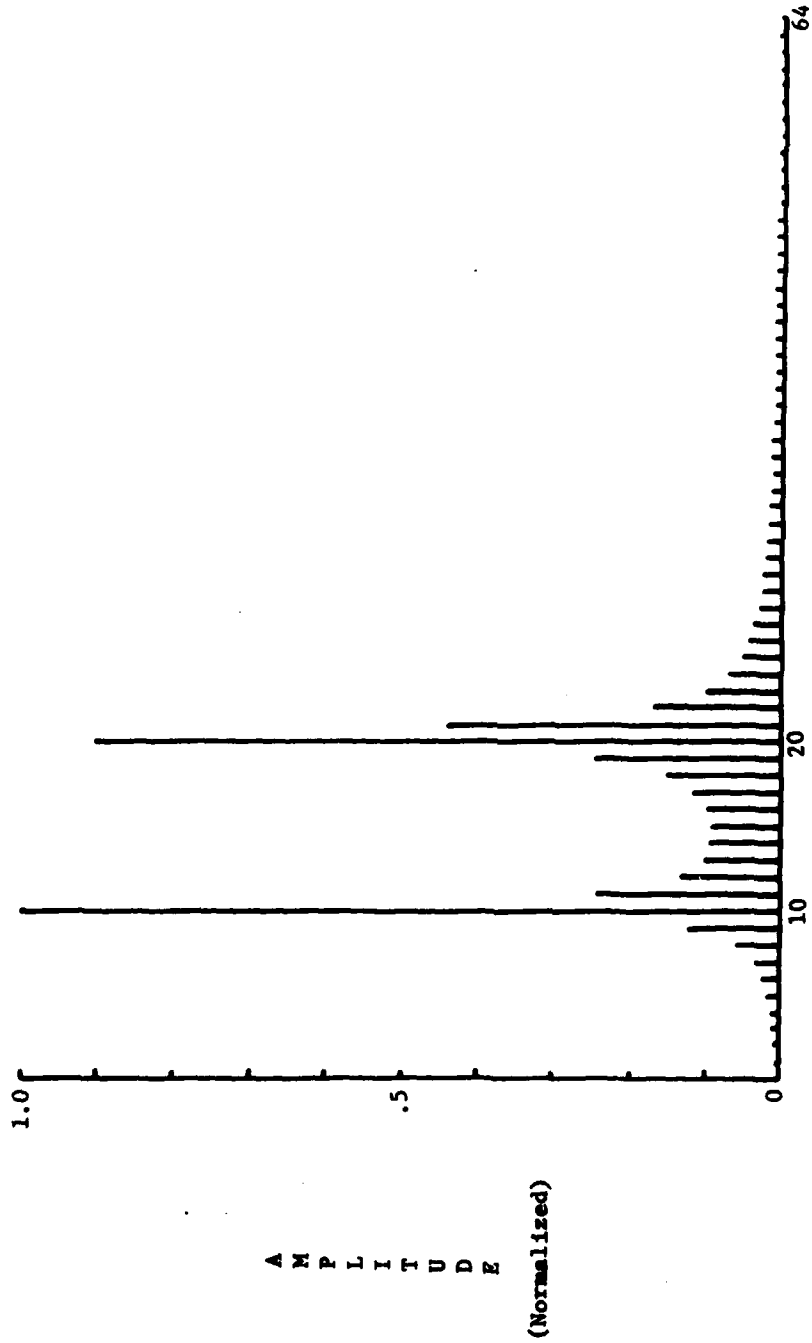


Figure 17. Complex horizontal FFT for 100m² trihedral at 3m and 100m² dihedral at 6m.

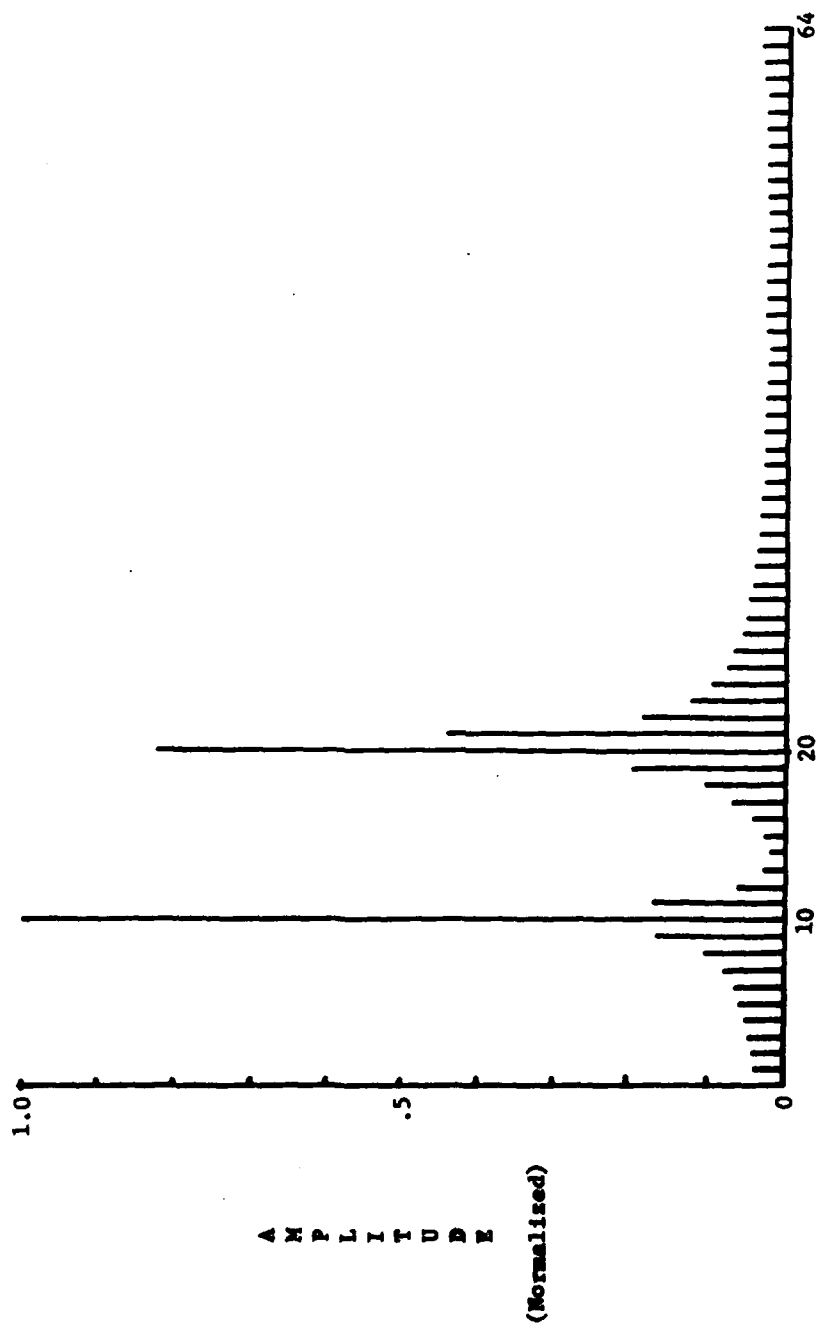


Figure 18. Complex vertical FFT for 100 m² trihedral at 3m and 100 m² dihedral at 6m.

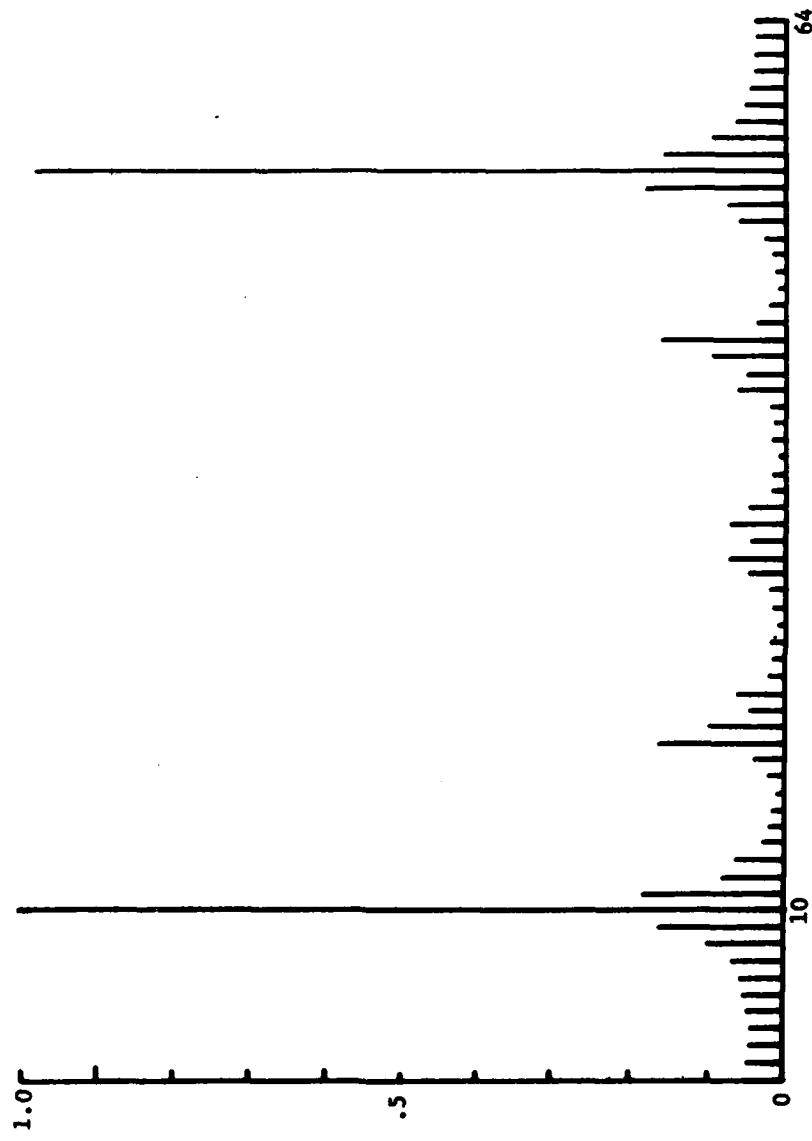


Figure 19. Real horizontal FFT for 100 m² trihedral 3 m and 100 m² dihedral at 6 m.

AMPLITUDE
(Normalised)

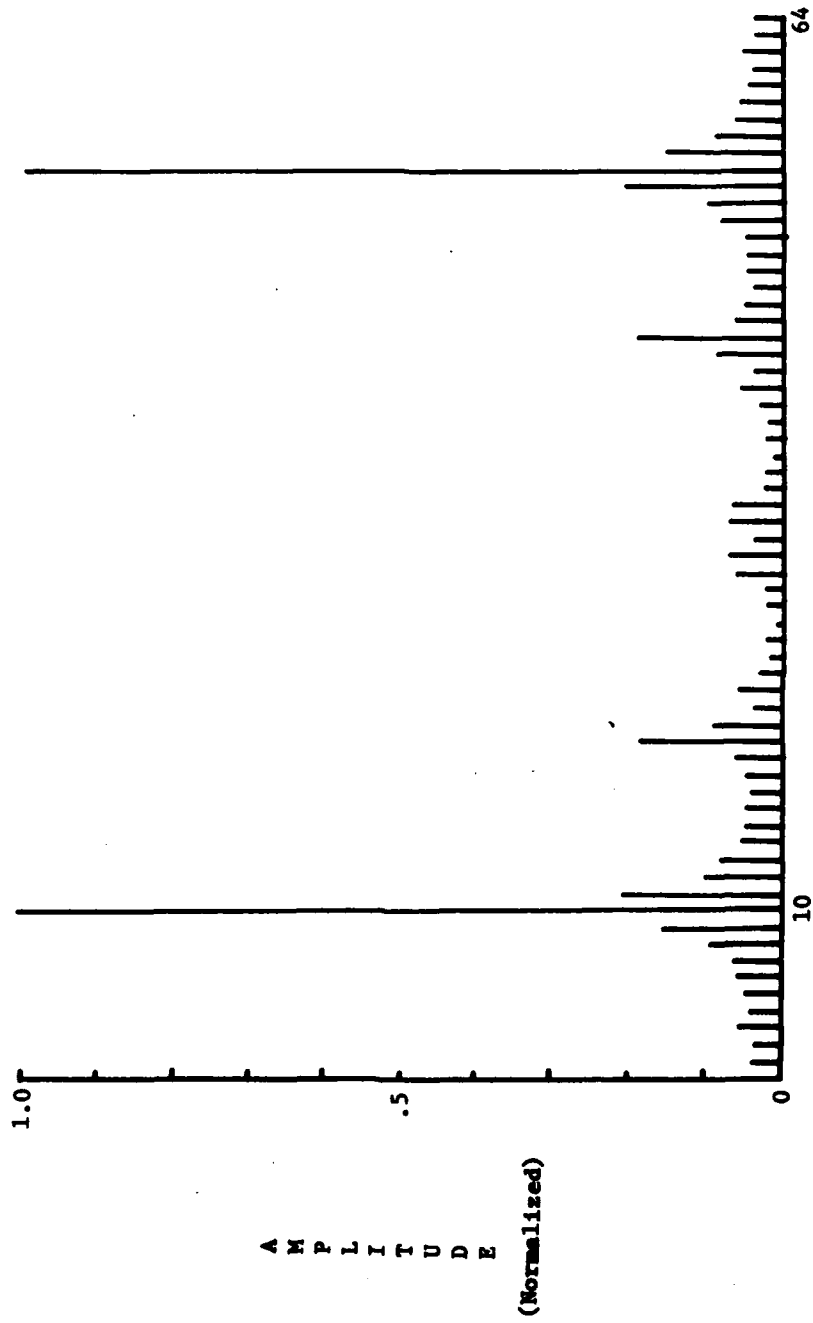


Figure 20. Real vertical FFT for 100 m² trihedral at 3 m and 100 m² dihedral at 6 m.

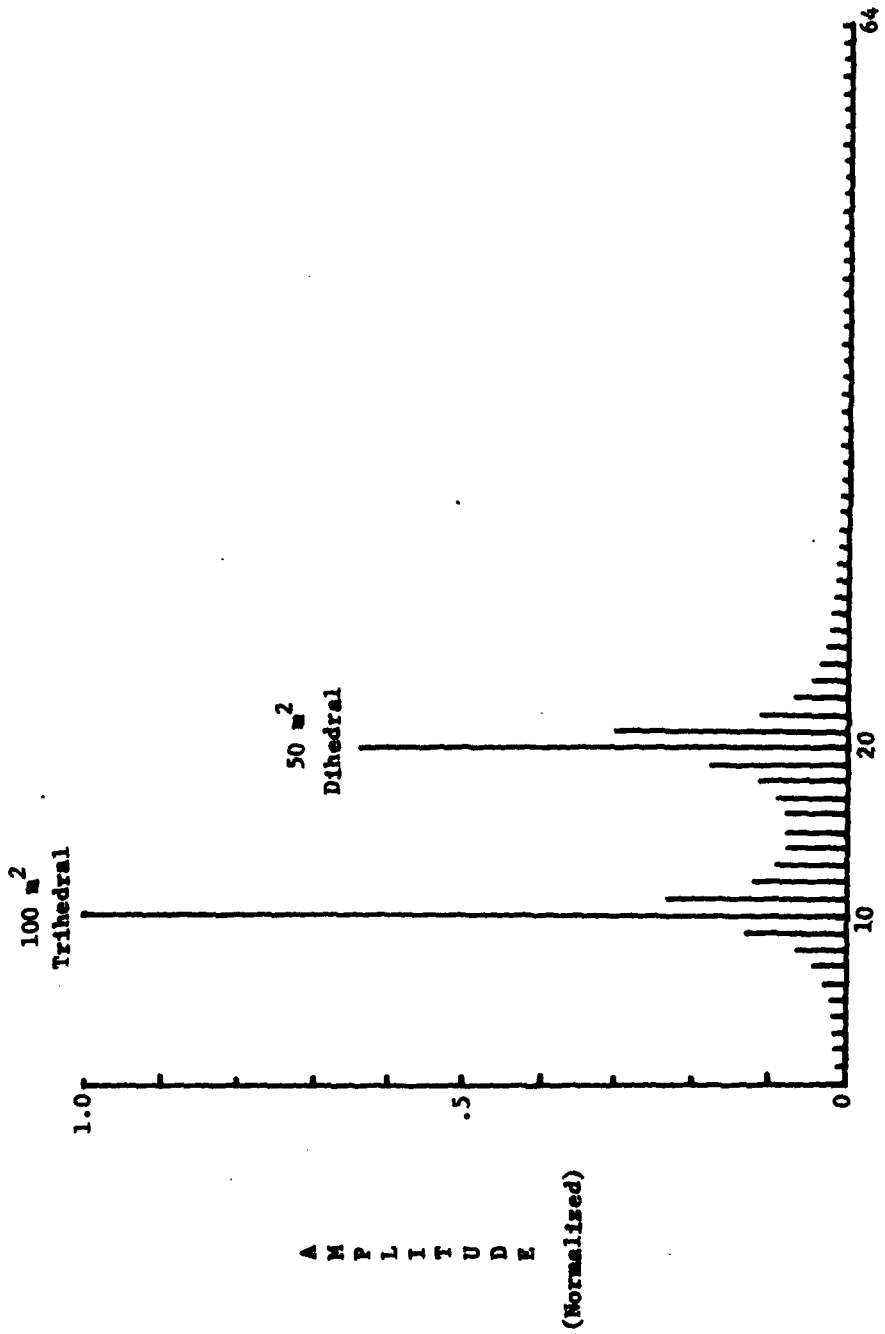


Figure 21. Real horizontal FFT for 100 m² trihedral at 3 m and 50 m² dihedral at 6 m.

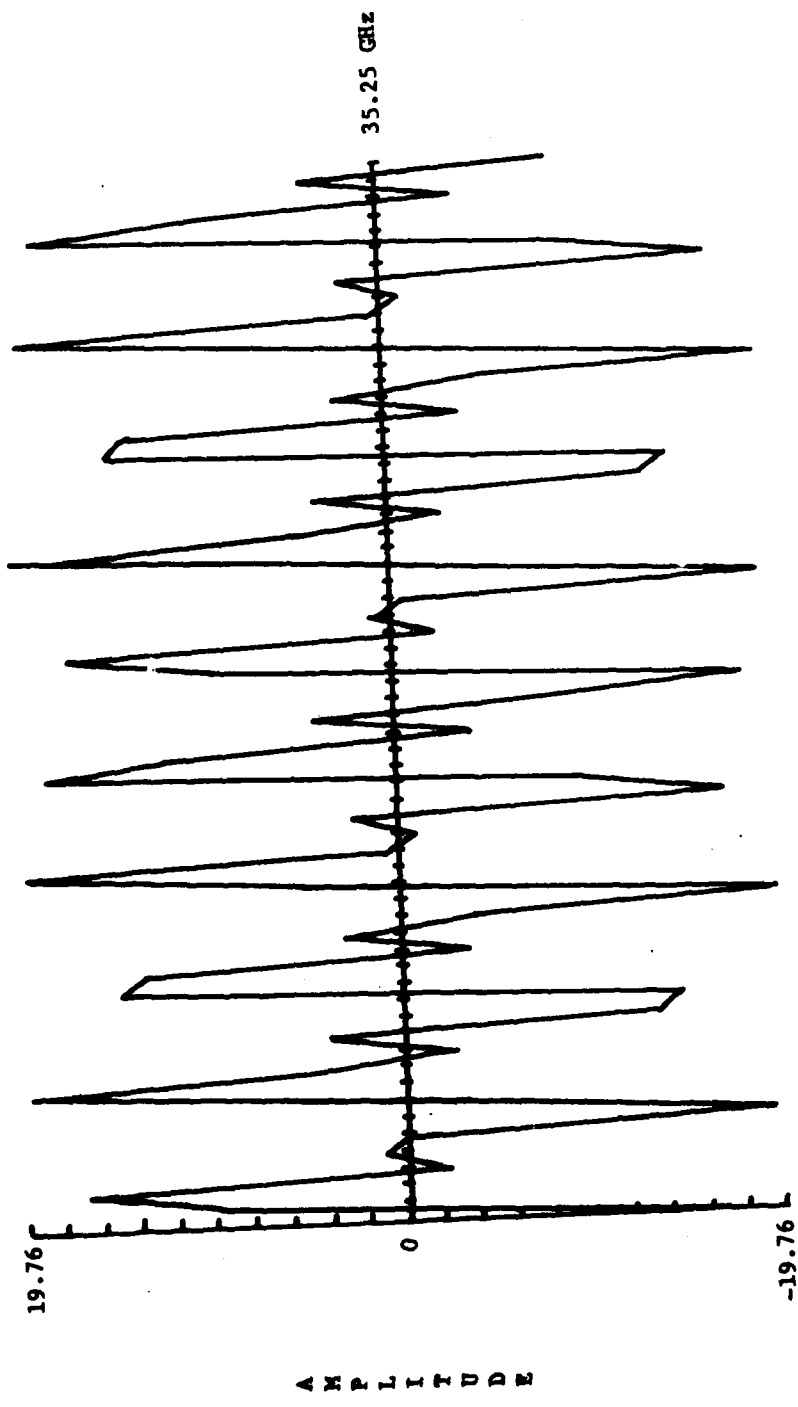


Figure 22. Horizontal in phase for 100 m² trihedral and 100 m² dihedral at 2.75 m and 5.90 m as a function of frequency (34.75 GHz to 35.25 GHz).

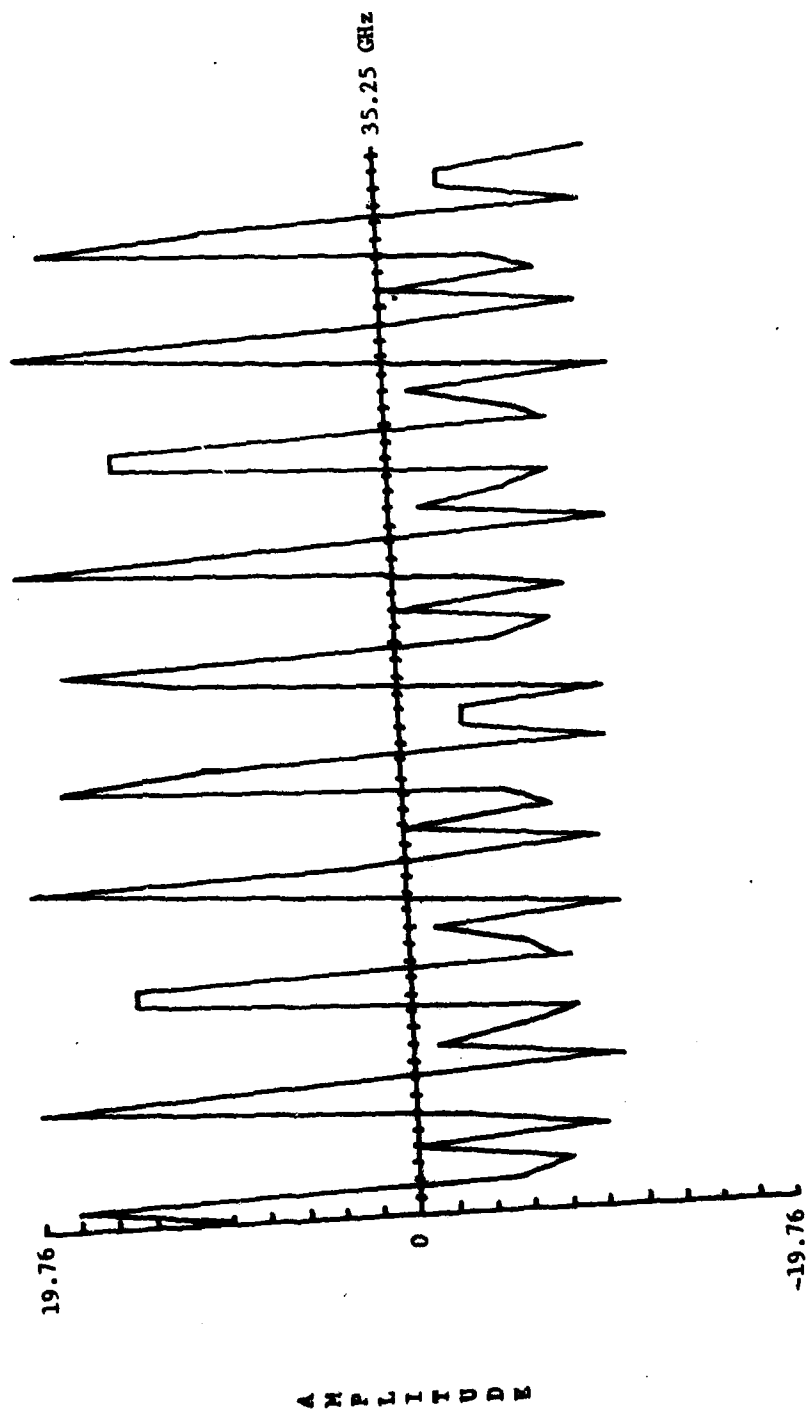


Figure 23. Horizontal quadrature for 100 m^2 trihedral and 100 m^2 dihedral at 2.95 m and 5.90 m as a function of frequency (34.75 GHz to 35.25 GHz).

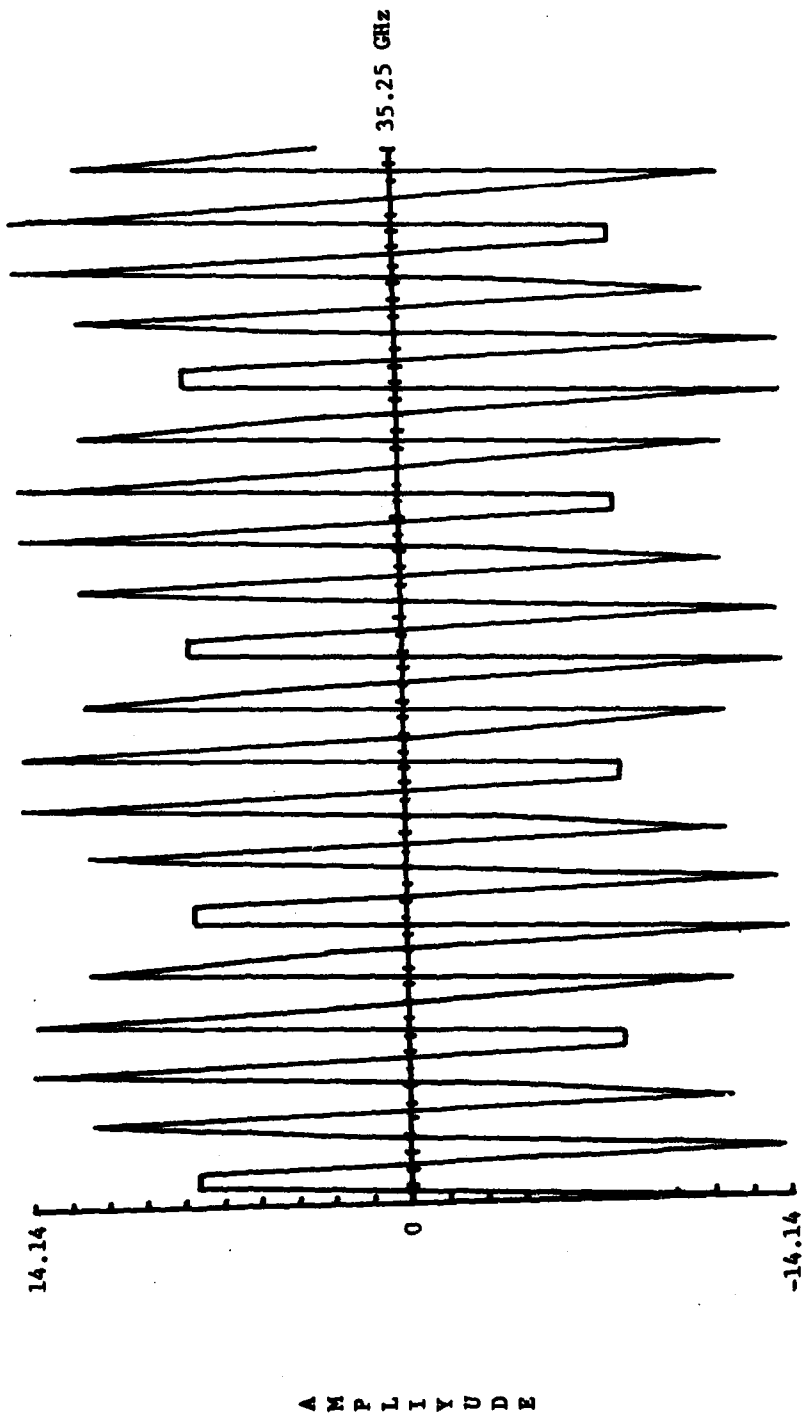


Figure 24. RHC in phase for 100 m^2 trihedral, 100 m^2 dihedral.

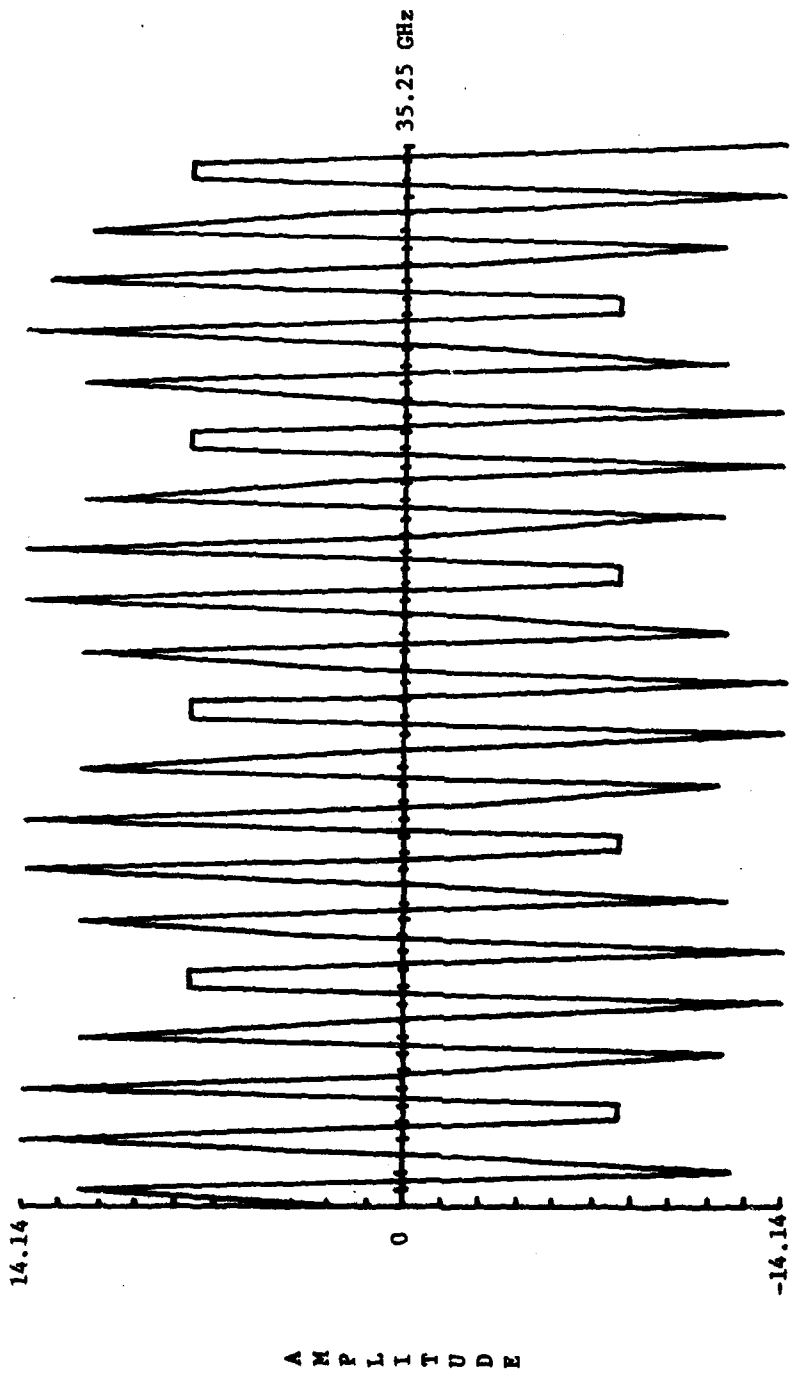


Figure 25. MHC quadrature for 100 m² trihedral, 100 m² dihedral.

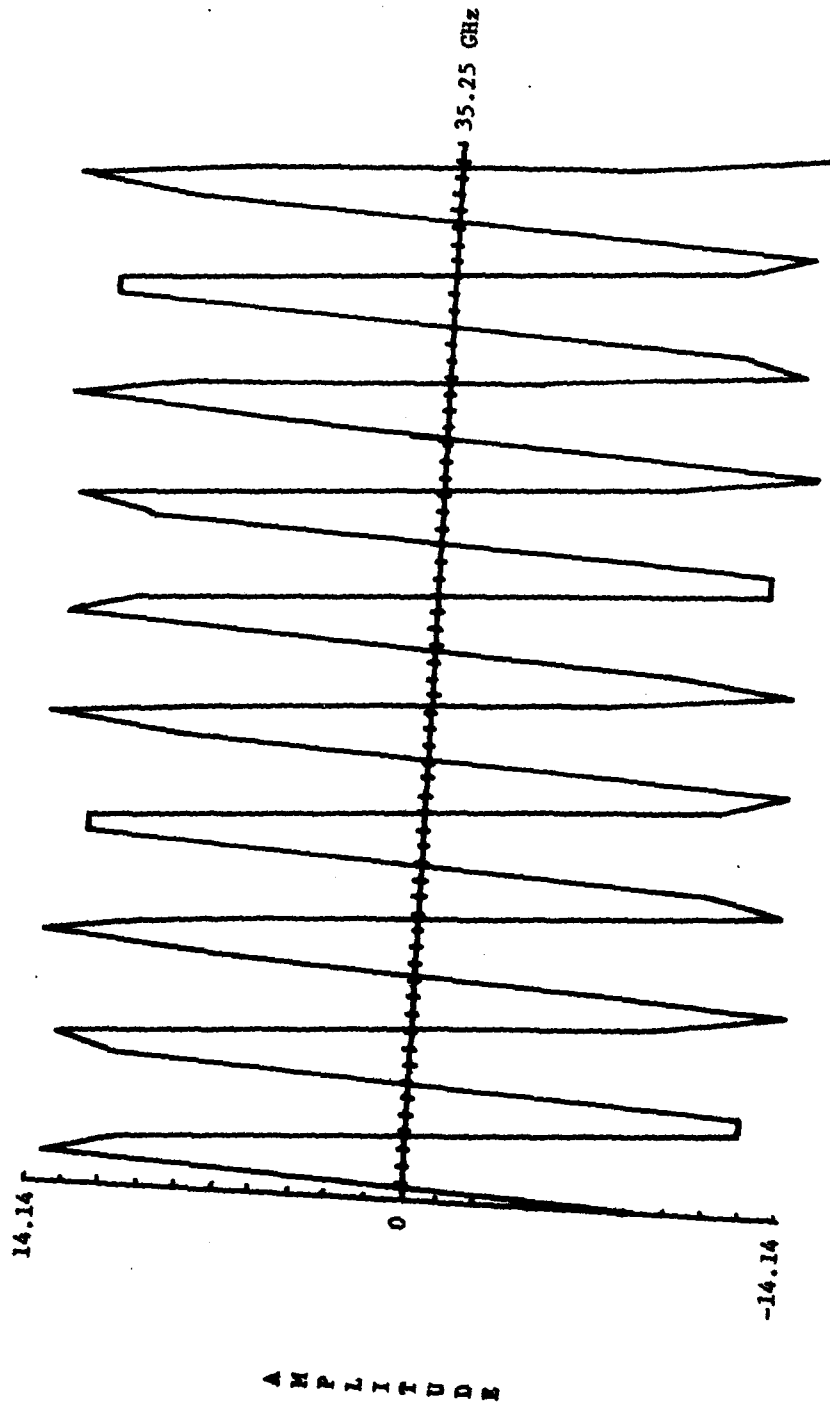


Figure 26. LHC in phase for 100 m² trihedral, 100 m² dihedral.

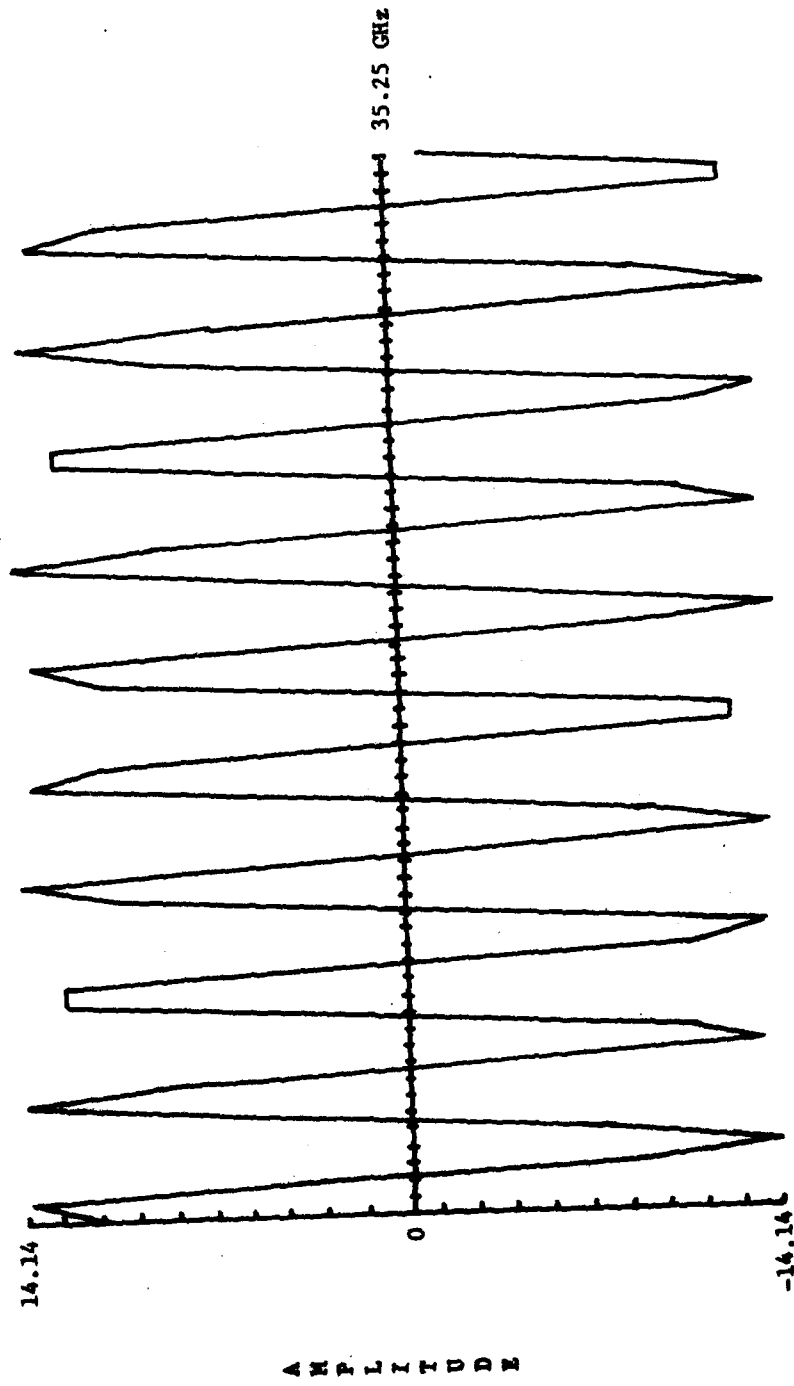


Figure 27. LHC quadrature for 100 m² trihedral 100 m² dihedral.

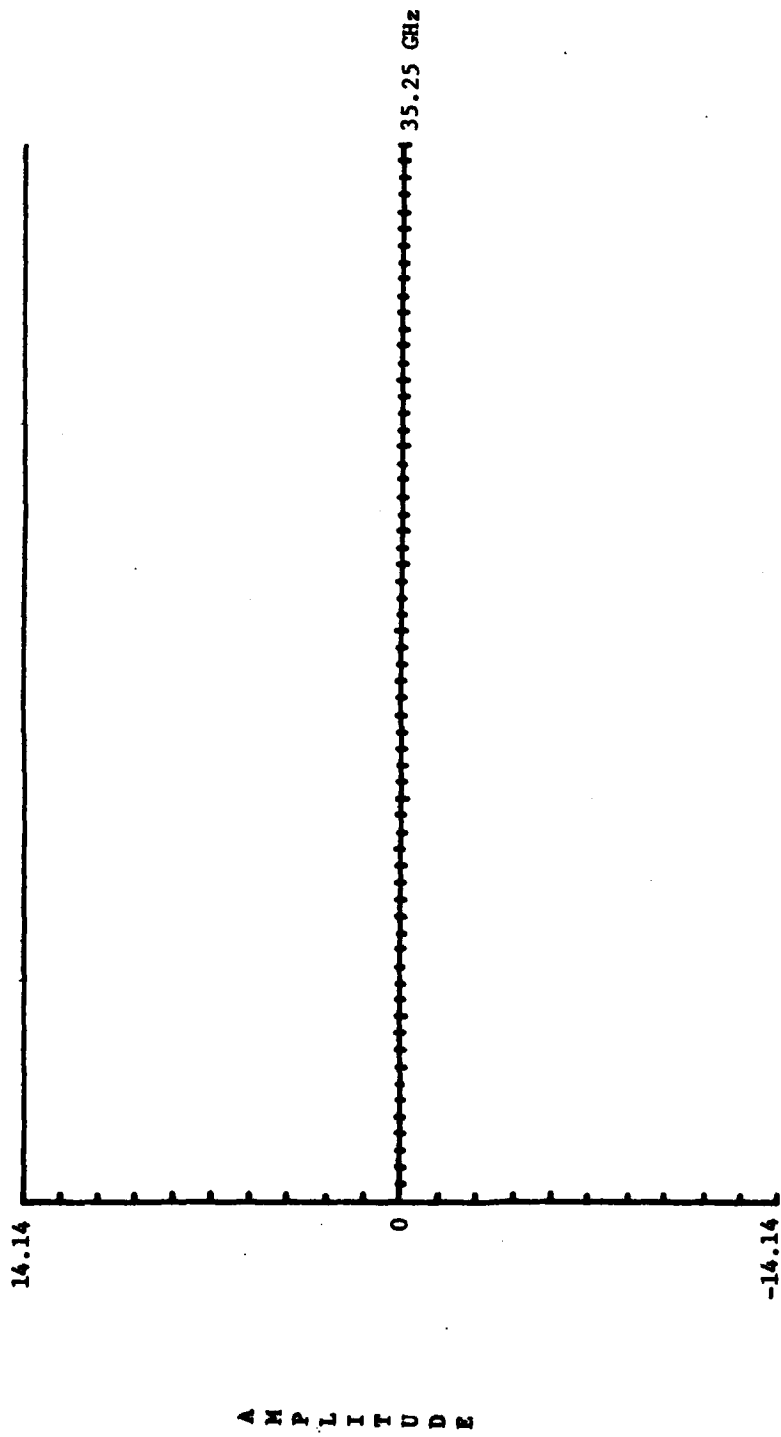


Figure 28. EHC return for 100 m² trihedral and 100 m² dihedral as a function of frequency.

$$\text{EHC} = \sqrt{R_1^2 + R_2^2}$$

f = 34.75 GHz to 35.25 GHz
64 steps

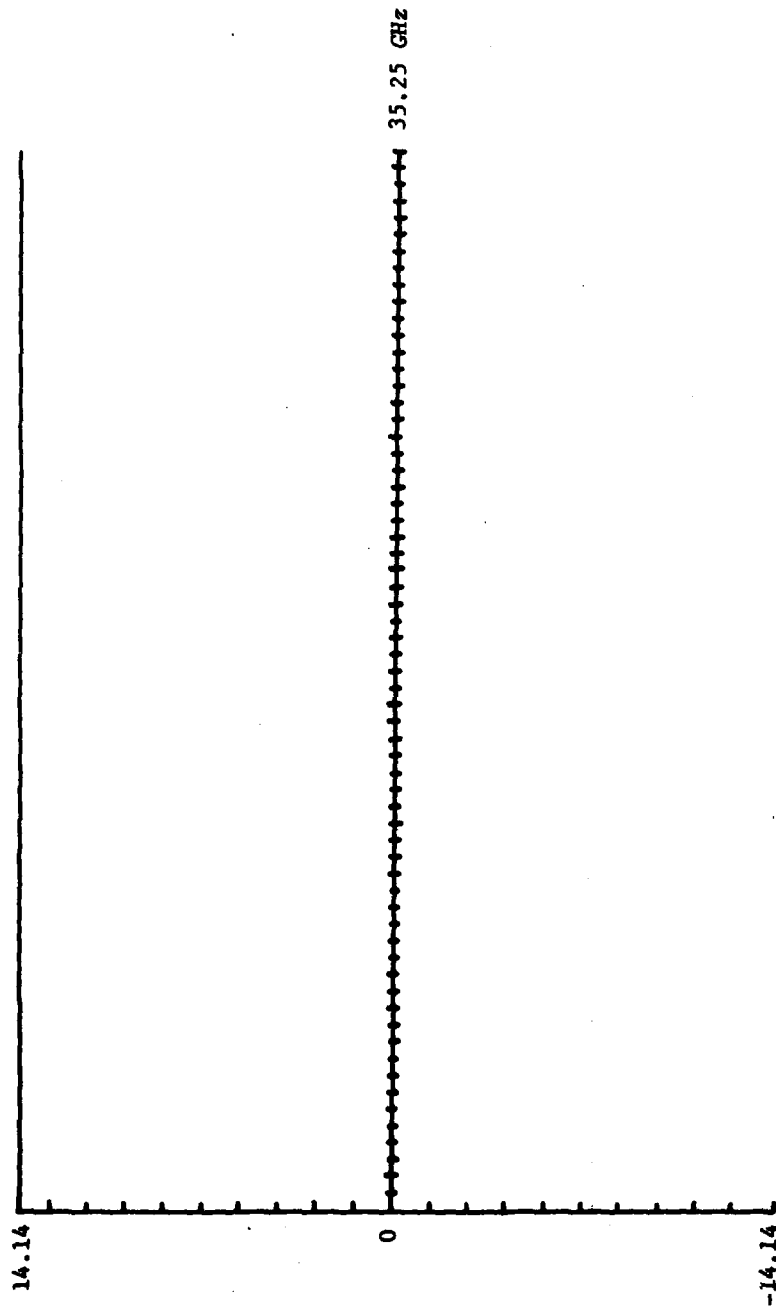


Figure 29. LHC return for 100 m² trihedral and 100 m² dihedral as a function of frequency

$$\text{LHC} = \sqrt{L1^2 + LQ^2}$$

f = 34.75 GHz to 35.25 GHz
64 steps

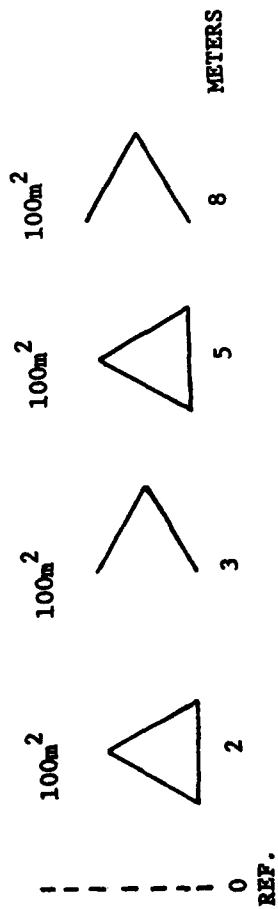


Figure 30. Four reflector array.

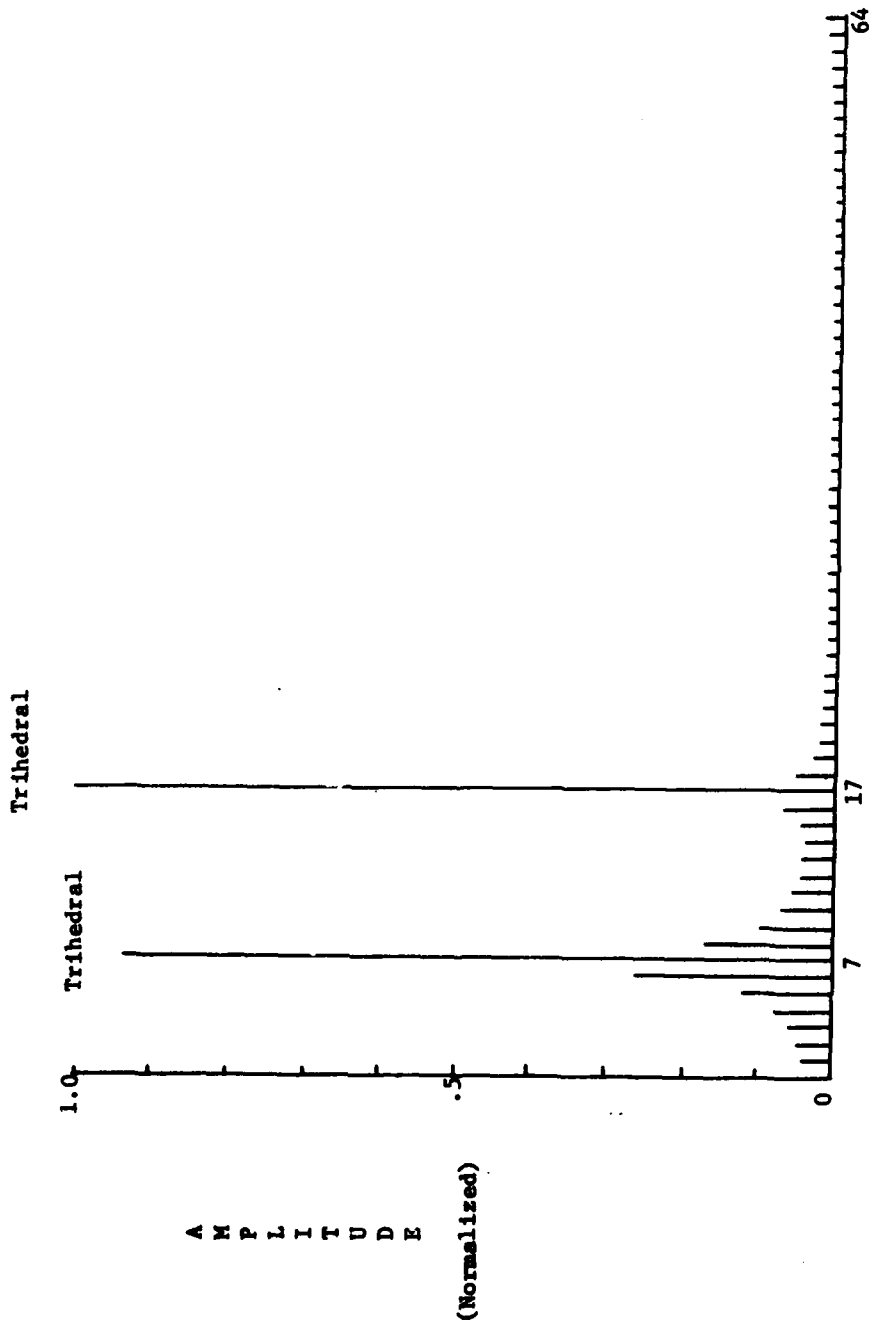


Figure 31. Complex LHC FFT for 100 m² trihedral @ 2m, 100 m² dihedral @ 5m, 100 m² trihedral @ 3m, and a 100 m² dihedral @ 8m.
Bandwidth = 500 MHz (d = .295 n), 34.75 GHz to 35.25 GHz.

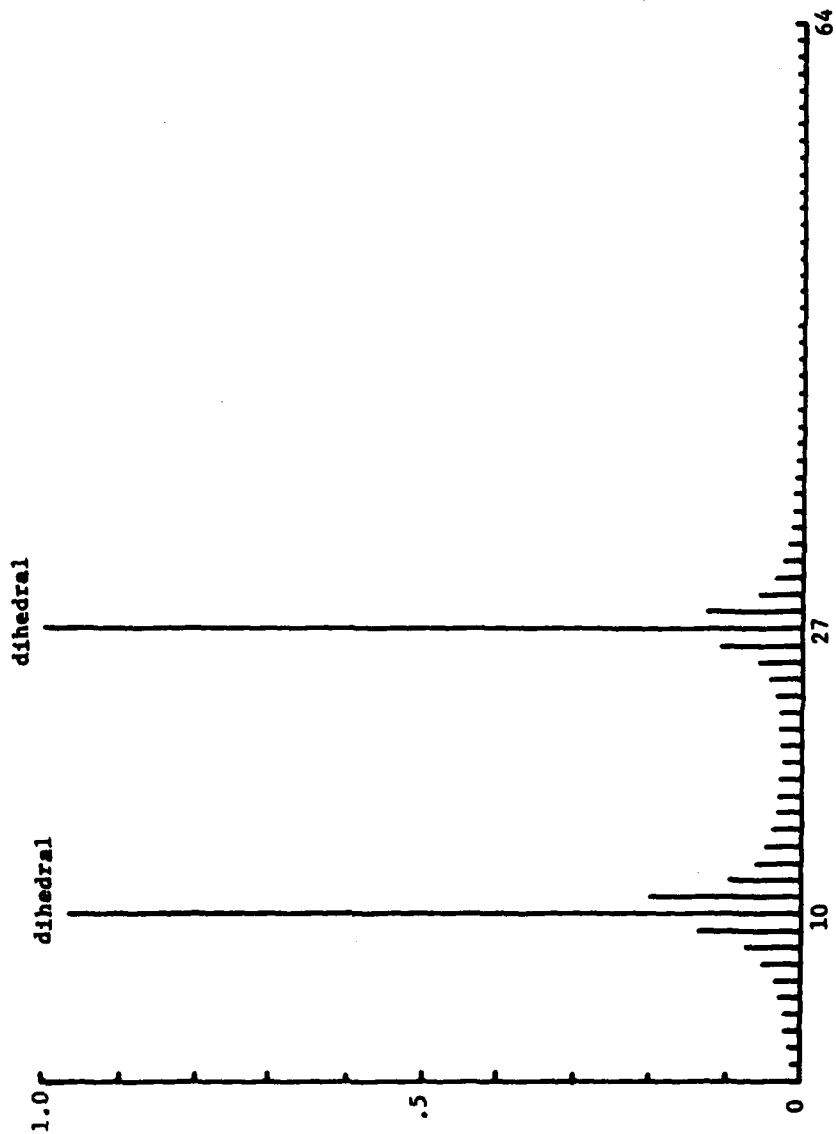


Figure 32. Complex RHC FFT for 4 reflector array.

A M P L I T U D E

(Normalized)

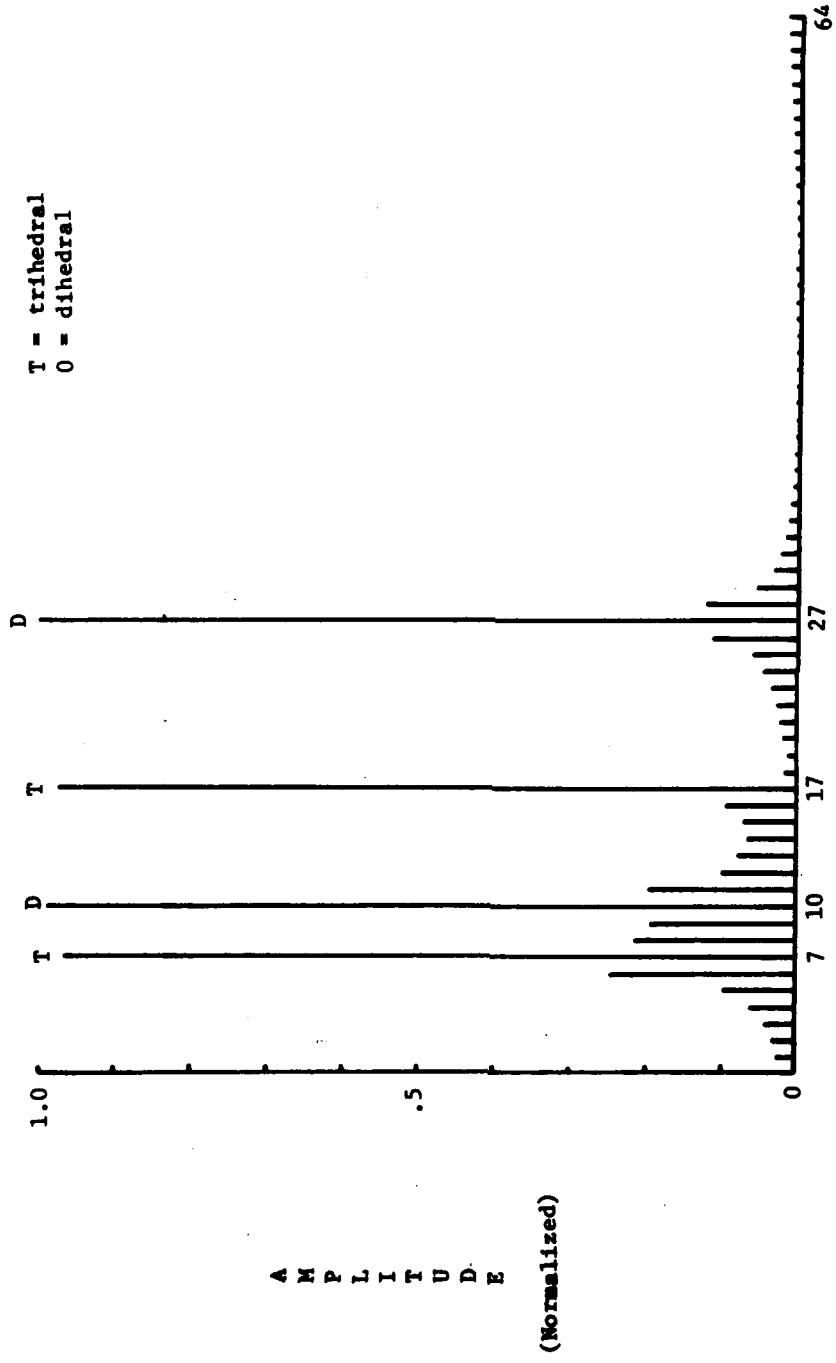


Figure 33. Complex horizontal FFT for 4 reflector array.

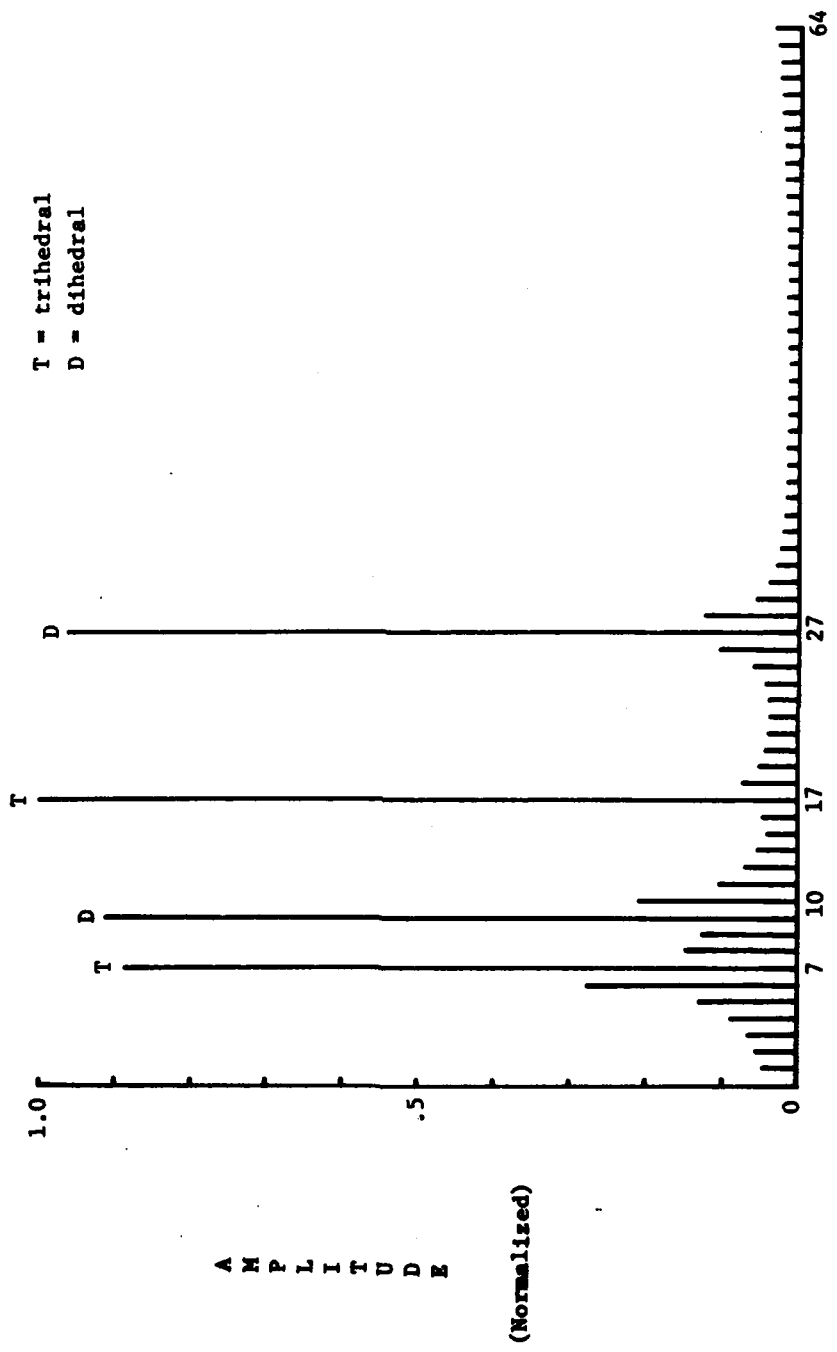


Figure 34. Complex vertical FFT for 4 reflector array.

$$\sum_{i=1}^{N_T} (N_T - i) = 6$$

$N_T = 4$ reflectors

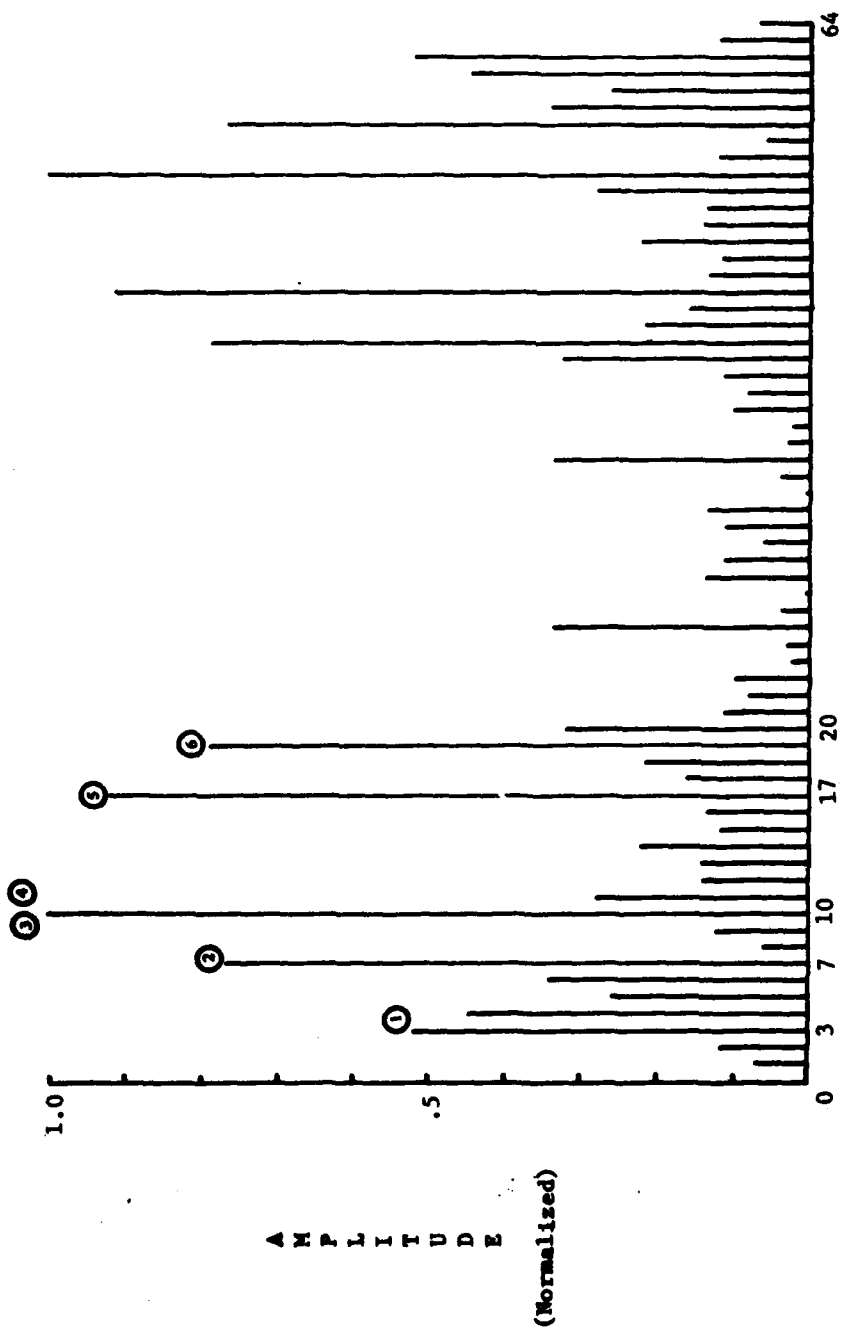


Figure 35. Real horizontal FFT for 4 reflector array.

$N_T = 4$ reflectors

$$\sum_{i=1}^{N_T} (N_T - i) = 6$$

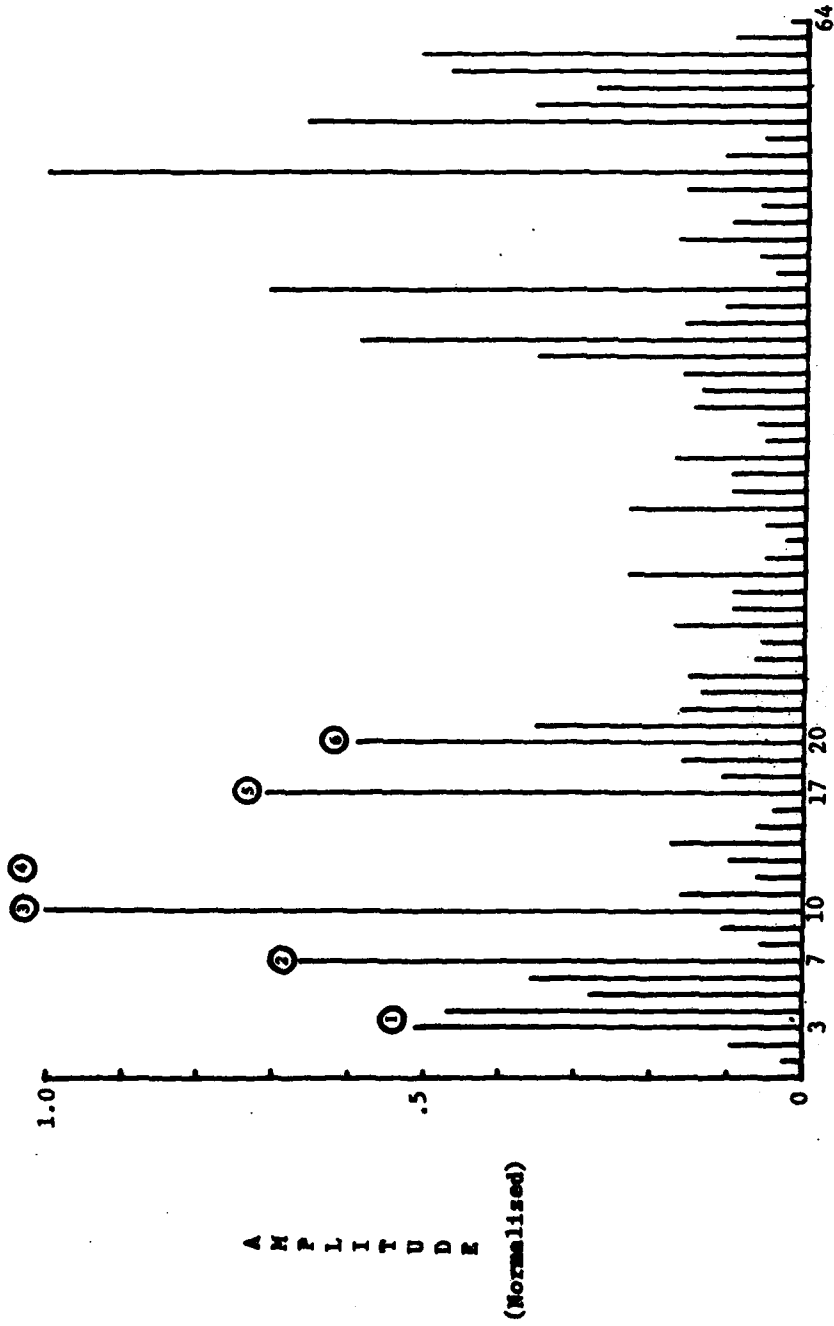


Figure 36. Real vertical FFT for 4 reflector array.

$$\sum_{i=1}^{N_L} (N_L - i) = 1$$

$N_L = 2$ dihedrals

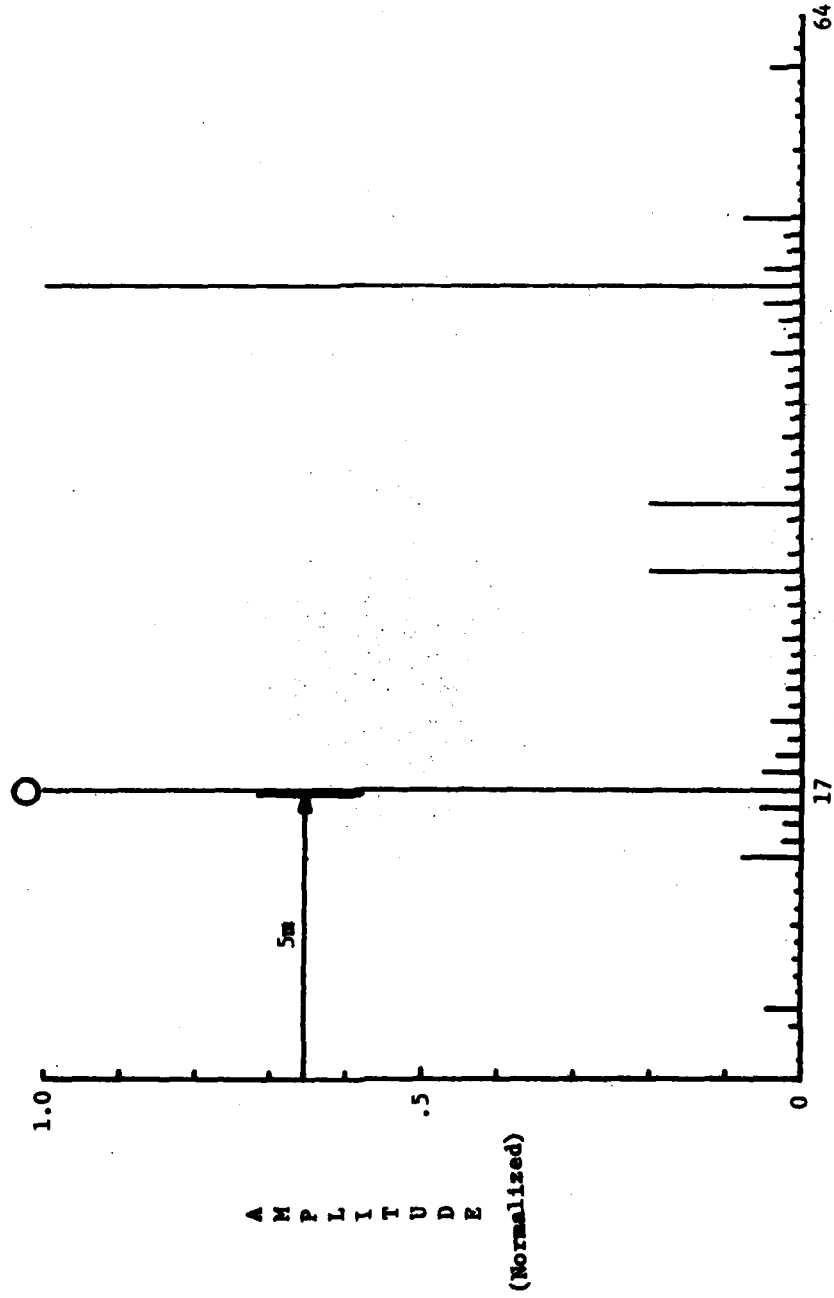


Figure 37. Real RHC FFT for 4 reflector array.

$$\sum_{i=1}^{N_L} (N_L - i) = 1$$

$N_L = 2$ trihedrals

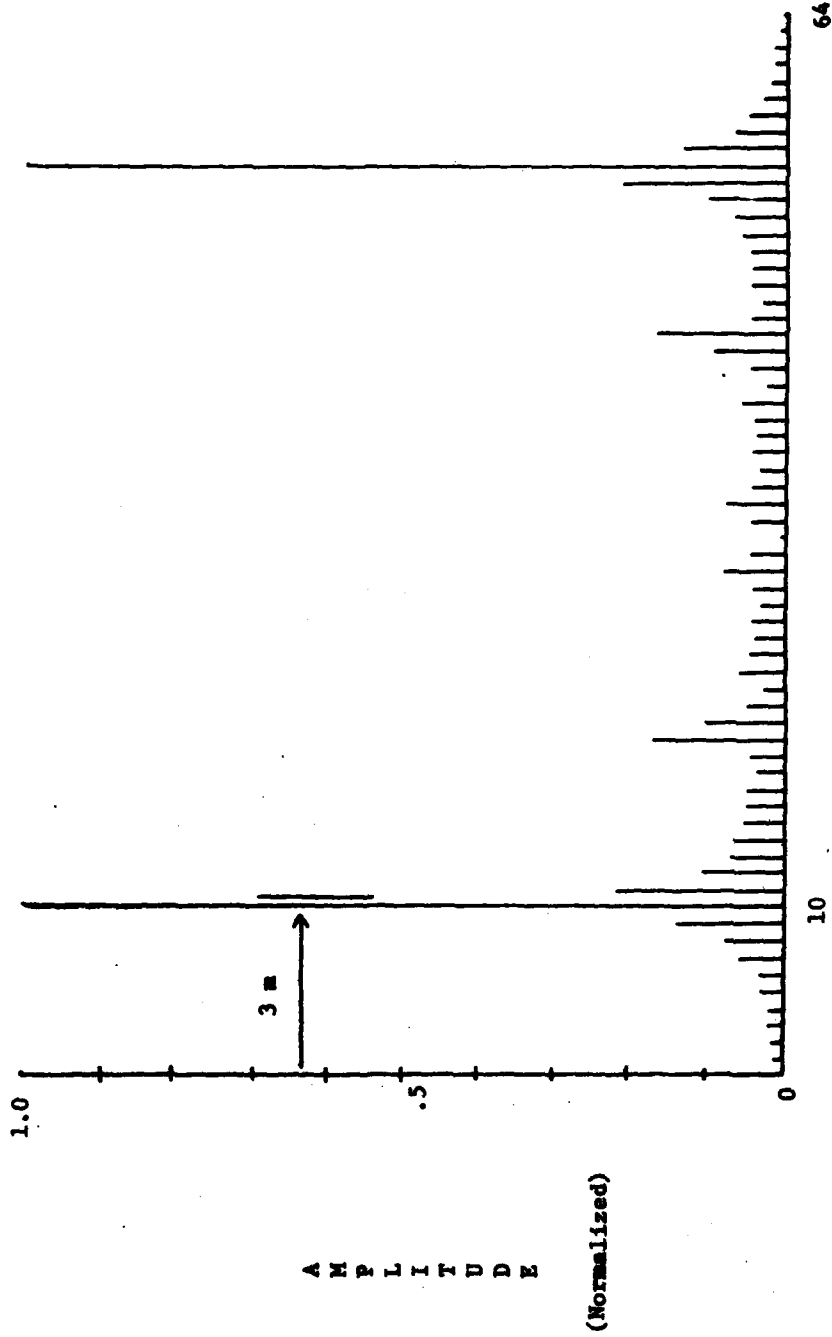


Figure 38. Real LHC FFT for 4 reflector array.

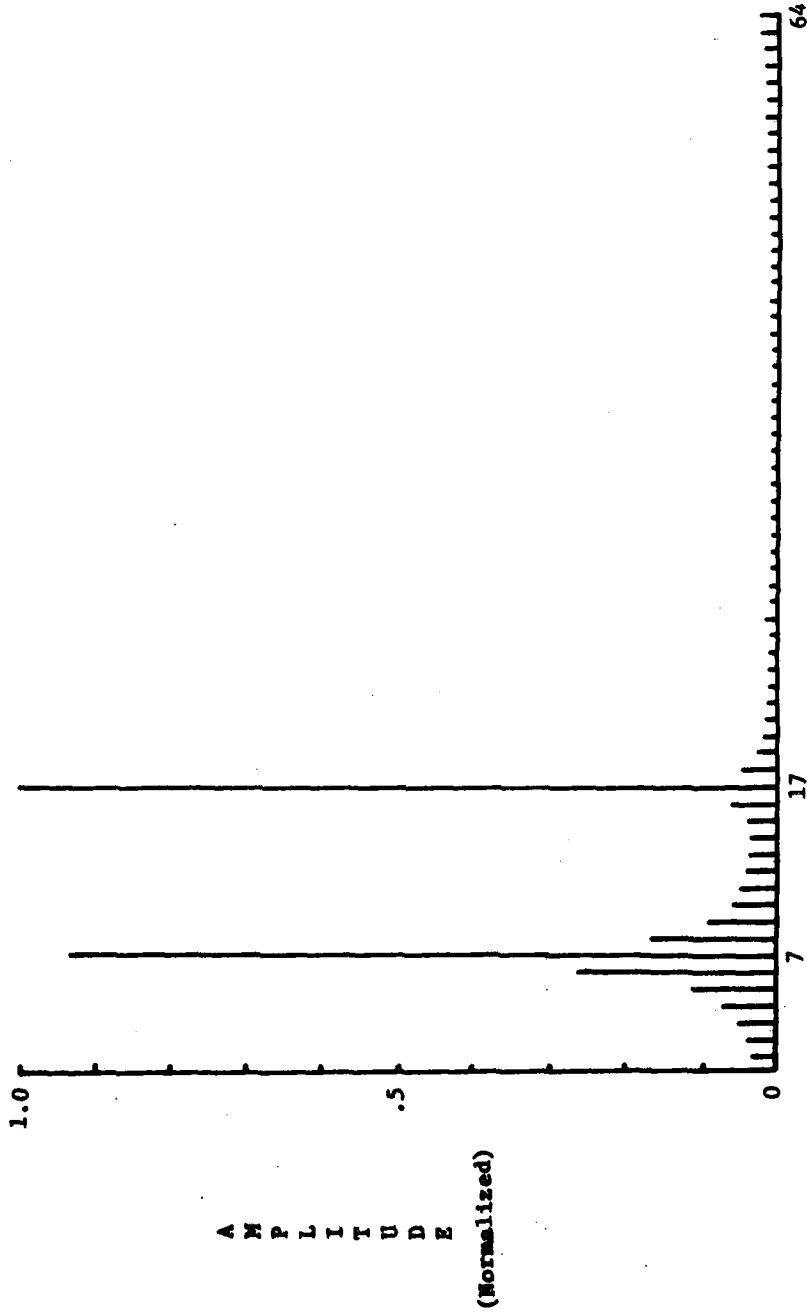


Figure 39. Complex LHC FFT for 50 db of antenna cross coupling.

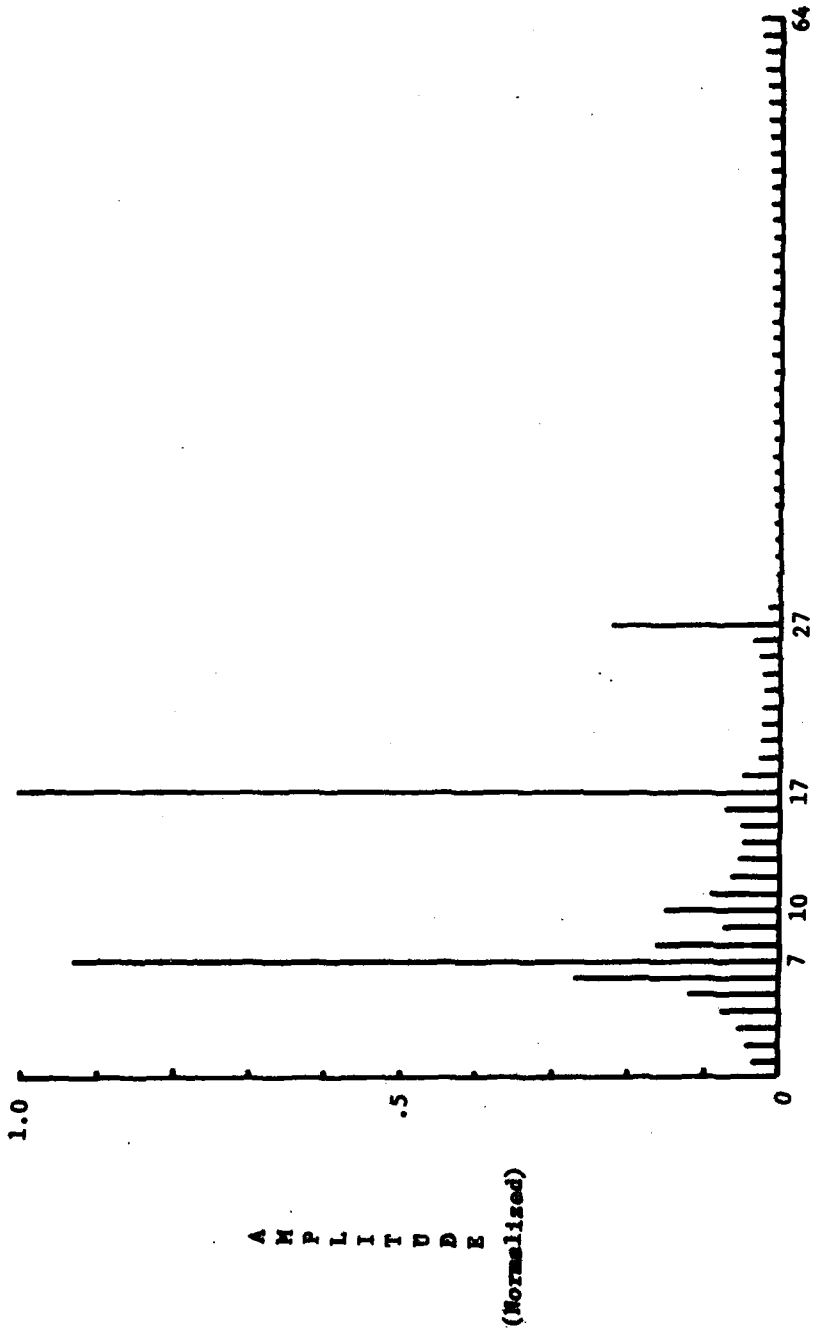


Figure 40. Complex LHC FFT for 20 db of antenna cross coupling.

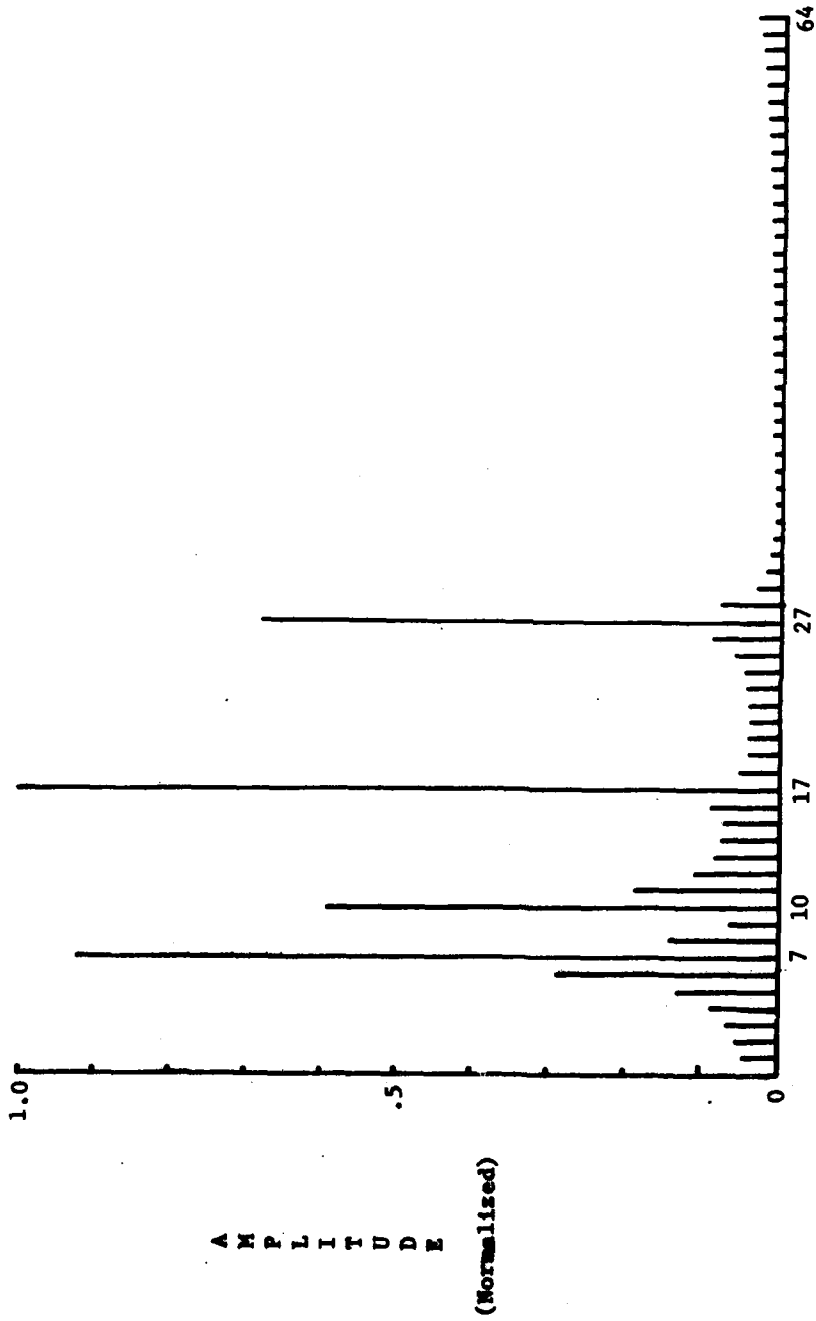


Figure 41. Complex LHC FFT for 10 db of antenna cross coupling.

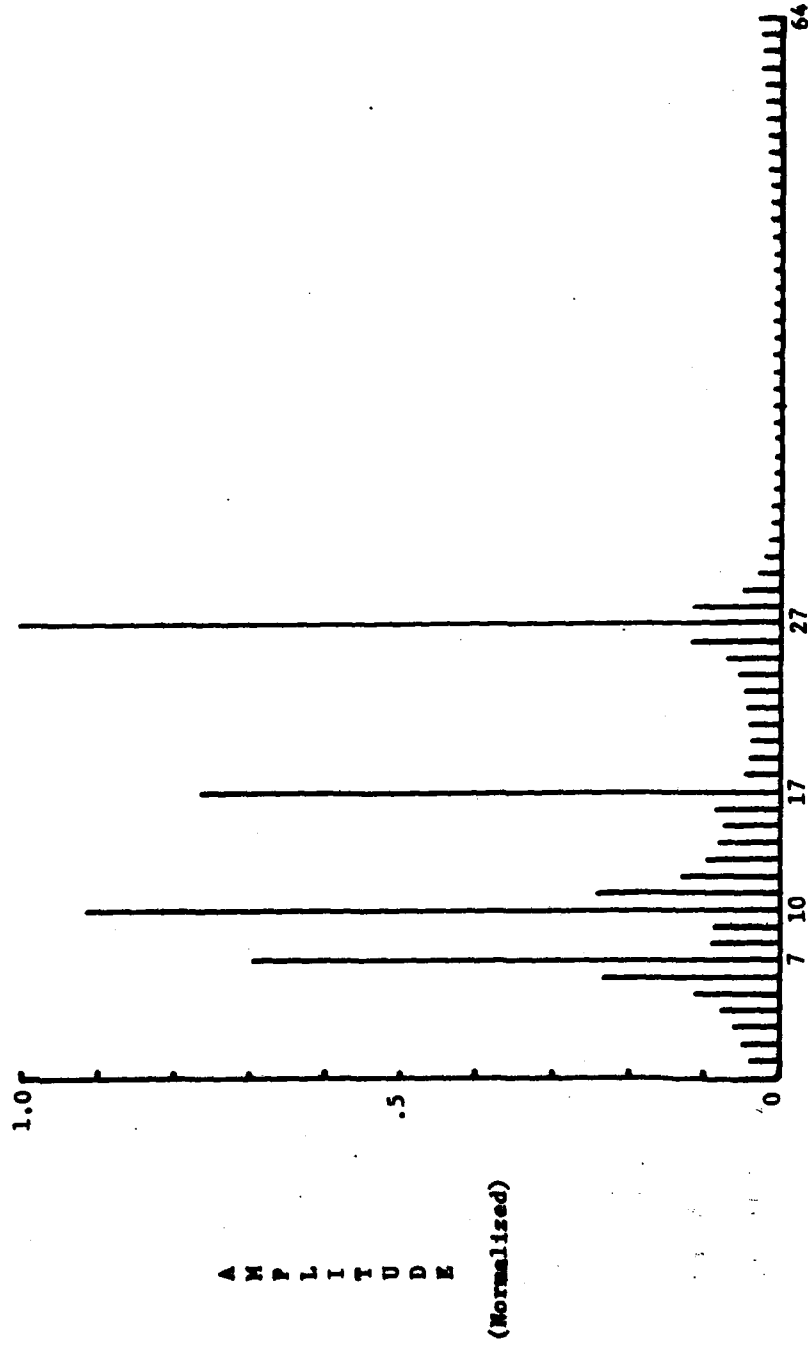


Figure 42. Complex LHC FFT for 3 db of antenna cross coupling.

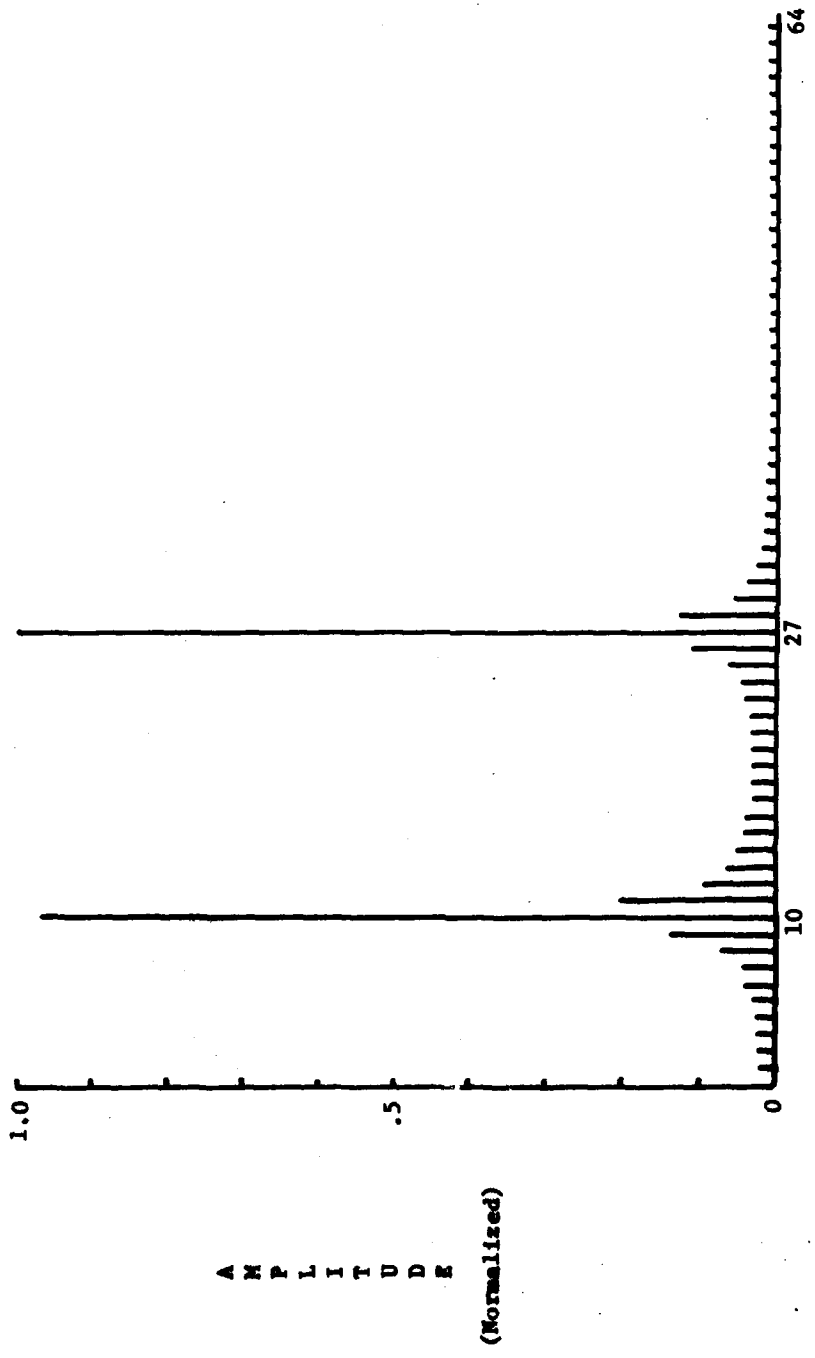


Figure 43. Complex RHC FFT for 50 db of antenna cross coupling.

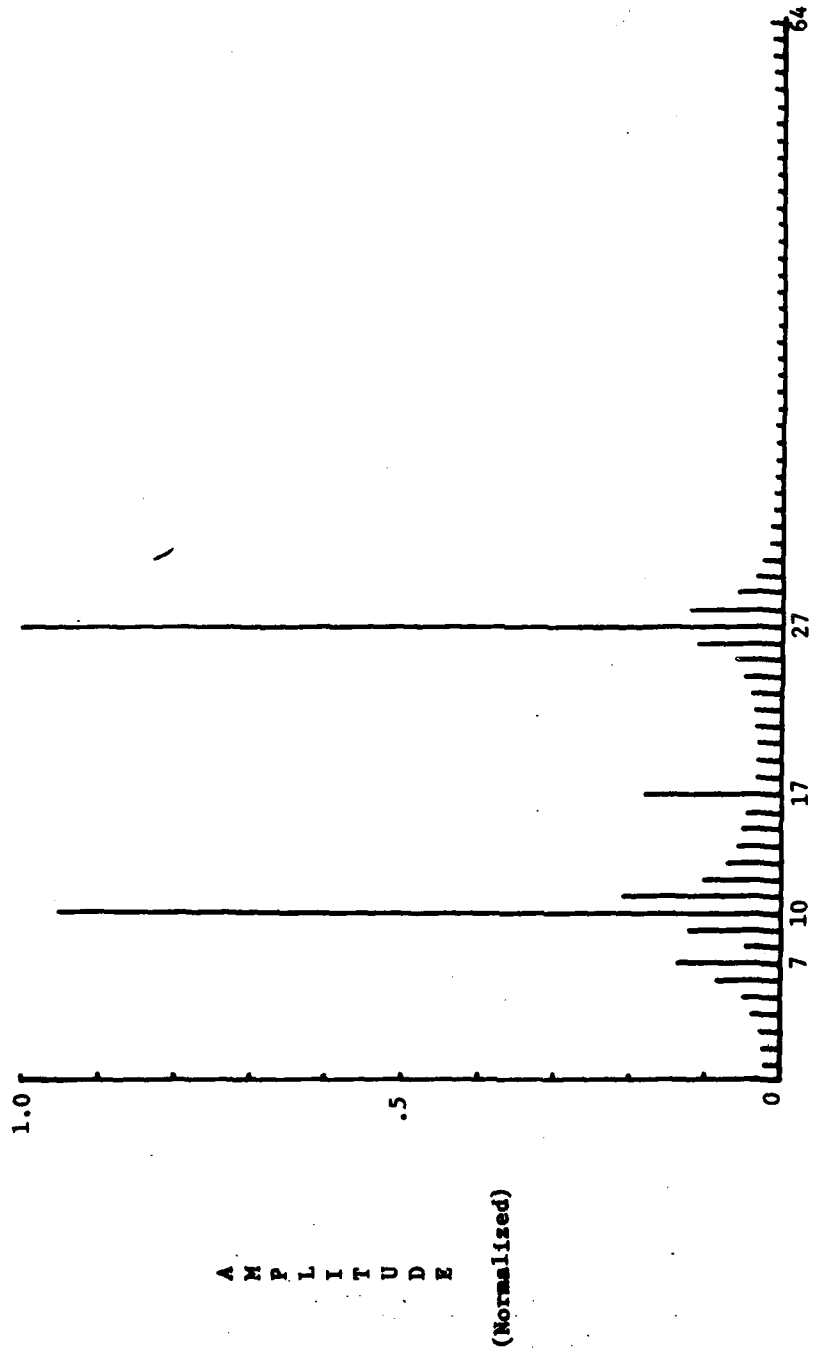


Figure 44. Complex RHC FFT for 20 db of antenna cross coupling.

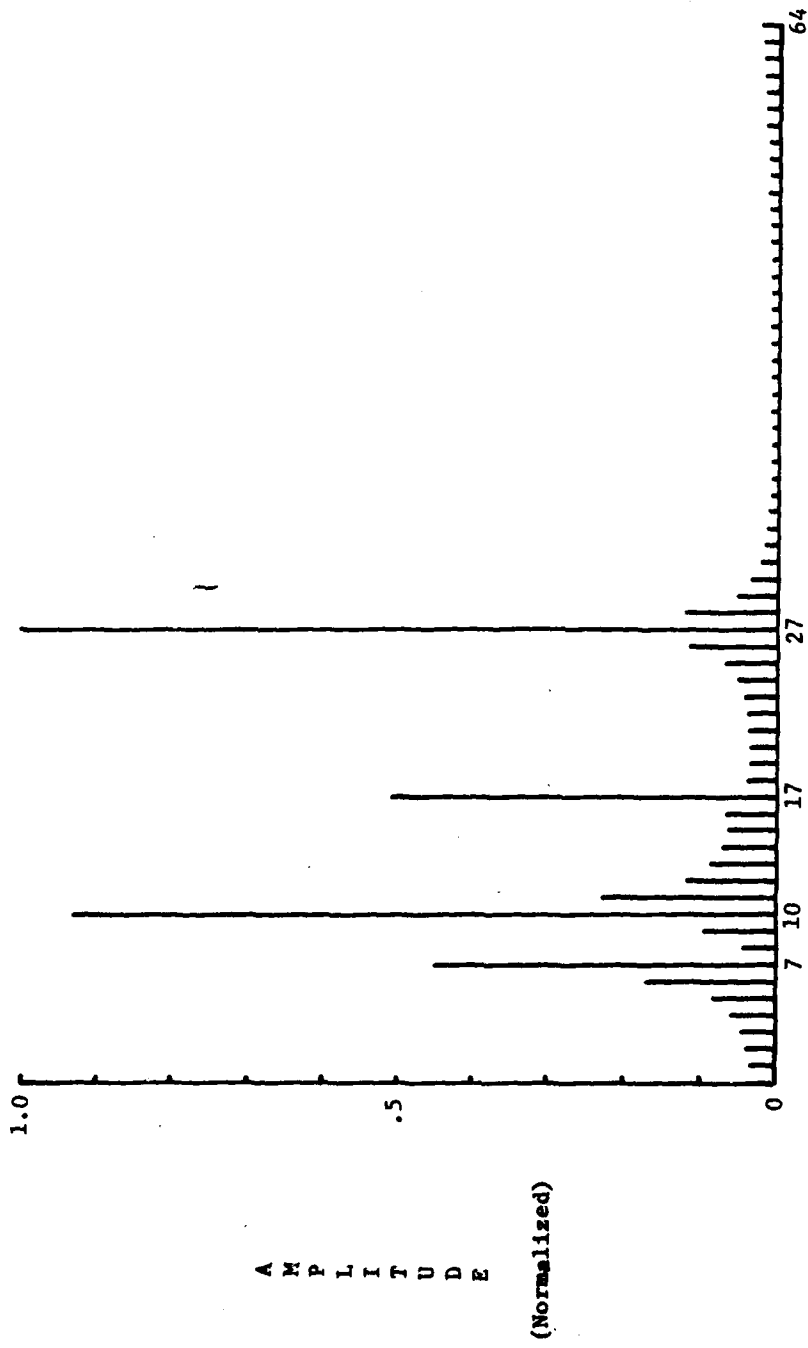


Figure 45. Complex RHC FFT for 10 db of antenna cross coupling.

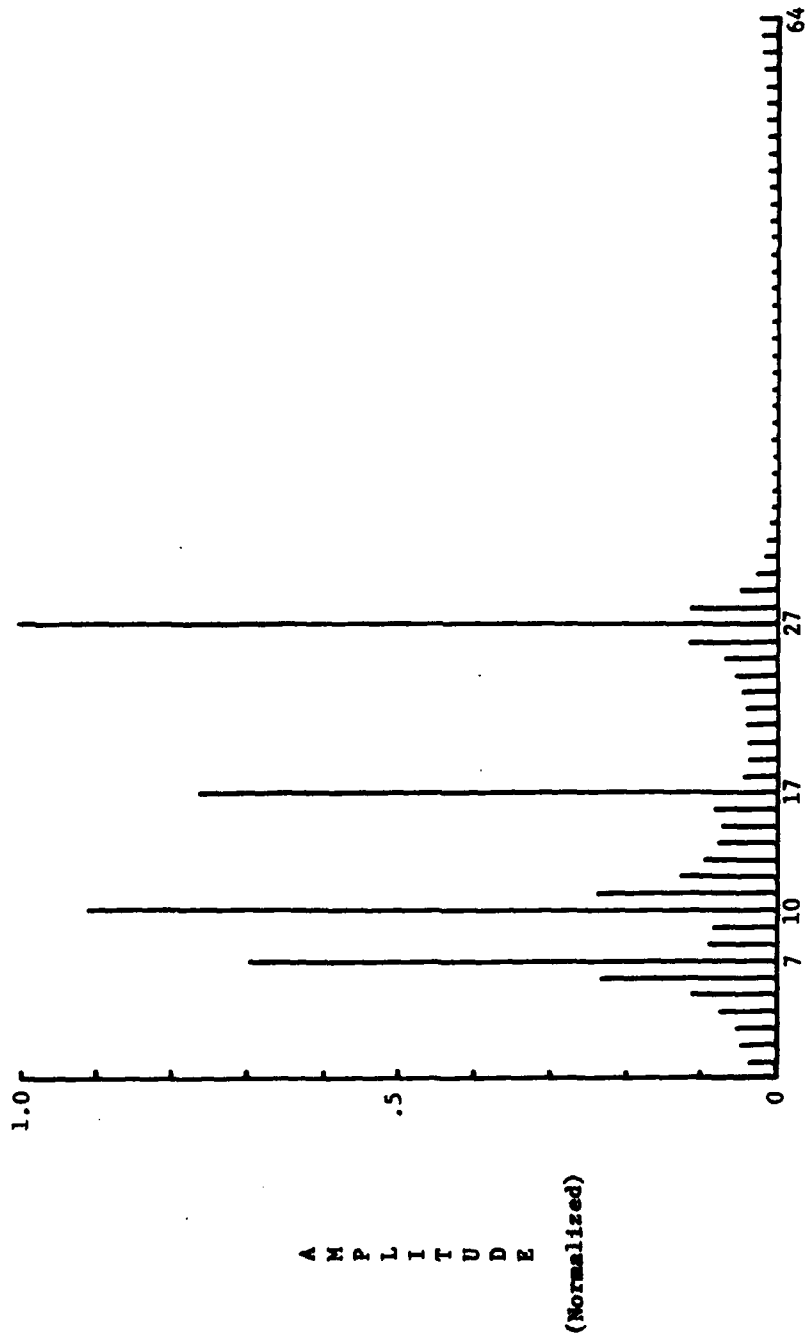


Figure 46. Complex RHC FFT for 3 db of antenna cross coupling.

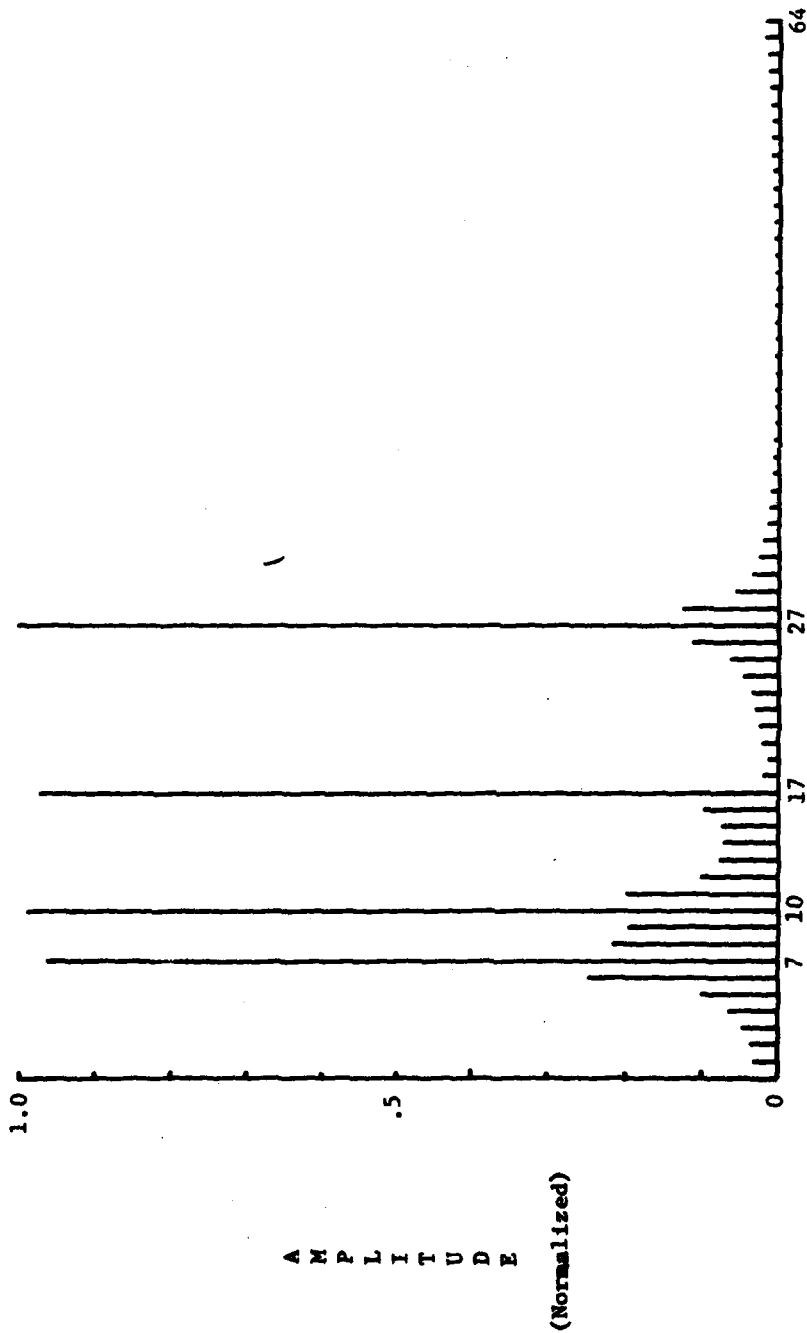


Figure 47. Complex horizontal FFT for 50 db of antenna cross coupling.

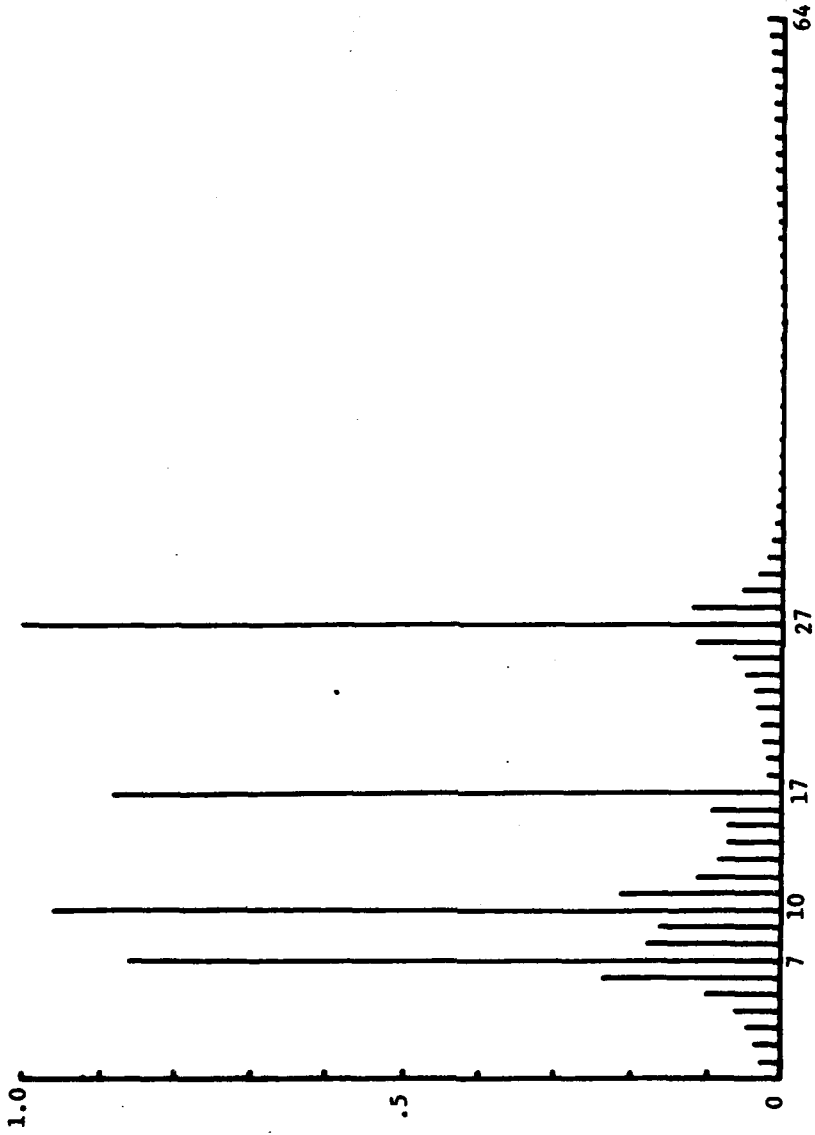


Figure 48. Complex horizontal FFT for 20 db of antenna cross coupling.

A
M
P
L
I
T
U
D
E

(Normalised)

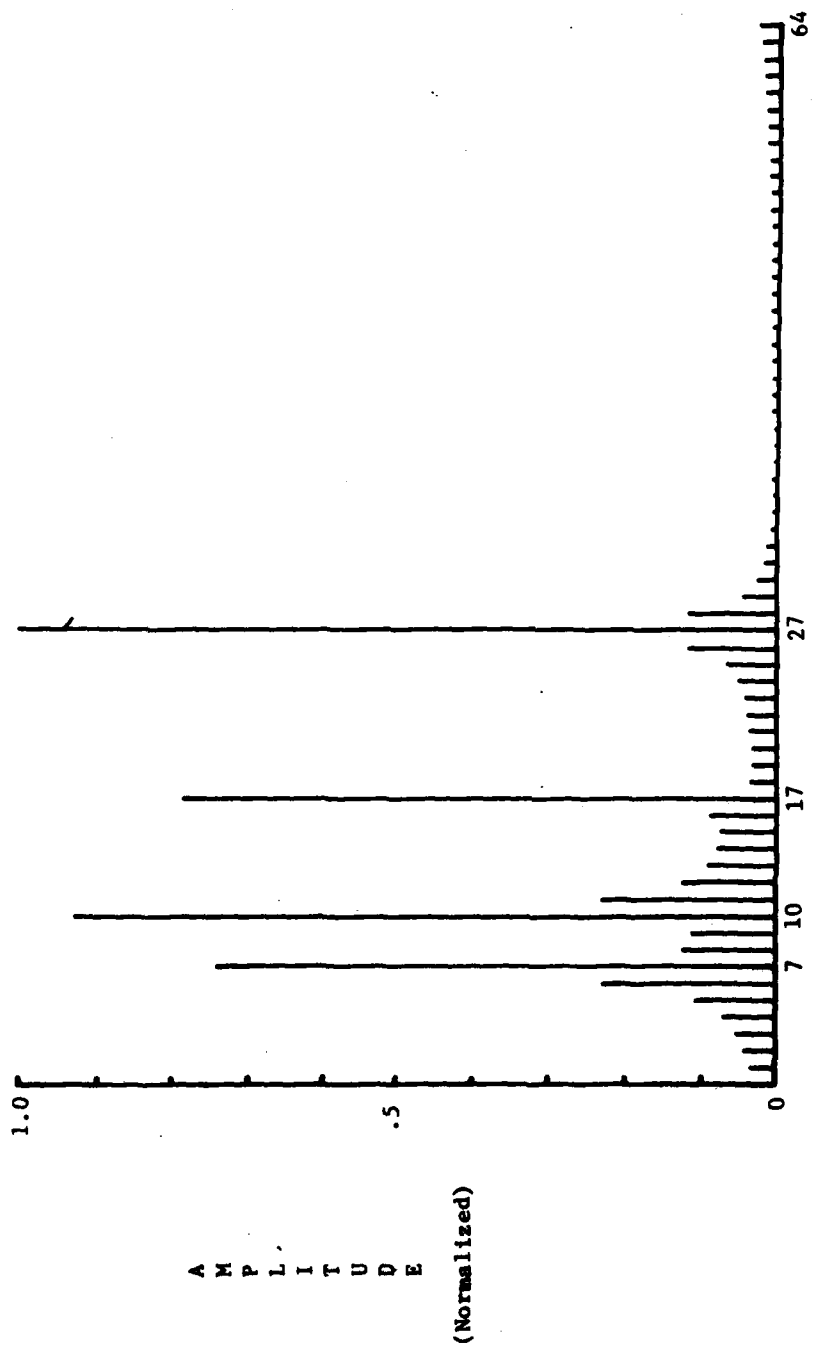


Figure 49. Complex horizontal FFT for 10 db of antenna cross coupling.

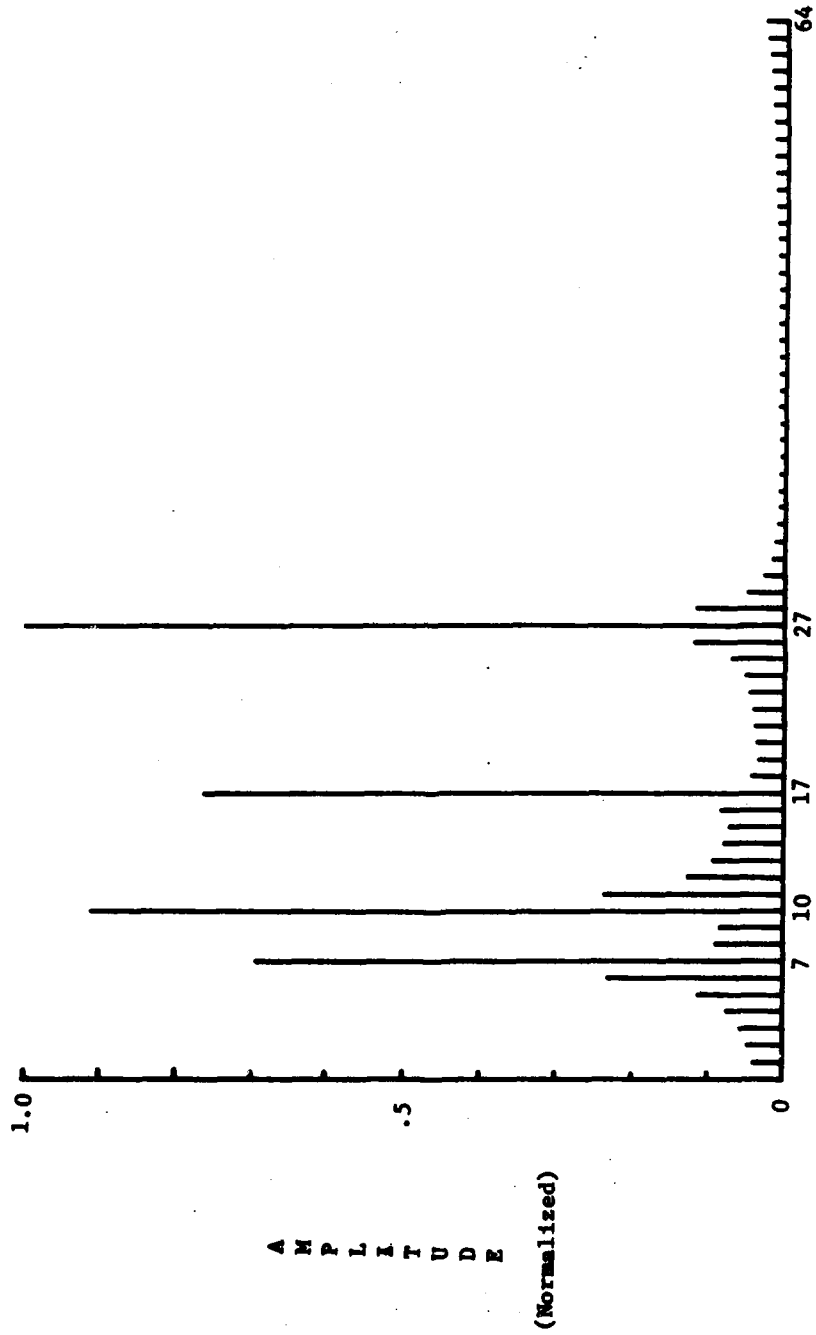


Figure 50. Complex horizontal FFT for 3 db of antenna cross coupling.

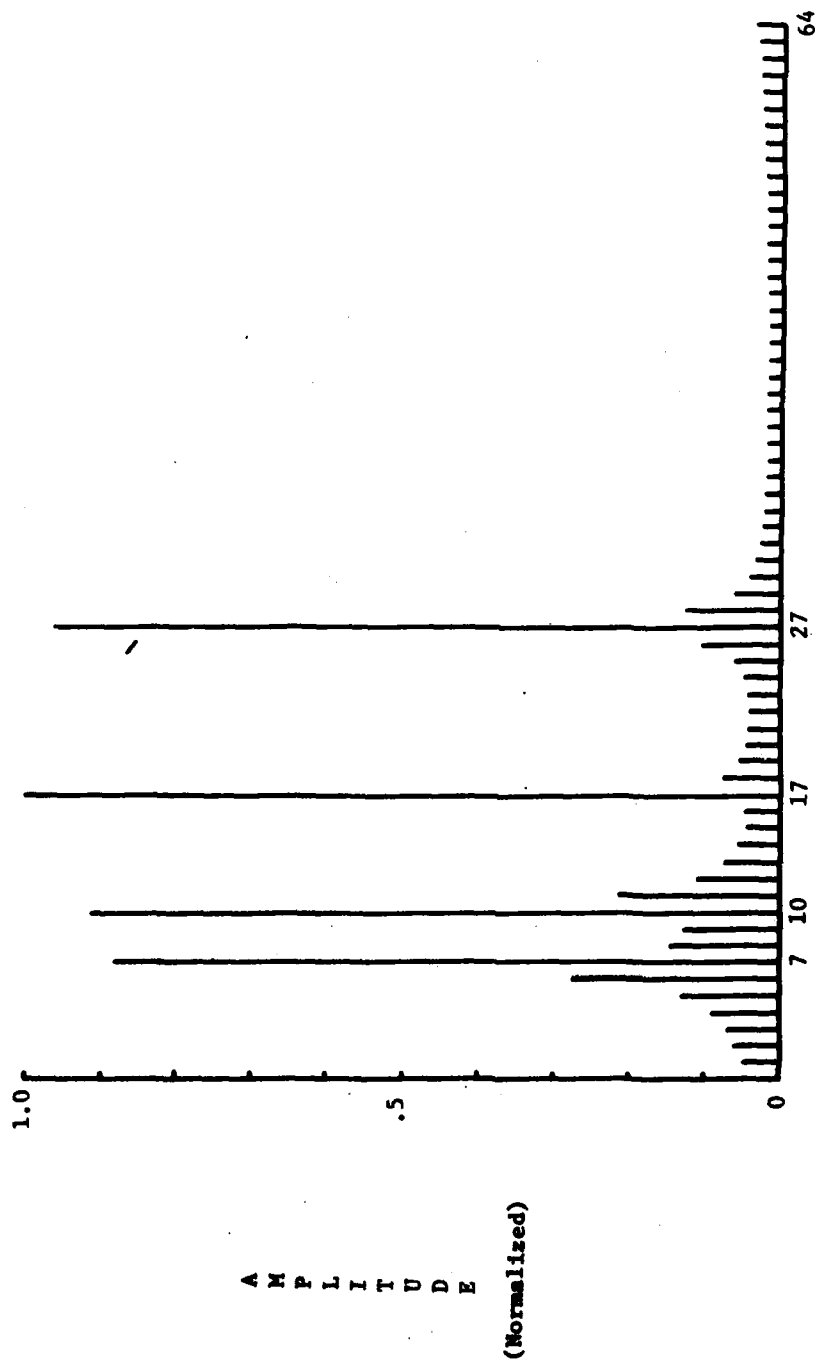


Figure 51. Complex vertical FFT for 50 db of antenna cross coupling.

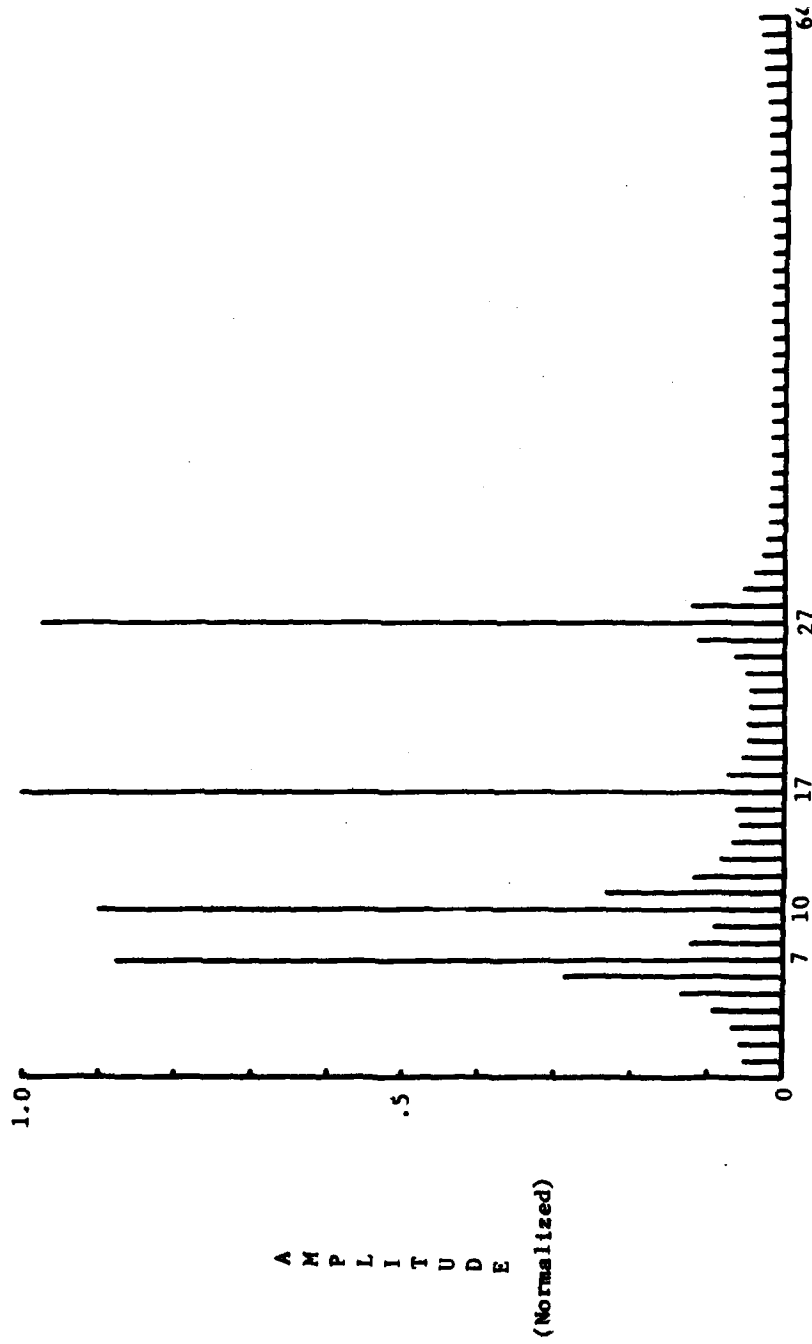


Figure 52. Complex vertical FFT for 20 db of antenna cross coupling.

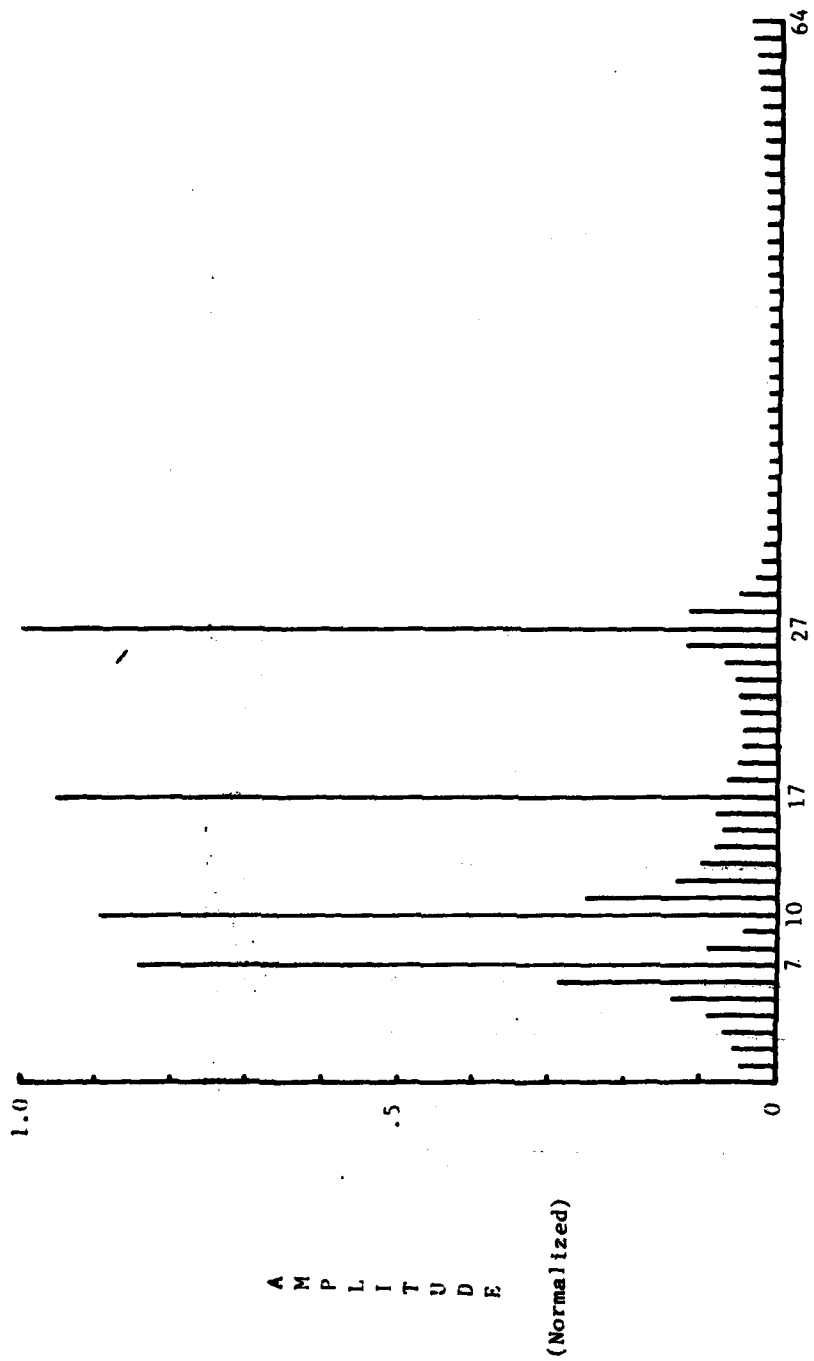


Figure 53. Complex vertical FFT for 10 db of antenna cross coupling.

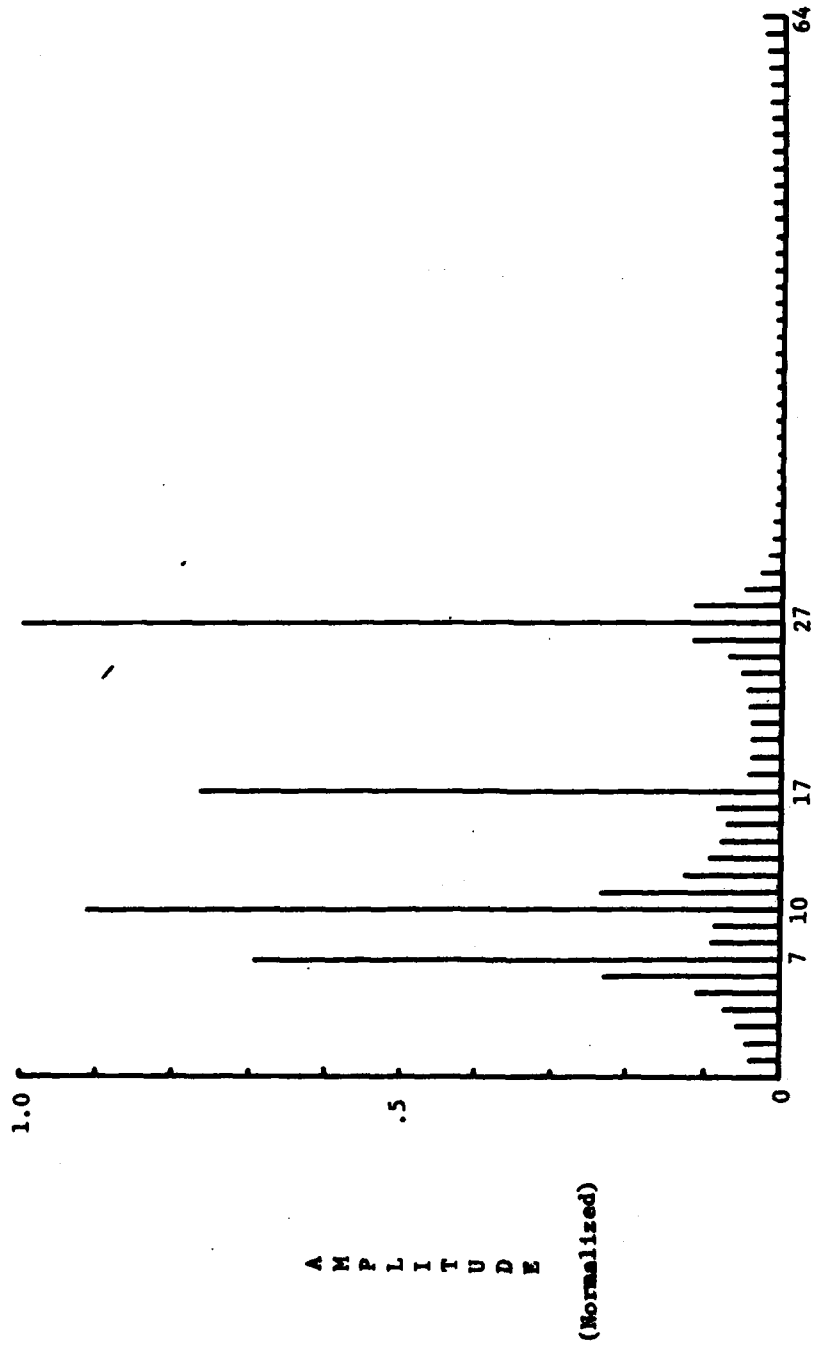


Figure 54. Complex vertical FFT for 3 db of antenna cross coupling.

SIMULATION

```

10 RAD
20 DIM P[20],O[20],L[20],E[20],A[20],R[20],I[20],KS[64,14]
30 DIM X[64,4]
40 MAT K=ZER
50 H=V=1
60 DISP "RATIO FOR CROSSCOUPLING IN DB";
70 INPUT R
80 R=10+(-R/10)
90 A=SQR(1-R)
100 B=SQR(R)
110 DISP "INPUT TRANSMIT WAVEFORM R,L,H,V ";
120 INPUT AS
130 IF AS="R" THEN 170
140 IF AS="L" THEN 190
150 IF AS="H" THEN 210
160 IF AS="V" THEN 230
170 N=-1
180 GOTO 240
190 N=+1
200 GOTO 240
210 V=0
220 GOTO 240
230 H=0
240 DISP "NUMBER ODD REF, AND EVEN REF. ";
250 INPUT N1,N2
260 FOR I=1 TO N1
270 DISP "ODD RCS AND DISTANCE" I;
280 INPUT P[I],O[I]
290 NEXT I
300 FOR I=1 TO N2
310 DISP "INPUT EVEN RCS,DIST AND ANGLE" I;
320 INPUT L[I],E[I],A[I]
330 A[I]=A[I]/(180/PI)
340 NEXT I
350 DISP "INPUT START FREQ. AND BANDWIDTH";
360 INPUT F,Q9
370 DISP "INPUT NUMBER OF FREQUENCY STEPS";
380 INPUT N9
390 F1=Q9/(N9-1)
400 FOR J=1 TO N9
410 K=4*PI*F/2.997E+08
420 V1=V2=V3=V4=H1=H2=H3=H4=0
430 FOR I=1 TO N1
440 Q=K*O[I]
450 P=SQR(P[I])
460 R[I]=-P*(A*H*COS(Q)+N*B*V*SIN(Q))
470 I[I]=P*(A*H*SIN(Q)-N*B*V*COS(Q))
480 H1=H1+R[I]
490 H2=H2+I[I]
500 NEXT I
510 FOR I=1 TO N2
520 Z=2*A[I]

```

SIMULATION (Cont'd)

```

530 Q=K*E[I]
540 L=SQR(L[I])
550 R1=L*(A*H*COS(Z)*COS(Q)+N*B*V*SIN(Z)*SIN(Q))
560 R2=L*(B*H*SIN(Z)*COS(Q)+N*A*V*SIN(Z)*SIN(Q))
570 R[I]=R1+R2
580 I1=L*(N*B*V*SIN(Z)*COS(Q)-A*H*COS(Z)*SIN(Q))
590 I2=L*(N*A*V*SIN(Z)*COS(Q)-B*H*SIN(Z)*SIN(Q))
600 I[I]=I1+I2
610 H3=H3+R[I]
620 H4=H4+I[I]
630 NEXT I
640 FOR I=1 TO N1
650 Q=K*O[I]
660 P=SQR(P[I])
670 R[I]=-P*(B*H*COS(Q)+N*A*V*SIN(Q))
680 I[I]=P*(B*H*SIN(Q)-N*A*V*COS(Q))
690 V1=V1+R[I]
700 V2=V2+I[I]
710 NEXT I
720 FOR I=1 TO N2
730 Z=2*A[I]
740 Q=K*E[I]
750 L=SQR(L[I])
760 R1=L*(A*H*SIN(Z)*COS(Q)+N*B*V*SIN(Z)*SIN(Q))
770 R2=-L*(B*H*COS(Z)*COS(Q)+N*A*V*COS(Z)*SIN(Q))
780 R[I]=R1+R2
790 I1=L*(N*B*V*SIN(Z)*COS(Q)-A*H*SIN(Z)*SIN(Q))
800 I2=L*(-N*A*V*COS(Z)*COS(Q)+B*H*COS(Z)*SIN(Q))
810 I[I]=I1+I2
820 V3=V3+R[I]
830 V4=V4+I[I]
840 NEXT I
850 K[J,1]=A*(H1+H3)+B*(V1+V3)
860 X1=K[J,1]
870 K[J,2]=A*(H2+H4)+B*(V2+V4)
880 Y1=K[J,2]
890 K[J,3]=A*(V1+V3)+B*(H1+H3)
900 X2=K[J,3]
910 K[J,4]=A*(V2+V4)+B*(H2+H4)
920 Y2=K[J,4]
930 K[J,5]=SQR(X1+2+Y1+2)
940 K[J,6]=SQR(X2+2+Y2+2)
950 B1=(X1-0)*(PI*(Y1<0)+PI/2)
960 IF X1=0 THEN 980
970 B1=B1+(ATN(Y1/X1)+PI*(X1<0)+2*PI*(X1>0 AND Y1<0))
980 B2=(X2-0)*(PI*(Y2<0)+PI/2)
990 IF X2=0 THEN 1010
1000 B2=B2+(ATN(Y2/X2)+PI*(X2<0)+2*PI*(X2>0 AND Y2<0))
1010 B9=B2-B1
1020 B9=B9*180/PI
1030 B9=B9+360*(B9<(-180))
1040 B9=B9-360*(B9>180)

```

SIMULATION (Concluded)

```
1050 K[J,7]=B9
1060 K[J,8]=0.707*(X1+Y2)
1070 K[J,9]=0.707*(Y1-X2)
1080 K[J,10]=0.707*(X1-Y2)
1090 K[J,11]=0.707*(Y1+X2)
1100 K[J,12]=SQR(K[J,8]+2+K[J,9]+2)
1110 K[J,13]=SQR(K[J,10]+2+K[J,11]+2)
1120 K[J,14]=F
1130 F=F1+F
1140 DISP J
1150 NEXT J
1160 DISP "FILE NUMBER";
1170 INPUT Z9
1180 STORE DATA Z9,K
1190 END
```

DATA FILE FORMAT

<u>Element #</u>	<u>Parameter</u>
1	HI
2	HQ
3	VI
4	VQ
5	H
6	V
7	B
8	RI
9	RQ
10	LI
11	LQ
12	R
13	L
14	F

FFT

```
10 RAD
20 DIM X(64),Y(64),MI(8),A(128),KS(64,14),A$(1)
30 MAT X=ZER
40 MAT Y=ZER
50 DISP "NEW FILE";
60 INPUT A$
70 IF A$="N" THEN 110
80 DISP "FILE NUMBER";
90 INPUT Q9
100 LOAD DATA Q9,K
110 DISP "REAL OR IMAGINARY FFT";
120 INPUT A$
130 IF A$="I" THEN 210
140 DISP "INPUT SUB-FILE#           ";
150 INPUT Z2
160 FOR I=1 TO 64
170 X(I)=0
180 Y(I)=K(I,Z2)
190 NEXT I
200 GOTO 270
210 DISP "INPUT Q AND I SUB-FILE #";
220 INPUT Z1,Z2
230 FOR I=1 TO 64
240 X(I)=K(I,Z1)
250 Y(I)=K(I,Z2)
260 NEXT I
270 N=6
280 N1=2+N
290 N2=N1
300 S=-1
310 L1=2+N
320 FOR I=1 TO N
330 M(I)=2+(N-I)
340 NEXT I
350 FOR L=1 TO N
360 N1=2+(L-1)
370 L2=INT(L1/N1)
380 L3=INT(L2/2)
390 K=0
400 FOR I1=1 TO N1
410 V=S*2*PI*K/L1
420 W1=COSV
430 W2=SINV
440 I2=L2*(I1-1)
450 FOR I=1 TO L3
460 J=I2+I
470 J1=J+L3
480 Q1=X(J1)*W1-Y(J1)*W2
490 Q2=Y(J1)*W1+X(J1)*W2
500 X(J1)=X(J)-Q1
510 Y(J1)=Y(J)-Q2
```

FFT (Concluded)

```

520 X[J]=X[J]+Q1
530 Y[J]=Y[J]+Q2
540 NEXT I
550 FOR I=2 TO N
560 I9=I
570 IF K<M[I] THEN 600
580 K=K-M[I]
590 NEXT I
600 K=K+M[I9]
610 NEXT I1
620 NEXT L
630 K=0
640 FOR J=1 TO L1
650 IF K<J THEN 720
660 H1=X[J]
670 H2=Y[J]
680 X[J]=X[K+1]
690 Y[J]=Y[K+1]
700 X[K+1]=H1
710 Y[K+1]=H2
720 FOR I=1 TO N
730 I9=I
740 IF K<M[I] THEN 770
750 K=K-M[I]
760 NEXT I
770 K=K+M[I9]
780 NEXT J
790 FOR I=1 TO L1
800 X[I]=X[I]/L1
810 Y[I]=Y[I]/L1
820 NEXT I
830 FOR I=1 TO N2
840 A[I]=(SQR(X[I]+2+Y[I]+2))
850 NEXT I
860 M1=-1E+99
870 M2=1E+99
880 FOR I=2 TO 64
890 IF A[I]<M1 THEN 910
900 M1=A[I]
910 IF A[I]>M2 THEN 930
920 M2=A[I]
930 NEXT I
940 SCALE 1,N2,0,M1
950 FOR I=2 TO N2
960 PLOT I,0
970 PLOT I,A[I],-1
980 NEXT I
990 PEN
1000 XAXIS 0
1010 M4=M1/10
1020 YAXIS 1,M4
1030 END

```

APPENDIX B

PRECEDING PAGE

TRANSFORMATION OF LINEAR TO CIRCULAR POLARIZATION

Circular polarization consists of two linear (horizontal and vertical) components with a $\pi/2$ phase shift between them. Using complex matrix notation, the following relationship between linear and circular polarization is obtained:

$$\begin{bmatrix} \vec{E}_R^T \\ \vec{E}_L^T \end{bmatrix} = \begin{bmatrix} 1 & -j \\ 1 & j \end{bmatrix} \begin{bmatrix} \vec{E}_H^T \\ \vec{E}_V^T \end{bmatrix}$$

$$\begin{bmatrix} \vec{E}_R^S \\ \vec{E}_L^S \end{bmatrix} = \begin{bmatrix} 1 & j \\ 1 & -j \end{bmatrix} \begin{bmatrix} \vec{E}_H^S \\ \vec{E}_V^S \end{bmatrix}$$

The transmitted and scattered linear components in terms of circular components will have the form:

$$\begin{bmatrix} \vec{E}_H^T \\ \vec{E}_V^T \end{bmatrix} = \begin{bmatrix} 1 & -j \\ 1 & j \end{bmatrix}^{-1} \begin{bmatrix} \vec{E}_R^T \\ \vec{E}_L^T \end{bmatrix}$$

$$\begin{bmatrix} \vec{E}_H^S \\ \vec{E}_V^S \end{bmatrix} = \begin{bmatrix} 1 & j \\ 1 & -j \end{bmatrix}^{-1} \begin{bmatrix} \vec{E}_R^S \\ \vec{E}_L^S \end{bmatrix}$$

Substituting these matrices into the original equations yields:

$$\begin{bmatrix} 1 & j \\ 1 & -j \end{bmatrix}^{-1} \begin{bmatrix} \vec{E}_R^S \\ \vec{E}_L^S \end{bmatrix} = \begin{bmatrix} S_{HH} & S_{HV} \\ S_{VH} & S_{VV} \end{bmatrix} \begin{bmatrix} 1 & -j \\ 1 & j \end{bmatrix}^{-1} \begin{bmatrix} \vec{E}_R^T \\ \vec{E}_L^T \end{bmatrix} \quad (A1)$$

$$[S]_{\text{Lin}} = \begin{bmatrix} S_{\text{HH}} & S_{\text{HV}} \\ S_{\text{VH}} & S_{\text{VV}} \end{bmatrix} = \text{Linear Scattering Matrix}$$

The linear scattering matrix is the transformation matrix between the linear transmitted energy and the linear scattered energy.

$$\begin{bmatrix} \vec{E}_H^{\text{S}} \\ \vec{E}_V^{\text{S}} \end{bmatrix} = \begin{bmatrix} S \\ \text{Lin} \end{bmatrix} \begin{bmatrix} \vec{E}_H^{\text{T}} \\ \vec{E}_V^{\text{T}} \end{bmatrix}$$

Solving (A1) for circular scattered components:

$$\begin{bmatrix} \vec{E}_R^{\text{S}} \\ \vec{E}_L^{\text{S}} \end{bmatrix} = \begin{bmatrix} 1 & j \\ 1 & -j \end{bmatrix} \begin{bmatrix} S \\ \text{Lin} \end{bmatrix} \begin{bmatrix} j & j \\ -1 & 1 \end{bmatrix} \begin{bmatrix} \vec{E}_R^{\text{T}} \\ \vec{E}_L^{\text{T}} \end{bmatrix}$$

$$\begin{bmatrix} \vec{E}_R^{\text{S}} \\ \vec{E}_L^{\text{S}} \end{bmatrix} = \frac{1}{2j} \begin{bmatrix} jS_{\text{HH}} - S_{\text{VH}} - S_{\text{HV}} - jS_{\text{VV}} & jS_{\text{HH}} - S_{\text{VH}} + S_{\text{HV}} + jS_{\text{VV}} \\ jS_{\text{HH}} + S_{\text{VH}} - S_{\text{HV}} + jS_{\text{VV}} & jS_{\text{HH}} + S_{\text{VH}} + S_{\text{HV}} - jS_{\text{VV}} \end{bmatrix} \begin{bmatrix} \vec{E}_R^{\text{T}} \\ \vec{E}_L^{\text{T}} \end{bmatrix}$$

The circular scattering matrix is defined as:

$$[S]_{\text{circ}} = \begin{bmatrix} S_{\text{RR}} & S_{\text{RL}} \\ S_{\text{LR}} & S_{\text{LL}} \end{bmatrix} = \text{Circular Scattering Matrix}$$

The transmitted and scattered circular components are related by the circular scattering matrix in the following manner:

$$\begin{bmatrix} \vec{E}_R^{\text{S}} \\ \vec{E}_L^{\text{S}} \end{bmatrix} = \begin{bmatrix} S \\ \text{circ} \end{bmatrix} \begin{bmatrix} \vec{E}_R^{\text{T}} \\ \vec{E}_L^{\text{T}} \end{bmatrix}$$

Equating coefficients and solving for the scattering matrix elements yields the following transformation equations:

$$S_{RR} = \frac{1}{2} (S_{HH} - S_{VV} + jS_{VH} + jS_{HV})$$

$$S_{RL} = \frac{1}{2} (S_{HH} + S_{VV} + jS_{VH} - jS_{HV})$$

$$S_{LR} = \frac{1}{2} (S_{HH} + S_{VV} - jS_{VH} + jS_{HV})$$

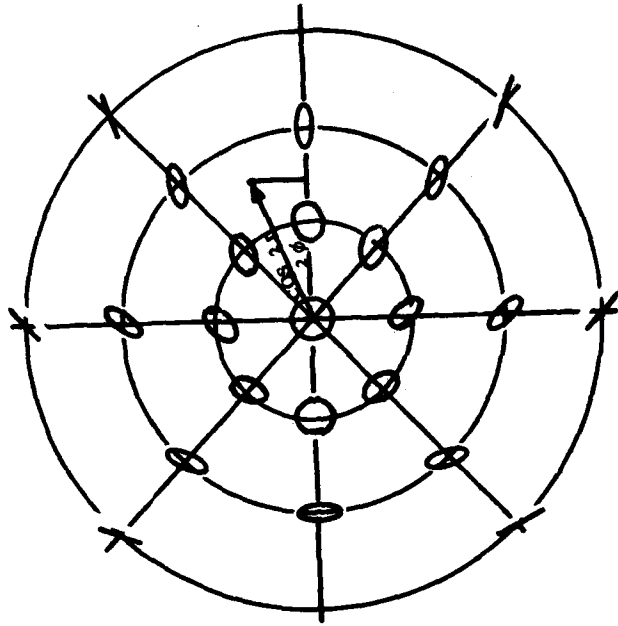
$$S_{LL} = \frac{1}{2} (S_{HH} - S_{VV} - jS_{VH} - jS_{HV})$$

APPENDIX C

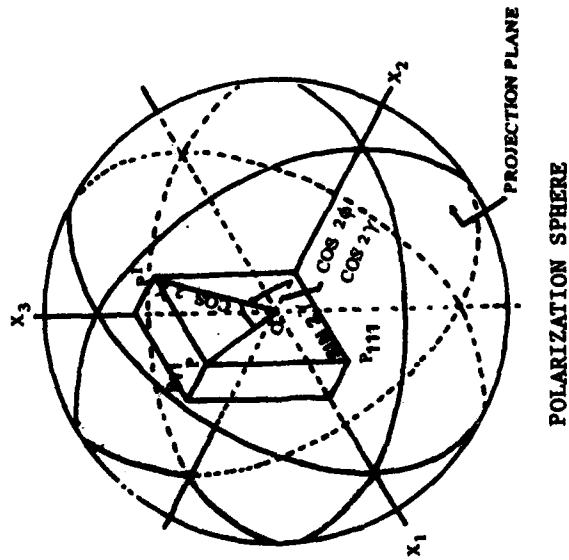
RECORDING FAC

POINCARÉ SPHERE

The Poincaré Sphere (or Polarization Sphere) is a means of representing polarization as a point in 3 dimensional space. A point on the sphere is defined by two double angles and the sign of one of the angles. The radius of the sphere is unity. Figure 55 shows a projection of the sphere. Circular polarization maps at the center of the projection, and linear polarizations at the perimeter. Some interest in using the Ploarization Sphere to differentiate between targets and clutter has arisen over the last few years. Figures 56 and 57 are mappings of real clutter data and the 4 reflector array described in the data section. The clutter data was obtained with 35 GHz radar. The clutter patch consisted of a pasture and tree line. Grazing angle was approximately 6° . RHC was transmitted. The reflector array data (100 m^2 trihedrals at 2 and 5 meters, 100 m^2 dihedrals at 3 and 8 meters) was generated with 20 dB of cross coupling (same as Radar). Figure 58 is a 100 m^2 trihedral at 3 meters and a 100 m^2 dihedral at 6 meters, 100 dB of coupling. Figure 59 is a 100 m^2 trihedral at 3 meters and a 50 m^2 dihedral at 3 meters, 100 dB of coupling.



POLARIZATION CHART



POLARIZATION SPHERE

Figure 55. Polarization sphere and polarization chart.

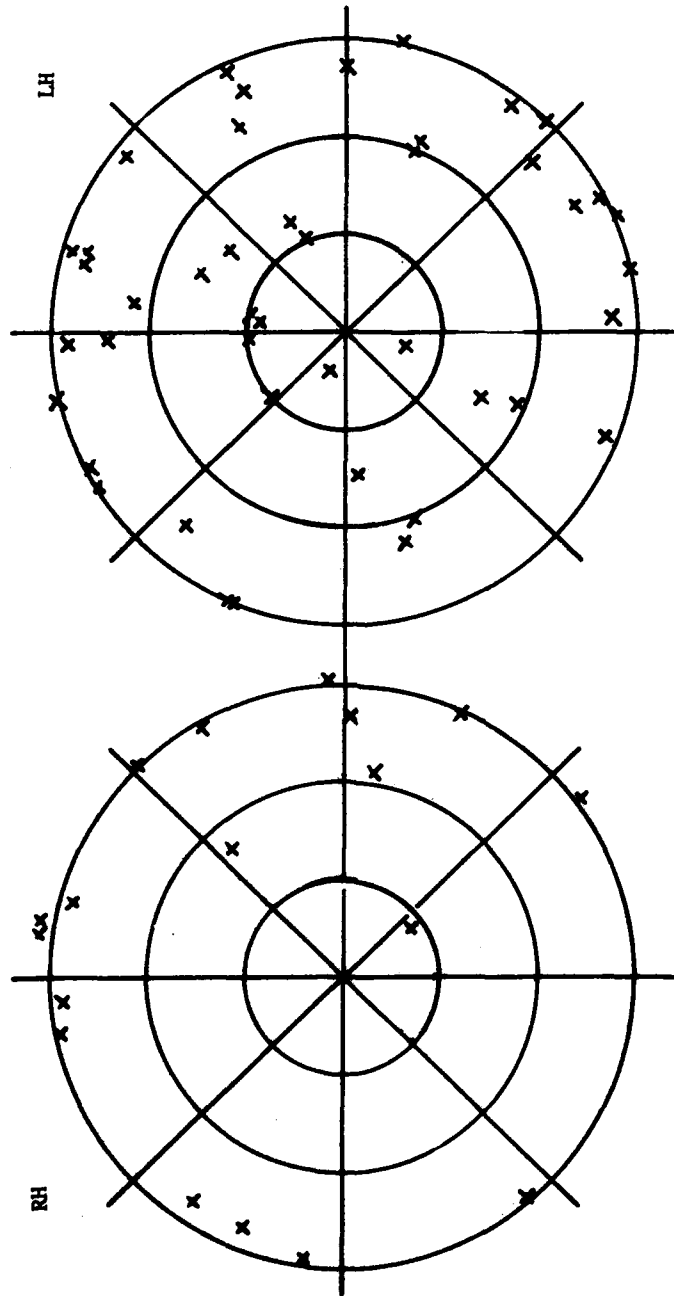


Figure 56. Poincaré sphere mapping of clutter patch.

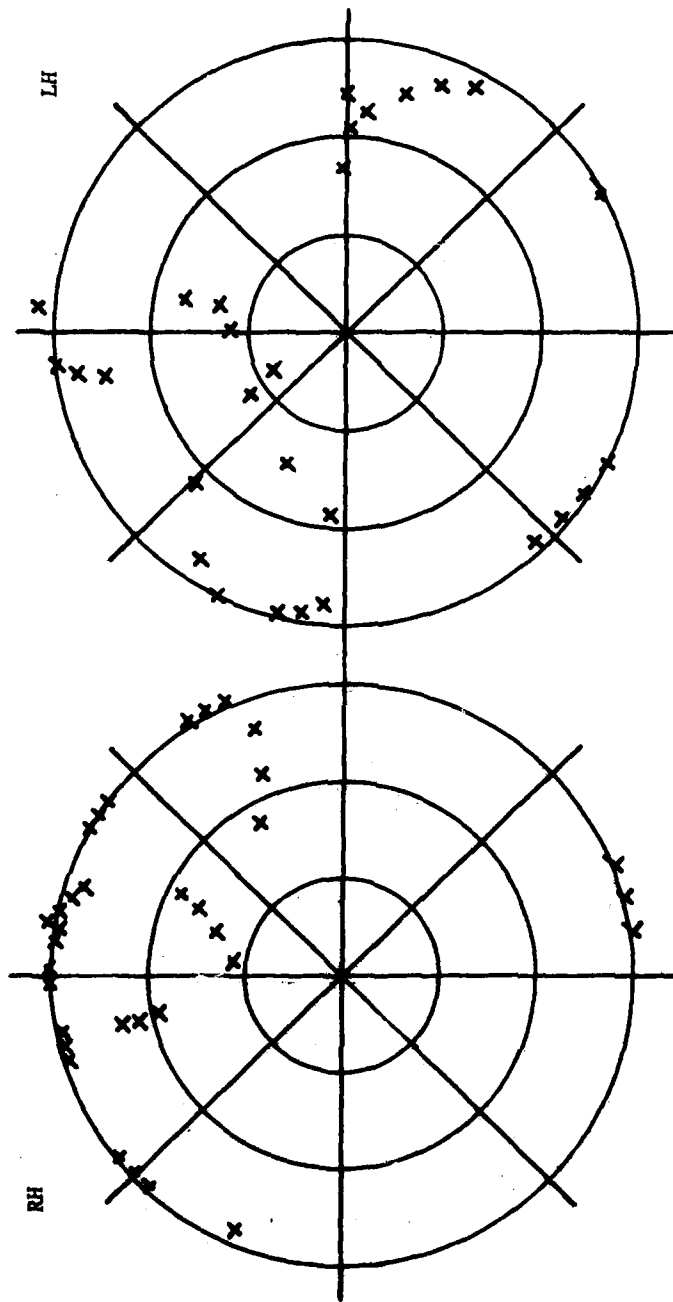


Figure 57. Poincaré sphere mapping of 4 reflector array
20 db of antenna cross coupling.

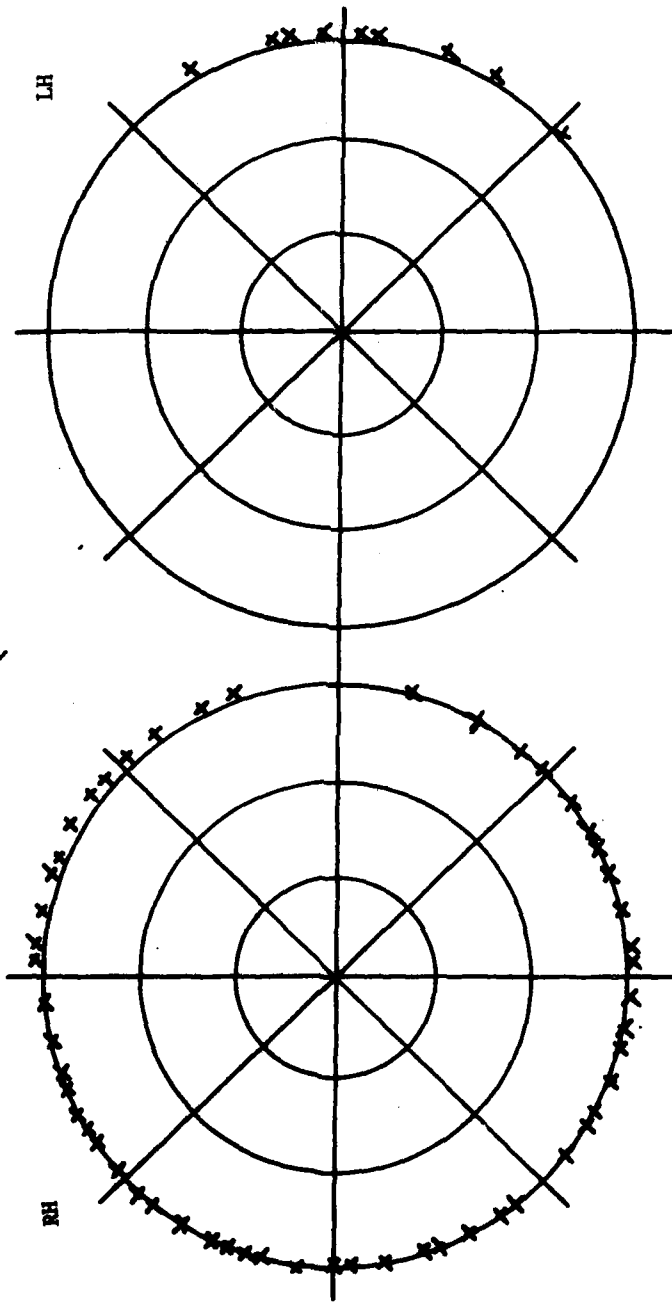


Figure 58. Poincaré sphere mapping of 100 m^2 trihedral and 100 m^2 dihedral at 3 and 6 meters.

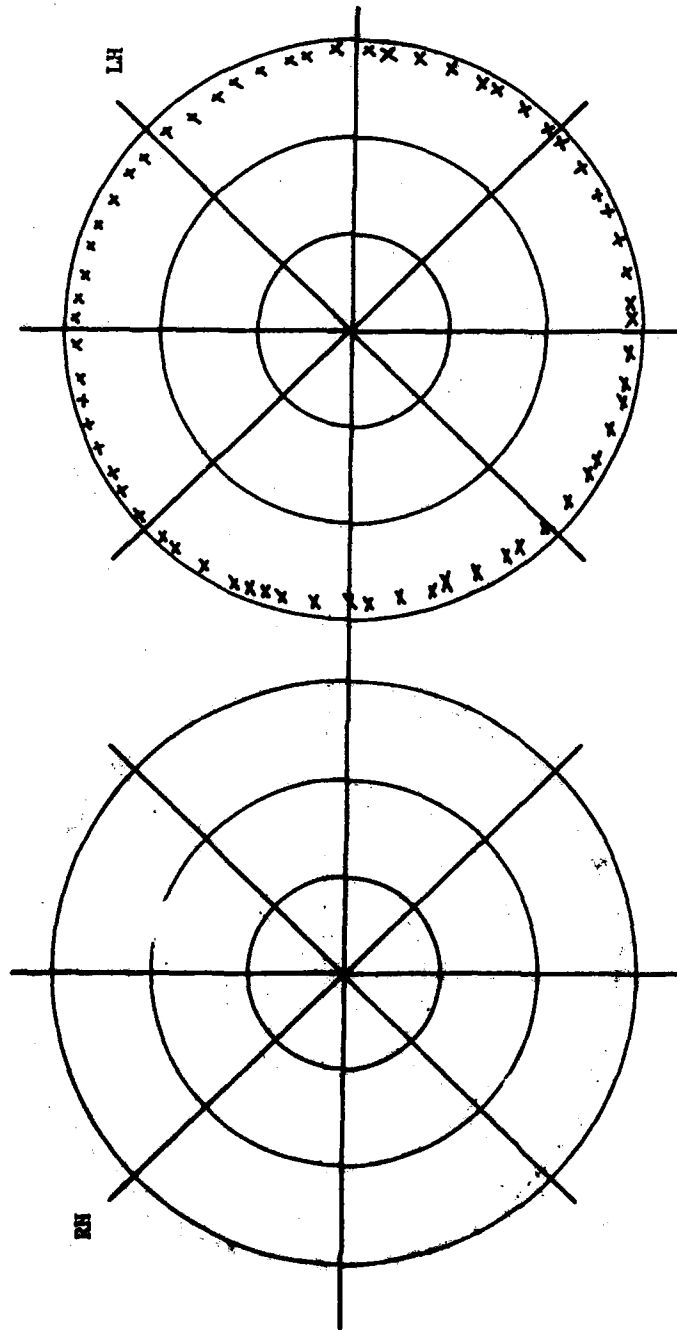
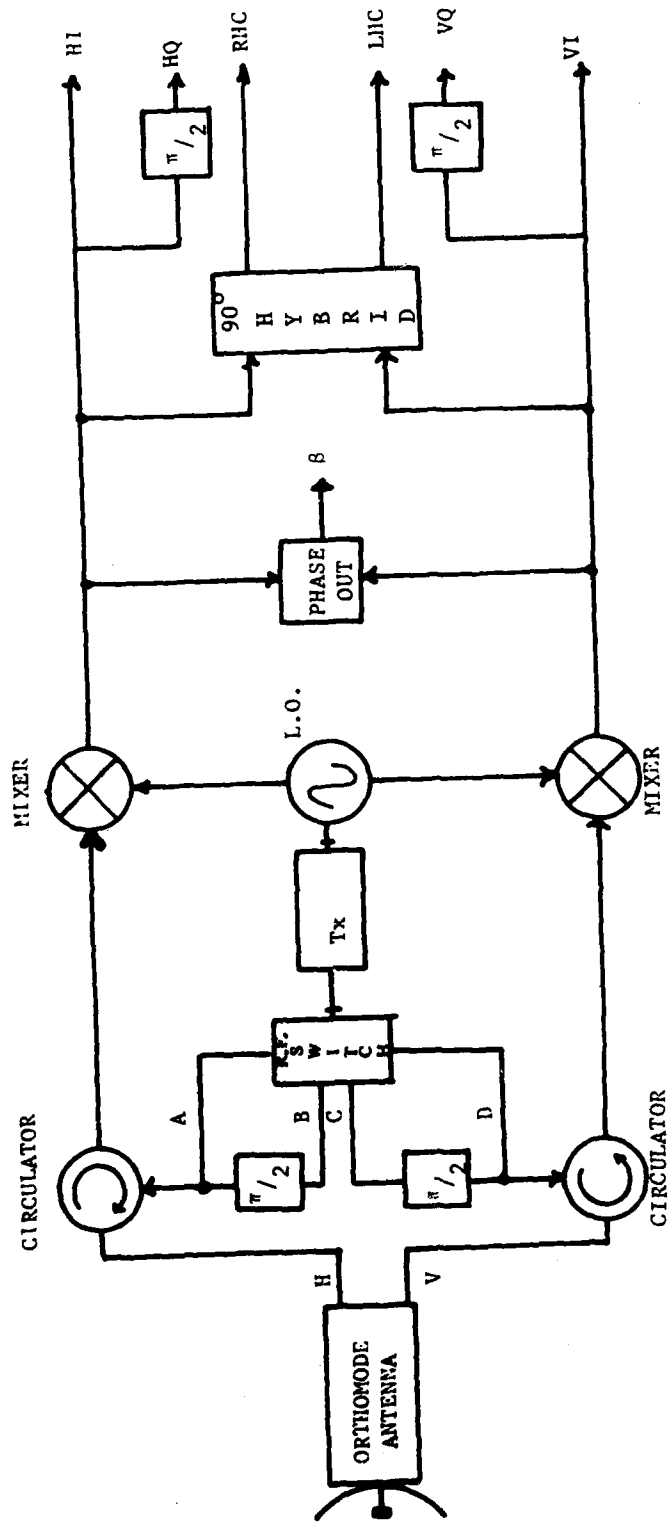


Figure 59. Poincaré sphere mapping of 100 m^2 trihedral and 50 m^2 dihedral at 3 and 6 meters.



R.F. SWITCH

- A = XMIT H
- D = XMIT V
- A+D = SMIT SLANT LEFT OR RIGHT
- A+C = XMIT LHC
- D+B = XMIT RHC

$$\beta = \phi_V - \phi_H$$

Figure 3. Block diagram of generic polarimetric radar.

AD A435 156

22
SIMPLE POLARIMETRIC SIMULATION FOR SMALL COMPUTERS(U)
ARMY MISSILE COMMAND REDSTONE ARSENAL AL ADVANCED

SENSOR'S DIRECTORATE J S COLE DEC 82 DRSMI-RE-83-8-1R

UNCLASSIFIED

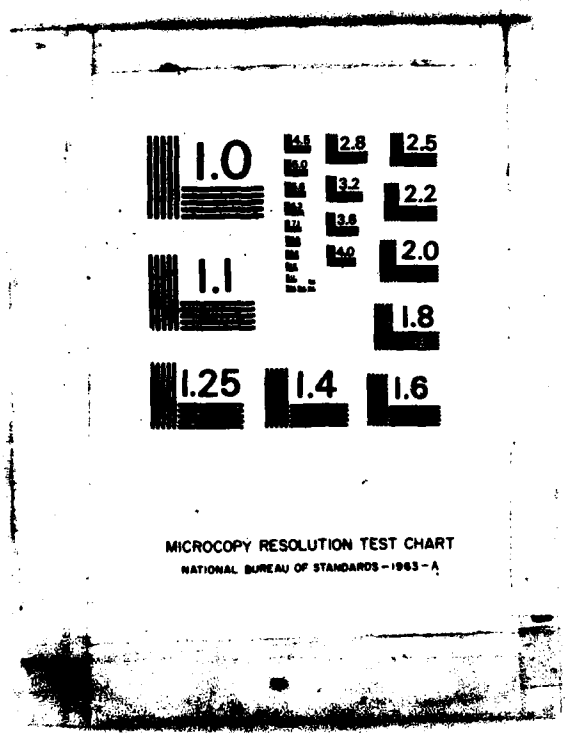
SBI AD 1950 462

F/G 17/9

NI



END
DATE
PRINTED
1 84



MICROCOPY RESOLUTION TEST CHART
NATIONAL BUREAU OF STANDARDS-1963-A

REFERENCES

¹IEEE STD 211-1977, "IEEE Standard Definitions of Terms for Radio Wave Propagation."

²G. Sinclair, "The Transmission and Reception of Elliptically Polarized Waves," Proc. IRE, VOL 38 pp 148-151, Feb 1950.

³J. R. Mentzer, "Scattering and Diffraction of Radio Waves," Pergamon Press, New York, 1955.

⁴J. R. Huynen, "Phenomenological Theory and Radar Targets," Ph.D. Dissertation, Drukkerij Bronder-Offset, N.V. Rotterdam, 1970.

⁵Dag T. Gjessing, "Adaptive Radar In Remote Sensing," Ann Arbor Science Publishers, Inc., Ann Arbor, Michigan, 1981.

DISTRIBUTION LIST

	<u>No. of Copies</u>
IIT Research Institute Guidance and Control Information and Analysis Center (GACIAC) 10 West 35th Street Chicago, IL 60616	1
Commander US Army Material Systems Analysis Activity ATTN: DRXSY-MP Aberdeen Proving Ground, MD 21005	1
Commander US Materiel Development and Readiness Command 5001 Eisenhower Avenue Alexandria, VA 22333	1
Commander Defense Advanced Research Projects Agency 1400 Wilson Boulevard Arlington, VA 22209	1
Commander US Army Research Office PO Box 12211 Research Triangle Park, NC 27709	1
Commander US Army Armament R&D Command Picatinny Arsenal Dover, NJ 07801	1
Commander US Army Armament R&D Command Ballistic Research Laboratories Aberdeen Proving Ground, MD 21005	1
Commander US Army Aviation R&D Command PO Box 209 St. Louis, MO 63166	1
Commander US Army Electronics R&D Command Atmospheric Sciences Laboratory White Sands Missile Range, NM 88002	1
Commander AVRADCOM ATTN: DRDAV-NC (Dr. Marner) 4300 Goodfellow Blvd St. Louis, MO 63120	1



DISTRIBUTION (Continued)

	<u>No. of Copies</u>
Commander US Army Electronics R&D Command US Army Electronic Warfare Laboratory Ft. Monmouth, NJ 07703	1
Commander US Army Electronics R&D Command Office of Missile Electronic Warfare White Sands Missile Range, NM 88022	1
Commander US Army Electronics R&D Command Combat Surveillance and Target Acquisition Laboratory Ft. Monmouth, NJ 07703	1
Commander US Army Electronics R&D Command Electronic Warfare Laboratory Ft. Monmouth, NJ 07703	1
Commander US Army Electronics R&D Command Electronics Technology and Devices Laboratory Ft. Monmouth, NJ 07703	1
Commander US Army Electronics R&D Command Night Vision and Electro-Optics Laboratory Ft. Belvoir, VA 22060	1
Commander US Army Electronics R&D Command Harry Diamond Laboratories 2800 Powder Mill Road Adelphi, MD 20783	1
Commander US Army Electronics R&D Command Project Manager, SOTAS Ft. Monmouth, NJ 07703	1
Commander US Army Mobility Equipment R&D Command Ft. Belvoir, VA 22060	1
Commander US Army Air Mobility Research and Development Laboratory AMES Research Center Moffett Field, CA 94035	1

DISTRIBUTION (Continued)

	<u>No. of Copies</u>
Commander US Army Tank-Automotive Command Warren, MI 48090	1
Commander US Army Missile Command Ballistic Missile Defense Advanced Technology Center PO Box 1500 Huntsville, AL 35807	1
Commander US Naval Research Laboratory ATTN: Code 5300, Radar Division Washington, DC 20390	1
Commander US Naval Air Development Center SEnsors & Avionics Technology Directorate Radar Division/Tactical Radar Branch Warminster, PA 18974	1
Commander US Naval Electronics Laboratory Center San Diego, CA 92152	1
Commander US Naval Surface Weapons Center Dahlgren, VA 22448	1
Commander US Naval Surface Weapons Center White Oak Laboratory Silver Spring, MD 20910	1
Commander US Naval Weapons Center China Lake, CA 93555	1
Commander US Air Force Systems Command US Air Force Armament Laboratory Eglin Air Force Base, FL 32542	1
Commander US Air Force Systems Command US Air Force Avionics Laboratory Wright-Patterson Air Force Base, OH 45433	1

DISTRIBUTION (Continued)

	<u>No. of Copies</u>
Commander US Air Force Systems Command Air Force Cambridge Research Laboratories Hanscom Air Force Base, MA 01731	1
Commander US Air Force Systems Command Rome Air Development Center Griffiss Air Force Base, NJ 13441	1
Director Division 8 MIT Lincoln Laboratory Lexington, MA 02173	1
Director Radar and Instrumentation Laboratory Engineering Experiment Station Georgia Institute of Technology Atlanta, GA 30332	1
Automation Industries, Inc. Vitro Laboratories Division 14000 Georgia Avenue Silver Spring, MD 20910	1
AIL Division Cutler-Hammer Deer Park Long Island, NY 11729	1
Bell Aerospace Textron, Inc. PO Box 1 Buffalo, NY 14240	1
Boeing Aerospace Company V. G. Vaden Research and Engineering Division Seattle, WA 98124	1
Emerson Electric Company Electronics and Space Division 8100 W. Florissant Avenue St. Louis, MO 63163	1
Environmental Research Institute of Michigan Radar and Optics Division PO Box 618 Ann Arbor, MI 48107	1

DISTRIBUTION (Continued)

	<u>No. of Copies</u>
Ford Aerospace & Communications Corporation Aeronutronics Division Ford Road Newport Beach, CA 92663	1
General Dynamics Suite 42, Holiday Center South Memorial Parkway Huntsville, AL 35801	1
Goodyear Aerospace Corporation Akron, OH 44315	1
Goodyear Aerospace Corporation Arizona Division Litchfield Park, AZ 85340	1
Lockheed Missile & Space Company, Inc. 4800 Bradford Drive Huntsville, AL 35807	1
Honeywell, Inc. Defense Systems Division 2600 Ridgway Parkway Minneapolis, MN 55413	1
Hughes Aircraft Corporation Advanced Missile Systems Division Canoga Park, CA 91304	1
Mark Resources Incorporated 4676 Admiralty Way Suite 303 Marina Del Rey, CA 90291	1
Martin Marietta Aerospace ATTN: R. C. Scott MP 205 PO Box 5837 Orlando, FL 32855	1
McDonnell Douglas Astronautics Company 3322 South Memorial Parkway, Suite 122 Huntsville, AL 35801	1
MITRE Corporation 4305 Middlesex Turnpike Bedford, MA 01730	1

DISTRIBUTION (Continued)

	<u>No. of Copies</u>
Norden Systems, Inc. 314 Norden Place Norwalk, CT 06856	1
Northrop Corporation Defense Systems Division 600 Hicks Road Rolling Meadows, IL 60008	1
Raytheon Company Equipment Development Laboratories 430 Boston Post Road Wayland, MA 01778	1
RCA Government and Commercial Systems 3322 South Memorial Parkway Suite 41 Huntsville, AL 35801	1
Riverside Research Institute 80 West End Avenue New York, NY 10023	1
Rockwell International Missile Systems division 3370 Miraloma Avenue PO Box 4128 Anaheim, CA 92803	1
Sperry Microwave Electronics PO Box 4648 Clearwater, FL 33518	1
Sperry Research Center 100 North Road Sudbury, MA 01776	1
SRI International 1611 North Kent Street Rosslyn Plaza Arlington, VA 22209	1
Technology Service Corporation 2811 Wilshire Boulevard Santa Monica, CA 90404	1
Teledyne Brown Engineering Cummings Research Park Huntsville, AL 35807	1

DISTRIBUTION (Continued)

	<u>No. of Copies</u>
Teledyne Micronetics 7155 Mission Gorge Road San Diego, CA 92120	1
Texas Instruments, Incorporated ATTN: Advanced Weapons Program Mail Stop 390 PO Box 6015 Dallas, TX 75222	1
TRW Defense and Space Systems Group 303 Williams Avenue, Suite 1231 Huntsville, AL 35801	1
Commander US Army Electronics R&D Command ATTN: DELET-M, Mr. N. Wilson DELCS-R, Mr. D. Foiani Mr. W. Fishbein Mr. W. Johnson Mr. E. Frost Mr. T. Ewanizky Ft. Monmouth, NJ 07703	1 1 1 1 1 1 1
Director Defense Advanced Research Projects Agency ATTN: Dr. James Tagnelia 1400 Wilson Boulevard Arlington, VA 22209	1
Commander US Air Force Systems Command US Air Force Armament Laboratory ATTN: Major R. Salema Eglin Air Force Base, FL 32542	1
Emerson Electric Company Electronics and Space Division ATTN: Mr. R. Hermann Mr. O. B. Mitchell 8100 W. Florissant St. Louis, MO 63136	1 1

DISTRIBUTION (Continued)

	<u>No. of Copies</u>
Georgia Institute of Technology Engineering Experiment Station ATTN: Dr. Robert McMillan Dr. Robert Shackelford Mr. James Gallager 347 Ferst Drive Atlanta, GA 30332	1 1 1
MIT Lincoln Laboratory Division 8 ATTN: Dr. Peter Tannenwald Dr. Harold Fetterman Dr. Jerry Waldman Lexington, MA 02173	1 1 1
Commander US Army ARRADCOM Bldg. 95 North DRDAR-SCF/IM (ATTN: W. Donally) Dover, NJ 07801	1
Chief Office of Missile Electronic Warfare US Army Electronic Warfare Lab ERADCOM ATTN: DELEW-M-STO, R. Blanco White Sands Missile Range, NM 88002	1
Department of the Army US Army Research Office ATTN: Information Processing Office PO Box 12211 Research Triangle Park, NC 27709	1
Sperry Research Center ATTN: Dr. R. M. Barnes 100 North Road Sudbury, MA 01776	1
System Planning Corporation Ray Harris 1500 Wilson Boulevard Arlington, VA 22209	1
Director Applied Technology Lab USARTL (AVRADCOM) ATTN: DAVDL-ATL-ASW (J. Shostak) Ft. Eustis, VA 23604	1

DISTRIBUTION (Continued)

	<u>No. of Copies</u>
DRSMI-LP, Mr. Voit	1
DRSMI-R, Dr. McCorkle	1
DRSMI-RN	1
DRSMI-RE, Mr. Lindberg	1
DRSMI-RE, Mr. Todd	1
DRSMI-RE, Mr. Pittman	1
DRSMI-REM, Mr. Haraway	1
DRSMI-REO, Mr. Ducote	1
DRSMI-RER, Mr. Low	1
DRSMI-RES, Mr. Hatcher	1
DRSMI-REG, Mr. Root	1
DRSMI-REL, Mr. Mangus	1
DRSMI-REL, Dr. Emmons	1
DRSMI-REL, Dr. Alexander	1
DRSMI-RN, Mr. Race	1
DRSMI-RR, Dr. Hartman	15
DRSMI-RPR	1
DRSMI-RPT, Record Set	1
DRSMI-REG, Mr. Sedenquist	1
DRSMI-REG, Mr. Russell	1
DRSMI-REG, Mr. D. Garner	1
DRSMI-REG, Mr. J. Cole	15

